Driver lines for studying associative learning in Drosophila

Yichun Shuai[1*], Megan Sammons[1,2], Gabriella Sterne[1,3], Karen Hibbard[1], He Yang[1], Ching-Po Yang[1,4], Claire Managan[1], Igor Siwanowicz[1], Tzumin Lee[1,4], Gerald M. Rubin[1], Glenn Turner[1], Yoshinori Aso[1*]

[1] Janelia Research Campus, Howard Hughes Medical Institute, 19700 Helix Drive, Ashburn, VA 20147, USA

[2] Current address: Technion-Israel Institute of Technology, 1 Efron St., Haifa 32000, Israel.

[3] Current address: Department of Biomedical Genetics, University of Rochester Medical Center, Rochester, NY, USA.

[4] Current address: Life Sciences Institute, University of Michigan, Ann Arbor, USA.

[*] Correspondence to: shuaiy@janelia.hhmi.org asoy@janelia.hhmi.org

Abstract

The mushroom body (MB) is the center for associative learning in insects. In Drosophila, intersectional split-GAL4 drivers and electron microscopy (EM) connectomes have laid the foundation for precise interrogation of the MB neural circuits. However, many cell types upstream and downstream of the MB remained to be investigated due to lack of driver lines. Here we describe a new collection of over 800 split-GAL4 and split-LexA drivers that cover approximately 300 cell types, including sugar sensory neurons, putative nociceptive ascending neurons, olfactory and thermo-/hygro-sensory projection neurons, interneurons connected with the MB-extrinsic neurons, and various other cell types. We characterized activation phenotypes for a subset of these lines and identified the sugar sensory neuron line most suitable for reward substitution. Leveraging the thousands of confocal microscopy images associated with the collection, we analyzed neuronal morphological stereotypy and discovered that one set of mushroom body output neurons, MBON08/MBON09, exhibits striking individuality and asymmetry across animals. In conjunction with the EM connectome maps, the driver lines reported here offer a powerful resource for functional dissection of neural circuits for associative learning in adult Drosophila.

Introduction

In the insect brain, the mushroom body (MB) serves as the center for associative learning (Figure 1A-C; reviewed in Modi et al., 2020; Davis, 2023). Information regarding conditioned stimulus (CS), such as odors and colors, is conveyed by projection neurons (PNs) to the calyx, the input region of the MB. Approximately 2,000 Kenyon cells (KCs), the MB's primary intrinsic neurons, represent the identity of sensory stimuli by their sparse activity patterns (Perez-Orive et al., 2002; Turner et al., 2008). Dopaminergic neurons (DANs) mediate signals of the unconditioned stimulus (US), such as sugar reward or electric shock punishment, to the MB (Burke et al., 2012; Kirkhart and Scott, 2015; Liu et al., 2012; Mao and Davis, 2009; Schwaerzel et al., 2003). DANs and MB output neurons (MBONs) collectively form 15 compartmental zones that tile down the length of the KC axons in the MB lobes (Aso et al., 2014a; Tanaka et al., 2008). Memories are stored as altered weights of synaptic connections between KCs and MB output neurons (MBONs) in each compartment (Hige et al., 2015a; Owald et al., 2015). Relative activity levels of MBONs across compartments represent the valence of the learned CS and drive memory-based behaviors (Aso et al., 2014b; Owald et al., 2015).

The recently completed electron microscopy (EM) connectomes of the Drosophila brain in larvae and adults revealed thousands of interneurons upstream of DANs, which convey reinforcement signals to the MB, and downstream of MBONs, which link the MB to premotor pathways and other higher-order brain centers (Dorkenwald et al., 2023; Eichler et al., 2017; Eschbach et al., 2020; Li et al., 2020; Scheffer et al., 2020; Winding et al., 2023; Zheng et al., 2018). Functional investigation of these interneuron cell types has been limited by the lack of cell-type-specific driver lines.

Using the intersectional split-GAL4 method (Luan et al., 2020, 2006), we previously generated 93 split-GAL4 driver lines that allowed for precise genetic access to 60 MB cell types, including most of the KCs, DANs, MBONs and other modulatory neurons in the MB lobe regions (Aso et al., 2014a). These lines have been instrumental in revealing the neural circuit logic by which the MB forms associative memories (Aso et al., 2019, 2014b; Awata et al., 2019; Berry et al., 2018; Dolan et al., 2018; Felsenberg et al., 2017; Handler et al., 2019; Hattori et al., 2017; Hige et al., 2015a, 2015b; Ichinose et al., 2015; König et al., 2019; Martinez-Cervantes et al., 2022; Masek et al., 2015; McCurdy et al., 2021; Pavlowsky et al., 2018; Plaçais et al., 2017; Sayin et al., 2019; Shyu et al., 2017; Tsao et al., 2018; Vogt et al., 2016; Wu et al., 2017; Yamada et al., 2023; Zhang et al., 2019).

Since the MB split-GAL4 lines were generated, new genetic and computational tools have expanded the cell types that can be targeted and facilitated the split-GAL4 design. Critically, a new collection of ZpGAL4DBD and p65ADZp hemidrivers became available (Dionne et al., 2018; Tirian and Dickson, 2017) and the expression patterns of the original GAL4 driver lines were imaged with higher-resolution confocal microscopy and Multi-Color-Flip-Out (MCFO) stochastic

labeling method to reveal the morphology of individual neurons (Meissner et al., 2023; Nern et al., 2015). Additionally, advanced tools for computational neuroanatomy were developed to aid the design of split-GAL4 driver lines (Bogovic et al., 2020; Costa et al., 2016; Masse et al., 2012; Meissner et al., 2023; Otsuna et al., n.d.). Leveraging these tools and resources, we have generated a collection of new split-GAL4 lines labeling MBONs, including the majority of atypical MBONs that have dendritic input both within the MB lobes and in adjacent brain regions (Rubin and Aso, 2023). In this report, we introduce a novel collection of approximately 800 split-GAL4 lines, covering sensory neurons for sugar, wind and nociception, projection neurons for olfactory, thermo/hygro-sensory and gustatory signals, ascending neurons from ventral nerve cord (VNC), cell types within the MB, and interneurons that connect with DANs and/or MBONs. While our primary objective was to generate driver lines for studying associative learning, the collection also includes cell types tailored for various other functions. We provide a lookup table that maps the corresponding EM neurons in the hemibrain connectome for these drivers to facilitate connectome-guided investigation of neural circuits. This expanded collection of driver lines will be instrumental for many future studies of Drosophila associative learning and beyond.

Results and Discussions

Split-GAL4 design and anatomical screening

To gain genetic access to the cell types that convey CS and US information to the MB and those mediating memory-based actions, we designed the screening to examine expression patterns of over 4,000 intersections of split-GAL4 hemidrivers. We selected 1,183 split-GAL4 lines representing various cell types in the central brain and the VNC for further characterization (Figure 1D). For these lines, we employed higher resolution confocal microscopy and visualized the individual neurons that compose each split-GAL4 pattern with the MCFO method. We eventually identified the 828 useful lines based on their specificity, intensity and non-redundancy. These fly lines are now publicly available through the webpage of the Janelia Flylight team project (http://www.janelia.org/split-gal4), where we have deposited a total of 28,376 confocal images from 6,374 tissue samples to document their expression patterns. We included lines with off-targeted expression, as they can be valuable for anatomical, developmental or imaging experiments, even if not suitable for behavioral experiments. Additionally, we retained drivers that intersected unintended cell types. Examples of confocal microscopy images are shown in Figure 1F and Figure 1-figure supplement 1.

We then sought to identify neurons labeled by our split-GAL4 lines to their counterparts in the hemibrain connectome volume (Scheffer et al., 2020). By utilizing confocal images registered to a standard brain, we matched neuronal cell types in each split-GAL4 line with those present in other lines and with the EM-reconstructed neurons (Figure 2A-D). This light microscopy (LM) to EM matching process allows us to locate the cell type of each driver line in the connectome map, enabling users to select driver lines for further functional investigations

105 based on their upstream and downstream synaptic partners (Figure 2E; Figure 2-figure
106 supplement 1-23).
107 Among the 828 lines, 355 lines exhibit relatively high specificity to a non-redundant set
108 of at least 319 distinct cell types. Figure 1E provides an overview of the categories of cell types
109 covered by these driver lines. Detailed information, including genotype, expression specificity,
110 matched EM cell type(s), and recommended driver for each cell type, can be found in
111 Supplementary File 1. A small subset of these lines have been previously used in studies (Aso et
112 al., n.d.; Dolan et al., 2019; Gao et al., 2019; Schretter et al., 2020; Takagi et al., 2017; Xie et al.,
113 2021; Yamada et al., 2023). All new transgenic lines generated in this study are listed in
114 Supplementary File 2.
115
116 **Drivers for the MB cell types, MBON-downstream and DAN-upstream**
117 Prior to the completion of the EM connectome map, we conducted parallel efforts to identify
118 cell types downstream of MBONs or upstream of DANs using confocal images of GAL4 drivers
119 registered to a standard brain (Bogovic et al., 2020). We searched for GAL4 drivers containing
120 cell types with potential connections to MBONs or DANs by quantifying the number of voxels
121 overlapping with MBON axons or DAN dendrites (Meissner et al., 2023; Otsuna et al., n.d.). We
122 then built split-GAL4 intersections from selected pairs of drivers from the established hemidriver
123 library (Dionne et al., 2018; Tirian and Dickson, 2017).
124 After matching with EM-reconstructed neurons, these efforts resulted in split-GAL4
125 drivers encompassing 111 cell types that connect with the DANs and MBONs (Figure 3). Several
126 of the cell types originally selected by LM were found to be not directly connected with MBONs
127 or DANs. Nevertheless, these lines can be valuable for investigating other behaviors. For
128 example, SS32237 was found to exhibit robust female-female aggression when activated
129 (Schretter et al., 2020).
130 In the hemibrain EM connectome, there are about 400 interneuron cell types that have
131 over 100 summed synaptic connections across the MBON and DAN population. Our newly
132 developed collection of split-GAL4 drivers covers 30 of these major interneuron cell types (Figure
133 3C). While this constitutes a small fraction, it includes cell types with remarkable connectivity
134 patterns. For instance, CRE011, present as a single neuron per hemisphere, integrates over 2,400
135 inputs from 9 types of MBONs. This is the highest number of synaptic inputs from MBONs among
136 all interneurons (Figure 3C). CRE011 provides cholinergic input to reward DANs (Figure 2E) and
137 neurons in the lateral accessory lobe, a premotor center housing dendrites of multiple
138 descending neurons (Kanzaki et al., 1994; Namiki et al., 2018). Another notable example is
139 SMP108, which integrates inputs from several glutamatergic MBONs and makes the highest
140 number of cholinergic connections to DANs involved in appetitive memory (Figure 3C). In a
141 recent study, we reported on SMP108's role in second-order conditioning (Yamada et al., 2023)
142 and its upstream neurons labeled in SS33917 in transforming appetitive memory into wind-

143 directed locomotion (Aso et al., 2023). Supplementary File 3 contains a list of these major
144 interneurons, along with available driver lines.
145 The current collection also contains 168 lines for cell types that have innervations within
146 the MB (Figure 3-figure supplement 1). These lines offer valuable tools to study cell types that
147 may have been overlooked previously. Notably, the SS48794 driver labels OA-VUMa2
148 octopaminergic neurons, which are the Drosophila equivalent of honeybee OA-VUMmx1
149 neurons, the first neurons identified as mediating US signals in an insect brain (Hammer, 1993).
150 Moreover, some drivers in this collection provide improved specificity. When combined with
151 previous collections (Aso et al., 2014a; Rubin and Aso, 2023), we now have coverage for 7 types
152 of Kenyon cells and 58 out of 68 cell types within the MB (excluding PNs) using split-GAL4 drivers.
153 Overall, this amounts to about 87% coverage for non-PN cell types within the MB and about 10%
154 coverage for MBON-downstream and DAN-upstream cell types (Supplementary File 3 and 4).
155
156 **Drivers for the antennal lobe projection neurons**
157 In Drosophila, the primary CS pathway to the MB involves the antennal lobe PNs that convey
158 olfactory signals. We have developed a set of driver lines for PNs and other cell types in the
159 antennal lobe (Supplementary File 1). This set includes 186 lines, covering 73 of the
160 approximately 180 PN types identified through EM connectome and LM studies (Bates et al.,
161 2020; Li et al., 2020; Lin et al., 2007; Tanaka et al., 2004; Zheng et al., 2022), encompassing both
162 uni- and multi-glomerular PNs (Figure 4 and 5; Supplementary File 5).
163 The antennal lobe, in addition to the 51 olfactory glomeruli, contains 7 glomeruli involved
164 in processing thermo- and hygro-sensory information (Enjin et al., 2016; Frank et al., 2015; Gallio
165 et al., 2011; Jenett et al., 2012; Liu et al., 2015; Marin et al., 2020; Stocker et al., 1990; Tanaka et
166 al., 2012). We provide 8 lines that cover sensory neurons projecting into these non-olfactory
167 glomeruli and 18 lines covering the projection neurons emanating from them (Figure 6;
168 Supplementary File 5).
169
170 **Drivers for reinforcement pathways**
171 Our understanding of the neural pathways that encode the US has been greatly advanced by
172 experiments that have tested the sufficiency of various neuronal cell types to substitute for the
173 US (Aso et al., 2010; Aso and Rubin, 2016; Chiang et al., 2011; Claridge-Chang et al., 2009; Hige
174 et al., 2015a; Huetteroth et al., 2015; Liu et al., 2012; Saumweber et al., 2018; Schroll et al., 2006;
175 Yamagata et al., 2015). These experiments leveraged thermogenic or optogenetic tools
176 expressed in specific neuronal cell types, especially DANs, to assess their functions in associative
177 learning. The approach to directly stimulate DANs, although valuable, bypasses the earlier US
178 processing pathways and potential feedback in the circuit. Because of this experimental caveat,
179 it is preferable to activate neurons at the sensory level of reward or punishment pathways to
180 faithfully replicate the natural activity of these DANs. In that way, DANs can be regulated by both

181 US sensory pathways and feedback pathways from MBONs. That is likely to be essential for the
182 successful execution of more continual learning tasks in which flies update memories based on
183 the current and past experiences (Felsenberg et al., 2017; Jiang and Litwin-Kumar, 2021;
184 McCurdy et al., 2021; Rajagopalan et al., 2022).

185 Our collection provides the starting point for generating the genetic tools needed for this
186 approach. For example, we have generated drivers for the cell types in the thermo-sensory
187 pathways, as well as PNs for odors with innate preference, such as CO2 and cVA (Datta et al.,
188 2008; Lin et al., 2013; Suh et al., 2004). These cell types are candidates to convey the
189 reinforcement signals to the MB and other brain regions for associative learning.

190 On the other hand, gustatory sensory neurons constitute the first layer of neurons that detect
191 food-related sensory signals (taste), which are conveyed to the MB through largely
192 uncharacterized pathways (Bohra et al., 2018; Burke et al., 2012; Deere et al., 2023; Kim et al.,
193 2017; Miyazaki et al., 2015; Sterne et al., 2021). GAL4 driver lines that recapitulate expression
194 patterns of gustatory receptors (GRs) have been generated and utilized for functional studies
195 (Dahanukar et al., 2007; Harris et al., 2015; Miyamoto et al., 2012; Wang et al., 2004; Yavuz et
196 al., 2014). However, these driver lines tend to contain a morphologically and functionally
197 heterogeneous set of sensory neurons (see for examples: Chen et al., 2022; Thoma et al., 2016)
198 and may contain off-targeted expressions. To address these limitations, we have generated
199 hemi-driver lines using GR-gene promoters to intersect specific subsets of gustatory sensory
200 neurons (Figure 7A).

201 We used this strategy to generate Gr64f-split-Gal4 lines and create clean drivers for
202 reward sensory neurons. In fruit flies, sugar is detected by sensory neurons located on different
203 taste organs of the body and also inside the brain (Fujii et al., 2015; Hiroi et al., 2002; Miyamoto
204 et al., 2012; Rodrigues and Siddiqi, 1978). Gr64f-Gal4, in which Gal4 is expressed under the
205 control of the promoter of the sugar receptor gene *Gr64f*, broadly labels sugar sensory neurons
206 (Dahanukar et al., 2007). However, Gr64f-Gal4 expresses in heterogeneous sets of sensory
207 neurons in the labellum, the tarsi and the labral sense organ (LSO) located along the pharynx. It
208 also labels subsets of olfactory receptor neurons and neurons innervating the abdominal
209 ganglion (Park and Kwon, 2011)(Figure 7 – figure supplement 1A), despite that whether these
210 cells endogenously express Gr64f is yet to be confirmed. This heterogeneity in Gr64f-Gal4
211 expression could limit its usage as the US in complex associative learning; while pairing odor with
212 the activation of Gr64f-Gal4 labeled neurons resulted in appetitive learning in a short learning
213 protocol, memory performance was severely compromised after long training protocols (Figure
214 7-figure supplemental 1B-C).

215 To refine Gr64f-Gal4 expression, we intersected Gr64f-GAL4DBD with various AD lines,
216 and obtained 16 stable split-GAL4 lines that have expression in distinct subsets of Gr64f neurons
217 (Figure 7). We examined the ability of these lines to serve as US in olfactory learning (Aso and
218 Rubin, 2016) and their potency to drive local search behaviors (Corfas et al., 2019)(Figure 8 and

Figure 8-figure supplemental 1). Additionally, we measured the walking speed of flies, as flies decrease walking while feeding (Thoma et al., 2016).

Among the Gr64f-split-GAL4 lines, SS87269 emerged as the best driver for substituting sugar reward in olfactory learning (Figure 8E). SS87269 expresses in the labellum and at least two types of tarsal sensory neurons, namely the ascending (atGRN) and the non-ascending segment-specific type (stGRN) (Figure 7E-F) but does not label pharyngeal sensory neurons. It also lacks expression in abdominal or olfactory sensory neurons that are likely off-targeted neurons found in the original Gr64f-GAL4. When odor presentation was paired with the activation of SS87269 neurons, flies formed robust appetitive memories even after extended training with high LED intensity (Figure 8E). Furthermore, and consistent with the idea that this subset of sensory neurons encodes appetitive food-related taste information, flies with SS87269 activation showed proboscis extension and reduced locomotion (Figure 8F-I; Figure 8 - figure supplemental 1 and Video 1-2). These flies also showed robust local search behavior during the post-activation period, i.e., an increased probability of revisiting the area where they experienced the activation (Figure 8F). Notably, the revisiting phenotype of SS87269 was stronger than the original Gr64f-GAL4 and any other Gr64f split-GAL4 drivers.

Two other lines SS88801 and SS88776, which label stGRNs or stGRNs along with labial expression, respectively (Figure 7K-L,I), showed moderate appetitive learning and reduced locomotion during activation (Figure 8E-F). Interestingly, however, the activation of stGRNs with SS88801 did not induce significant local search behaviors (Figure 8F and Figure 8-figure supplement 1). This finding could be valuable for investigating reinforcement circuits involved in promoting local search by comparing pathways from labial and tarsal sensory neurons to the MB and central complex.

In contrast to SS87269, two other resulting lines, SS87278 and SS87279, express in cells that appear to convey aversive signals. Activation of these lines induced an increase in walking speed during activation (Figure 8F) and reduced the probability of return at the offset of LED activation. Also, flies became progressively less mobile during the inter-trial interval period (Figure 8G). The reduced locomotion in the interval period was also observed with the original Gr64f-GAL4 (Figure 8G) and a bitter-taste driver, Gr66a-GAL4 (data not shown). With extended training using SS87278 and SS87279, the preference to the paired odor eventually became negative (Figure 8E). These drivers label distinct subsets of sensory neurons projecting to the abdominal ganglion (Figure 7N-O). The innervation of SS87278 inside the abdominal ganglion is similar to that of Gr66a-GAL4 (Figure 7P) (Dunipace et al., 2001), which is known to label multidendritic sensory neurons in the adult Drosophila abdomen (Shimono et al., 2009). Examining projection patterns in fly bodies with whole-animal agar sections, we found that sensory neurons in SS87278 also project to the abdominal body surface (Figure 7J), likely representing the class IV multidendritic neurons that detect multimodal nociceptive stimuli (Hwang et al., 2007; Ohyama et al., 2015). GAL4 expression in these aversive sensory neurons

may thereby explain the compromised learning performance with the original Gr64f-GAL4. The refinement with SS87269 now allows for specific manipulation of the rewarding subset of gustatory sensory neurons thereby permitting training with an extended number of trials. While we have not yet conducted anatomical screening, LexADBD lines generated with Gr64f, Gr43a, Gr66a, Gr28b promoters (Figure 7A) should enable similar refinement of these sensory neuron lines. We also made a small number of lines for cell types in the subesophageal zone (SEZ) area (Figure 8-figure supplemental 2), which complement previous collections of drivers for gustatory interneurons (Otto et al., 2020; Sterne et al., 2021).

Lastly, we generated driver lines for putative ascending nociceptive pathways. We determined the activation preference for 581 combinations of ZpGAL4DBD and p65ADZp hemidrivers in the circular arena (Figure 9A, Supplementary File 1). We found one driver, SS01159, that showed the most robust avoidance of LED quadrants and demonstrated behavioral components that are characteristic to nociception, including backward walking, turning, increased speed, and jumping upon activation (Figure 9B-D, and Video 3). This driver labels a group of ascending neurons (Figure 9E), which likely carry nociceptive signals from the body and legs to the brain. We then generated drivers for subsets of these ascending neurons guided by single neuron morphologies of cells in SS01159 determined by MCFO stochastic labeling (Nern et al., 2015). Altogether we generated approximately 100 lines for ascending neurons (examples shown in Figure 9E). While not completely matched to EM cell types due to only a portion of their morphologies being available in the hemibrain volume, these lines serve as a valuable resource for querying reinforcement pathways.

Morphological individuality and asymmetry

Despite the recent progress in the EM connectome field, EM-based methods remain prohibitively expensive to examine morphological individuality of neurons across animals. In our efforts to annotate confocal images of split-GAL4 lines, we occasionally encountered samples with atypical morphologies (Figure 10). For example, one V_l2PN neuron, which typically projects to the lateral horn of the ipsilateral hemisphere, exhibited a peculiar morphology in one brain sample, where its axon crossed the midline and projected to the contralateral hemisphere, yet it still reached the correct target area within the lateral horn of the opposite side (Figure 10A). Another instance involved a DPM neuron, the sole serotonergic neuron of the MB lobes. While typical brain samples contain only one DPM neuron per hemisphere, we found a brain with two DPM neurons in one hemisphere (Figure 10B). In this case, the DPM projections exhibited an atypical innervation of the calyx of the mushroom body. We also found examples involving MBONs. The dendrites of MBON-α1 are typically confined inside the α lobe of the MB, but we discovered a case of MBON-α1 in addition projecting to the ellipsoid body (Figure 10C). MBON-α3 displayed striking variability in soma positions, but only subtle variability in axonal projections (Figure 10D). The table in Figure 10E summarizes additional examples of the atypical morphologies of MBONs.

These examples of atypical morphology were observed only once in dozens of samples, and thus can be considered as erroneous projections either resulting from stochastic developmental processes, or possibly caused by ectopic expression of reporter proteins on the plasma membrane.

In contrast to these seemingly erroneous morphological variations, we found highly reproducible individuality and asymmetry of morphology for two MBONs labeled by MB083C. This split-GAL4 driver line invariably labels two cells in each hemisphere in 169 brain samples examined with four different reporters and in both sexes (57 males and 112 females; Figure 11-figure supplement 1). In all samples, these MBONs arborized dendrites in the γ3 and β′1 compartments. An obvious mistargeting of the axon was observed in only one sample, suggesting highly consistent development of these MBONs (Figure 11A-B). However, MCFO method visualized two distinct morphologies of these MBONs: MBON08 arborizes dendrites in the γ3 compartment of both hemispheres, whereas MBON09 arborize dendrites in ipsilateral γ3 and contralateral β′1 (Figure 11C-H)(Aso et al., 2014a). β′1 compartment was always labeled in both hemispheres for all 169 samples, suggesting that MBON09 represents at least one of the two cells in each hemisphere. The second cell can be either MBON08 or MBON09. In MCFO experiments, we observed 21 instances of MBON08 and 188 instances of MBON09 (Figure 11I). Based on the likelihood, we expect 65% of flies contain four MBON09, while the remaining 35% of flies likely have at least one MBON08. Consistent with the low occurrence of MBON08, we never observed a brain with MBON08 on both hemispheres (Figure 11J). When MBON08 and MBON09 coexist, MBON09 arborized in the lateral part of the ipsilateral γ3 and MBON08 arborize in the medial part of the contralateral γ3 (Figure 11E-H). This seemingly extended γ3 compartment innervated by MBON08 is not part of γ4, because it did not overlap with DANs in the γ4 (Figure 11-figure supplement 2A-B). Although MBON08 was not found in brain samples used for the hemibrain or FAFB EM connectome (Dorkenwald et al., 2023; Scheffer et al., 2020; Zheng et al., 2018), DANs in the γ3 could be subdivided to two groups that innervate the medial or lateral part of the γ3 (Figure 11-figure supplement 2C) (Li et al., 2020), possibly reflecting heterogeneity on the MBON side. In larval brains, two MBONs that correspond to adult MBON08/09 exhibit identical morphology (Eichler et al., 2017; Saumweber et al., 2018; Truman et al., 2023). Therefore, one of these MBONs acquires distinct morphology as MBON08 during metamorphosis at 21/209 odds, resulting in an asymmetric output pathway of the MB; We have never observed a brain with MBON08 on both hemispheres, and therefore MBON08 likely to appear in only one hemisphere, if at all (Figure 11J). This asymmetry could be one source of turning handedness and idiosyncratic learning performance (de Bivort et al., 2022; Smith et al., 2022) , given that MBON09 forms extensive connection with other MBONs and fan-shaped body neurons (Li et al., 2020) and that activity of MBON08/MBON09 has strong influence on turning (Aso et al., 2014b, n.d.; Matheson et al., 2022).

333 **Conversion to split-LexA**
334 Split-GAL4 lines can be converted into split-LexA lines by replacing the GAL4 DNA binding domain
335 with that of LexA (Ting et al., 2011). To broaden the utility of our collection, we have generated
336 over 20 LexADBD lines to test the conversions of split-GAL4 to split-LexA. The majority (22 out of
337 34) of the resulting split-LexA lines exhibited very similar expression patterns to their
338 corresponding original split-GAL4 lines (Figure 12). For the failed cases, the expression level was
339 either undetectable or too weak.
340
341 **Concluding Remarks**
342 The ability to define and manipulate a small group of neurons is crucial for studying neural
343 circuits. Here, we have generated and characterized driver lines targeting specific cell types that
344 are likely to be a part of associative learning circuits centered on the MB. We have provided these
345 driver lines with a comprehensive lookup table linking these cell types with the EM hemibrain
346 connectome. These lines, together with preceding collections of drivers (see for examples: Aso
347 et al., 2014a; Aso and Rubin, 2016; Davis et al., 2020; Dolan et al., 2018; Rubin and Aso, 2023;
348 Shuai et al., 2015; Sterne et al., 2021; Strother et al., 2017; Tuthill et al., 2013; Wang et al., 2021;
349 Wolff and Rubin, 2018; Wu et al., 2016), collectively constitute a powerful resource for precise
350 functional interrogation of associative learning in adult Drosophila melanogaster, and will be a
351 foundation to reveal conserved principles of neural circuits for associative learning.
352
353 **Materials and Methods**
354 **Fly strains**
355 *Drosophila melanogaster* strains were reared at 22℃ and 60% humidity on standard cornmeal food in
356 12:12 hour light:dark cycle. The genotypes of all split-GAL4 and split-LexA driver lines released here are
357 listed in the Supplementary File 1. The new collection of split-GAL4 drivers reported here was designed
358 based on confocal image databases (http://flweb.janelia.org) (Jenett et al., 2012; Tirian and Dickson,
359 2017), and screening expression patterns of p65ADZp and ZpGAL4DBD combinations as described
360 previously (Aso et al., 2014a; Pfeiffer et al., 2010).
361
362 **Immunohistochemistry**
363 Brains and ventral nerve cords of 3-10 days old flies were dissected, fixed and immunolabeled and imaged
364 with confocal microscopes (Zeiss LSM710, LSM780 or LSM880) as previously described (Aso et al., 2014a;
365 Jenett et al., 2012; Meissner et al., 2023; Nern et al., 2015). The detailed protocols and videos are available
366 at https://www.janelia.org/project-team/flylight/protocols.
367
368 **Behavioral assays**
369 For flies expressing CsChrimson (Klapoetke et al., 2014), the food was supplemented with retinal (0.2 mM
370 all-trans-retinal prior to eclosion and then 0.4 mM). Two- to six-day old adult females were collected and
371 sorted on a Peltier cold plate 2-4 days before testing in behavioral assays. Flies were starved for 40–48
372 hr on 1% agar before they were subjected to behavioral experiments. Olfactory conditioning and

373 optogenetic activation experiments were performed as previously described using the modified four-field
374 olfactory arena equipped with the 627 nm LED board and odor mixers (Aso and Rubin, 2016; Pettersson,
375 1970). The odors were diluted in paraffin oil: pentyl acetate (PA, 1:10000, v/v) and ethyl lactate (EL,
376 1:10000, v/v). Videos were taken at 30 frames per second and analyzed using Fiji and Caltech FlyTracker
377 (Eyjolfsdottir et al., 2014).
378
379 **LM-EM matching**
380 The confocal microscopy images of different split-GAL4 lines were registered to a common template
381 JRC2018_unisex (Bogovic et al., 2020) and organized in Janelia Workstation software
382 (https://github.com/JaneliaSciComp/workstation). Color depth MIP mask search (Otsuna et al., n.d.) was
383 used to search through the EM neuron library (hemibrain 1.2.1) for matching candidates. The searching
384 target was obtained by either creating a mask on the full confocal image or using neurons of interest
385 manually segmented in VVD viewer (https://github.com/takashi310/VVD_Viewer)(Wan et al., 2012).
386 SWC files of top-matching EM neuron candidates were loaded into VVD viewer together with the confocal
387 microscopy images in the same standard brain coordinates. By rotating the 3d images and manually
388 scrutinizing the branching patterns, we picked the best matching candidate. Typically, we had high
389 confidence of LM-to-EM matching for the line that labels only one cell per hemishere. For instance, we
390 could unambiguously match the cell in SS67721 with SMP108 in the EM hemibrain volume. Our
391 confidence of LM-to-EM matching tended to be lower for the lines that label multiple cells, because
392 neurons of similar morphologies could be labeled together in those lines.
393
394 **Connectivity analysis**
395 Connectivity information was retrieved from neuPrint (neuprint.janelia.org), a publicly accessible website
396 hosting the "hemibrain" dataset (Scheffer et al., 2020). For cell types, we used cell type name assignments
397 reported in Sheffer et al., 2020. Only connections of the cells in the right hemisphere were used due to
398 incomplete connectivity in the left hemisphere. The 3D renderings of neurons presented were generated
399 using the visualization tools of NeuTu (Zhao et al., 2018) or VVD viewer .
400
401 **Statistics**
402 Statistical comparisons were performed on GraphPad Prism 7.0 using one-way ANOVA followed by
403 Dunnett's test for multiple comparisons. Sample size was not predetermined based on pilot experiments.
404
405
406 **Supplemental information**
407 **Supplementary File 1 A list of released driver lines and their corresponding EM neurons.**
408 Listed are stable split-GAL4 lines (SS, MB) and split-LexA lines (SL). Drivers are grouped by the anatomical
409 regions where they have their primary expression. Recently released MBON lines (Rubin and Aso, 2023)
410 are also included. Matching to EM cell types in the hemibrain v1.2.1 dataset was performed by an
411 algorithmic search of the morphologies of EM skeletons, followed by manual evaluation of proposed
412 matches using 3D visualization software. The best-matching candidates are listed. Where multiple
413 candidates seem valid, the alternatives are listed in the note column. In some cases, a matching EM

414 BodyId can be found in the hemibrain v1.2.1 dataset but an EM cell type has not been defined; these are
415 listed as TBD. Number of cells observed in light microscopy (LM) or electron microscopy (EM) are from
416 one hemisphere, unless otherwise stated. A descriptive cell type column is included, which uses
417 conventional names (if available) to facilitate searching and includes cell types with weak/stochastic
418 expression (bracketed) or putative cell types with less matching confidence. When there are multiple
419 drivers for the same cell type(s), one is chosen as the primary driver based on specificity, consistency, and
420 expression strength. Abbreviations: AL, antennal lobe; ORNs, olfactory receptor neurons; AL LNs,
421 antennal lobe local interneurons; PNs, projection neurons; MB, mushroom body; KCs, Kenyon cells;
422 MBONs, mushroom body output neurons; DANs, dopaminergic neurons; LH, lateral horn; LHONs, lateral
423 horn output neurons; LHLNs, lateral horn local neurons; SNP, superior neuropils; CRE, crepine; CX, central
424 complex; LAL, lateral accessory lobe; ANs, ascending neurons; DNs, descending neurons; OANs,
425 octopaminergic neurons; 5-HT, serotonergic neurons; OL, optic lobe; VLNP, ventrolateral neuropils; INP,
426 inferior neuropils (other than crepine); VMNP, ventromedial neuropils; PENP, periesophageal neuropils;
427 GNG, gnathal ganglia; VNC, ventral nerve cord; N.D., not determined.
428
429 **Supplementary File 2 New transgenic flies generated in this study.**
430 The enhancer fragments, insertion sites, and inserted chromosomes used to construct the lines are listed.
431 For some of the transgenes, an additional version with a *p10* 3'-UTR (Pfeiffer et al., 2012) was generated
432 to increase the expression.
433
434 **Supplementary File 3 Coverage of MBON-downstream and DAN-upstream**
435 Connection matrix between MB interneurons and DANs and MBONs. A threshold was set to exclude
436 connections with a low number of neuron-neuron connections, specifically, 10 connections for MBON to
437 a downstream neuron and 5 connections for upstream neurons to a DAN (Li et al., 2020). Recurrent
438 neurons are defined as cell types receiving input from MBONs and supplying output to DANs.
439
440 **Supplementary File 4 Updated list of driver lines for cell types within the MB excluding Kenyon**
441 **cells.**
442 This includes new or improved split-GAL4 and split-LexA lines from the present study, lines from the Aso
443 2014 collection (Aso et al., 2014a), a recent MBON collection (Rubin and Aso, 2023), MB630B (Aso and
444 Rubin, 2016), SS01308 (Aso et al., 2019), MB063B (Dolan et al., 2019), SS46348 (Otto et al., 2020), and
445 some regular Gal4 lines VT43924-Gal4.2 (Amin et al., 2020) and G0239 (Chiang et al., 2011). Lines listed
446 in boldface are generally of higher quality.
447
448 **Supplementary File 5 Coverage of PN cell types**
449 A list of split-GAL4 lines and their coverage of PNs of the antennal lobe. Shading indicates expression level.
450 Many of the multi-glomerular PN (mPN) cell types cannot be easily differentiated based on light
451 microscopy images, so they are listed as a broad mPN category in the table.
452

453 **Video1 Activation phenotypes with SS87269**

454 An exemplar video of activation phenotypes of flies of the genotype SS87269/UAS-CsChrimson-mVenus
455 attP18. Flies receive six consecutive 60s trials; during each trial a 10s LED activation was presented (from
456 10-20s) as indicated. The trajectories of individual flies over the previous 5 s are shown.

457 **Video 2 Proboscis extension upon SS87269 activation for flies walking on a ball**

458 Flies were thorax-fixed by tethering to a pin and allowed to walk on an air-floated foam ball. Proboscis
459 activities were tracked with the Animal Part Tracker (https://github.com/kristinbranson/APT).
460

461 **Video 3 Activation preference of SS01159 in the LED choice experiment.**
462 An exemplar video of LED choices of flies of the genotype SS01159/UAS-CsChrimson-mVenus attP18.
463 The trajectories of individual flies over the previous 5 s are shown. 625 nm LED was on from 30 s to 60 s
464 and from 90 s to 120 s, and the lit quadrants are indicated.
465

466 **Acknowledgments**

467 We thank members of the Y.A., G.M.R. and G.T. laboratories for technical assistance and valuable
468 comments on the manuscript. We thank all the members of Janelia Flylight, fly facility and scientific
469 computing for constructing split-GAL4 drivers and generating confocal microscopy images.

470 **Author contributions**

471 Conceptualization, G.M.R., G.T., L.T. and Y.A.; Formal Analysis and Investigation, Y.S., M.S., G.B.., K.H.,
472 C.Y., C.M.., I.S., and Y.A.; Writing, Y.S., G.M.R., G.T., G.S., and Y.A.; Supervision, G.M.R., G.T., T.L., and Y.A..;
473 Funding Acquisition, G.M.R., G.T., T.L. and Y.A.

474 **Competing interests**

475 The authors declare no competing interests.

476

477 **References**

478 Amin H, Apostolopoulou AA, Suárez-Grimalt R, Vrontou E, Lin AC. 2020. Localized inhibition in the
479 Drosophila mushroom body. *Elife* **9**. doi:10.7554/eLife.56954
480 Aso Y, Hattori D, Yu Y, Johnston RM, Iyer NA, Ngo T-TB, Dionne H, Abbott LF, Axel R, Tanimoto H, Rubin
481 GM. 2014a. The neuronal architecture of the mushroom body provides a logic for associative
482 learning. *Elife* **3**:e04577.
483 Aso Y, Ray RP, Long X, Bushey D, Cichewicz K, Ngo T-T, Sharp B, Christoforou C, Hu A, Lemire AL, Tillberg
484 P, Hirsh J, Litwin-Kumar A, Rubin GM. 2019. Nitric oxide acts as a cotransmitter in a subset of
485 dopaminergic neurons to diversify memory dynamics. *Elife* **8**. doi:10.7554/eLife.49257

Aso Y, Rubin GM. 2016. Dopaminergic neurons write and update memories with cell-type-specific rules. *Elife* **5**. doi:10.7554/eLife.16135

Aso Y, Sitaraman D, Ichinose T, Kaun KR, Vogt K, Belliart-Guérin G, Plaçais P-Y, Robie AA, Yamagata N, Schnaitmann C, Rowell WJ, Johnston RM, Ngo T-TB, Chen N, Korff W, Nitabach MN, Heberlein U, Preat T, Branson KM, Tanimoto H, Rubin GM. 2014b. Mushroom body output neurons encode valence and guide memory-based action selection in Drosophila. *Elife* **3**:e04580.

Aso Y, Siwanowicz I, Bräcker L, Ito K, Kitamoto T, Tanimoto H. 2010. Specific dopaminergic neurons for the formation of labile aversive memory. *Curr Biol* **20**:1445–1451.

Aso Y, Yamada D, Bushey D, Hibbard K, Sammons M, Otsuna H, Shuai Y, Hige T. n.d. Neural circuit mechanisms for transforming learned olfactory valences into wind-oriented movement. doi:10.1101/2022.12.21.521497

Awata H, Takakura M, Kimura Y, Iwata I, Masuda T, Hirano Y. 2019. The neural circuit linking mushroom body parallel circuits induces memory consolidation in. *Proc Natl Acad Sci U S A* **116**:16080–16085.

Bates AS, Schlegel P, Roberts RJV, Drummond N, Tamimi IFM, Turnbull R, Zhao X, Marin EC, Popovici PD, Dhawan S, Jamasb A, Javier A, Serratosa Capdevila L, Li F, Rubin GM, Waddell S, Bock DD, Costa M, Jefferis GSXE. 2020. Complete Connectomic Reconstruction of Olfactory Projection Neurons in the Fly Brain. *Curr Biol* **30**:3183–3199.e6.

Berry JA, Phan A, Davis RL. 2018. Dopamine Neurons Mediate Learning and Forgetting through Bidirectional Modulation of a Memory Trace. *Cell Rep* **25**:651–662.e5.

Bogovic JA, Otsuna H, Heinrich L, Ito M, Jeter J, Meissner G, Nern A, Colonell J, Malkesman O, Ito K, Saalfeld S. 2020. An unbiased template of the Drosophila brain and ventral nerve cord. *PLoS One* **15**:e0236495.

Bohra AA, Kallman BR, Reichert H, VijayRaghavan K. 2018. Identification of a Single Pair of Interneurons for Bitter Taste Processing in the Drosophila Brain. *Curr Biol* **28**:847–858.e3.

Burke CJ, Huetteroth W, Owald D, Perisse E, Krashes MJ, Das G, Gohl D, Silies M, Certel S, Waddell S. 2012. Layered reward signalling through octopamine and dopamine in Drosophila. *Nature* **492**:433–437.

Chen H-L, Motevalli D, Stern U, Yang C-H. 2022. A functional division of sweet taste neurons that is value-based and task-specific. *Proc Natl Acad Sci U S A* **119**. doi:10.1073/pnas.2110158119

Chiang A-S, Lin C-Y, Chuang C-C, Chang H-M, Hsieh C-H, Yeh C-W, Shih C-T, Wu J-J, Wang G-T, Chen Y-C, Wu C-C, Chen G-Y, Ching Y-T, Lee P-C, Lin C-Y, Lin H-H, Wu C-C, Hsu H-W, Huang Y-A, Chen J-Y, Chiang H-J, Lu C-F, Ni R-F, Yeh C-Y, Hwang J-K. 2011. Three-dimensional reconstruction of brain-wide wiring networks in Drosophila at single-cell resolution. *Curr Biol* **21**:1–11.

Claridge-Chang A, Roorda RD, Vrontou E, Sjulson L, Li H, Hirsh J, Miesenböck G. 2009. Writing memories with light-addressable reinforcement circuitry. *Cell* **139**:405–415.

Corfas RA, Sharma T, Dickinson MH. 2019. Diverse Food-Sensing Neurons Trigger Idiothetic Local Search in Drosophila. *Curr Biol* **29**:1660–1668.e4.

Costa M, Manton JD, Ostrovsky AD, Prohaska S, Jefferis GSXE. 2016. NBLAST: Rapid, Sensitive Comparison of Neuronal Structure and Construction of Neuron Family Databases. *Neuron* **91**:293–311.

Dahanukar A, Lei Y-T, Kwon JY, Carlson JR. 2007. Two Gr genes underlie sugar reception in Drosophila. *Neuron* **56**:503–516.

Datta SR, Vasconcelos ML, Ruta V, Luo S, Wong A, Demir E, Flores J, Balonze K, Dickson BJ, Axel R. 2008. The Drosophila pheromone cVA activates a sexually dimorphic neural circuit. *Nature* **452**:473–477.

Davis FP, Nern A, Picard S, Reiser MB, Rubin GM, Eddy SR, Henry GL. 2020. A genetic, genomic, and computational resource for exploring neural circuit function. *Elife* **9**. doi:10.7554/eLife.50901

Davis RL. 2023. Learning and memory using Drosophila melanogaster: a focus on advances made in the fifth decade of research. *Genetics*. doi:10.1093/genetics/iyad085

534 de Bivort B, Buchanan S, Skutt-Kakaria K, Gajda E, Ayroles J, O'Leary C, Reimers P, Akhund-Zade J, Senft
535 R, Maloney R, Ho S, Werkhoven Z, Smith MA-Y. 2022. Precise Quantification of Behavioral
536 Individuality From 80 Million Decisions Across 183,000 Flies. *Front Behav Neurosci* **16**:836626.
537 Deere JU, Sarkissian AA, Yang M, Uttley HA, Martinez Santana N, Nguyen L, Ravi K, Devineni AV. 2023.
538 Selective integration of diverse taste inputs within a single taste modality. *Elife* **12**.
539 doi:10.7554/eLife.84856
540 Dionne H, Hibbard KL, Cavallaro A, Kao J-C, Rubin GM. 2018. Genetic Reagents for Making Split-GAL4
541 Lines in. *Genetics* **209**:31–35.
542 Dolan M-J, Belliart-Guérin G, Bates AS, Frechter S, Lampin-Saint-Amaux A, Aso Y, Roberts RJV, Schlegel P,
543 Wong A, Hammad A, Bock D, Rubin GM, Preat T, Plaçais P-Y, Jefferis GSXE. 2018. Communication
544 from Learned to Innate Olfactory Processing Centers Is Required for Memory Retrieval in
545 Drosophila. *Neuron* **100**:651–668.e8.
546 Dolan M-J, Frechter S, Bates AS, Dan C, Huoviala P, Roberts RJ, Schlegel P, Dhawan S, Tabano R, Dionne
547 H, Christoforou C, Close K, Sutcliffe B, Giuliani B, Li F, Costa M, Ihrke G, Meissner GW, Bock DD, Aso
548 Y, Rubin GM, Jefferis GS. 2019. Neurogenetic dissection of the Drosophila lateral horn reveals major
549 outputs, diverse behavioural functions, and interactions with the mushroom body. *Elife* **8**.
550 doi:10.7554/eLife.43079
551 Dorkenwald S, Matsliah A, Sterling AR, Schlegel P, Yu S-C, McKellar CE, Lin A, Costa M, Eichler K, Yin Y,
552 Silversmith W, Schneider-Mizell C, Jordan CS, Brittain D, Halageri A, Kuehner K, Ogedengbe O,
553 Morey R, Gager J, Kruk K, Perlman E, Yang R, Deutsch D, Bland D, Sorek M, Lu R, Macrina T, Lee K,
554 Bae JA, Mu S, Nehoran B, Mitchell E, Popovych S, Wu J, Jia Z, Castro M, Kemnitz N, Ih D, Bates AS,
555 Eckstein N, Funke J, Collman F, Bock DD, Jefferis GSXE, Seung HS, Murthy M, FlyWire Consortium.
556 2023. Neuronal wiring diagram of an adult brain. *bioRxiv*. doi:10.1101/2023.06.27.546656
557 Dunipace L, Meister S, McNealy C, Amrein H. 2001. Spatially restricted expression of candidate taste
558 receptors in the Drosophila gustatory system. *Curr Biol* **11**:822–835.
559 Eichler K, Li F, Litwin-Kumar A, Park Y, Andrade I, Schneider-Mizell CM, Saumweber T, Huser A, Eschbach
560 C, Gerber B, Fetter RD, Truman JW, Priebe CE, Abbott LF, Thum AS, Zlatic M, Cardona A. 2017. The
561 complete connectome of a learning and memory centre in an insect brain. *Nature* **548**:175–182.
562 Enjin A, Zaharieva EE, Frank DD, Mansourian S, Suh GSB, Gallio M, Stensmyr MC. 2016. Humidity Sensing
563 in Drosophila. *Curr Biol* **26**:1352–1358.
564 Eschbach C, Fushiki A, Winding M, Schneider-Mizell CM, Shao M, Arruda R, Eichler K, Valdes-Aleman J,
565 Ohyama T, Thum AS, Gerber B, Fetter RD, Truman JW, Litwin-Kumar A, Cardona A, Zlatic M. 2020.
566 Recurrent architecture for adaptive regulation of learning in the insect brain. *Nat Neurosci* **23**:544–
567 555.
568 Eyjolfsdottir E, Branson S, Burgos-Artizzu XP, Hoopfer ED, Schor J, Anderson DJ, Perona P. 2014.
569 Detecting Social Actions of Fruit FliesComputer Vision – ECCV 2014. Springer International
570 Publishing. pp. 772–787.
571 Felsenberg J, Barnstedt O, Cognigni P, Lin S, Waddell S. 2017. Re-evaluation of learned information in
572 Drosophila. *Nature* **544**:240–244.
573 Frank DD, Jouandet GC, Kearney PJ, Macpherson LJ, Gallio M. 2015. Temperature representation in the
574 Drosophila brain. *Nature* **519**:358–361.
575 Fujii S, Yavuz A, Slone J, Jagge C, Song X, Amrein H. 2015. Drosophila sugar receptors in sweet taste
576 perception, olfaction, and internal nutrient sensing. *Curr Biol* **25**:621–627.
577 Gallio M, Ofstad TA, Macpherson LJ, Wang JW, Zuker CS. 2011. The coding of temperature in the
578 Drosophila brain. *Cell* **144**:614–624.
579 Gao R, Asano SM, Upadhyayula S, Pisarev I, Milkie DE, Liu T-L, Singh V, Graves A, Huynh GH, Zhao Y,
580 Bogovic J, Colonell J, Ott CM, Zugates C, Tappan S, Rodriguez A, Mosaliganti KR, Sheu S-H, Pasolli
581 HA, Pang S, Xu CS, Megason SG, Hess H, Lippincott-Schwartz J, Hantman A, Rubin GM, Kirchhausen

582 T, Saalfeld S, Aso Y, Boyden ES, Betzig E. 2019. Cortical column and whole-brain imaging with
583 molecular contrast and nanoscale resolution. *Science* **363**. doi:10.1126/science.aau8302
584 Hammer M. 1993. An identified neuron mediates the unconditioned stimulus in associative olfactory
585 learning in honeybees. *Nature* **366**:59–63.
586 Handler A, Graham TGW, Cohn R, Morantte I, Siliciano AF, Zeng J, Li Y, Ruta V. 2019. Distinct Dopamine
587 Receptor Pathways Underlie the Temporal Sensitivity of Associative Learning. *Cell*.
588 doi:10.1016/j.cell.2019.05.040
589 Harris DT, Kallman BR, Mullaney BC, Scott K. 2015. Representations of Taste Modality in the Drosophila
590 Brain. *Neuron* **86**:1449–1460.
591 Hattori D, Aso Y, Swartz KJ, Rubin GM, Abbott LF, Axel R. 2017. Representations of Novelty and
592 Familiarity in a Mushroom Body Compartment. *Cell* **169**:956–969.e17.
593 Hige T, Aso Y, Modi MN, Rubin GM, Turner GC. 2015a. Heterosynaptic Plasticity Underlies Aversive
594 Olfactory Learning in Drosophila. *Neuron* **88**:985–998.
595 Hige T, Aso Y, Rubin GM, Turner GC. 2015b. Plasticity-driven individualization of olfactory coding in
596 mushroom body output neurons. *Nature* **526**:258–262.
597 Hiroi M, Marion-Poll F, Tanimura T. 2002. Differentiated Response to Sugars among Labellar
598 Chemosensilla in Drosophila. *jzoo* **19**:1009–1018.
599 Huetteroth W, Perisse E, Lin S, Klappenbach M, Burke C, Waddell S. 2015. Sweet taste and nutrient value
600 subdivide rewarding dopaminergic neurons in Drosophila. *Curr Biol* **25**:751–758.
601 Hwang RY, Zhong L, Xu Y, Johnson T, Zhang F, Deisseroth K, Tracey WD. 2007. Nociceptive Neurons
602 Protect Drosophila Larvae from Parasitoid Wasps. *Curr Biol* **17**:2105–2116.
603 Ichinose T, Aso Y, Yamagata N, Abe A, Rubin GM, Tanimoto H. 2015. Reward signal in a recurrent circuit
604 drives appetitive long-term memory formation. *Elife* **4**:e10719.
605 Jenett A, Rubin GM, Ngo T-TB, Shepherd D, Murphy C, Dionne H, Pfeiffer BD, Cavallaro A, Hall D, Jeter J,
606 Iyer N, Fetter D, Hausenfluck JH, Peng H, Trautman ET, Svirskas RR, Myers EW, Iwinski ZR, Aso Y,
607 DePasquale GM, Enos A, Hulamm P, Lam SCB, Li H-H, Laverty TR, Long F, Qu L, Murphy SD, Rokicki
608 K, Safford T, Shaw K, Simpson JH, Sowell A, Tae S, Yu Y, Zugates CT. 2012. A GAL4-driver line
609 resource for Drosophila neurobiology. *Cell Rep* **2**:991–1001.
610 Jiang L, Litwin-Kumar A. 2021. Models of heterogeneous dopamine signaling in an insect learning and
611 memory center. *PLoS Comput Biol* **17**:e1009205.
612 Kanzaki R, Ikeda A, Shibuya T. 1994. [引用] Morphology and physiology of pheromone-triggered flip-flop
613 descending interneurons of the male silkworm moth, Bombyx mori. *J Comp Physiol A*.
614 Kim H, Kirkhart C, Scott K. 2017. Long-range projection neurons in the taste circuit of Drosophila. *Elife* **6**.
615 doi:10.7554/eLife.23386
616 Kirkhart C, Scott K. 2015. Gustatory learning and processing in the Drosophila mushroom bodies. *J*
617 *Neurosci* **35**:5950–5958.
618 König C, Khalili A, Niewalda T, Gao S, Gerber B. 2019. An optogenetic analogue of second-order
619 reinforcement in Drosophila. *Biol Lett* **15**:20190084.
620 Li F, Lindsey JW, Marin EC, Otto N, Dreher M, Dempsey G, Stark I, Bates AS, Pleijzier MW, Schlegel P,
621 Nern A, Takemura S-Y, Eckstein N, Yang T, Francis A, Braun A, Parekh R, Costa M, Scheffer LK, Aso Y,
622 Jefferis GS, Abbott LF, Litwin-Kumar A, Waddell S, Rubin GM. 2020. The connectome of the adult
623 Drosophila mushroom body provides insights into function. *Elife* **9**. doi:10.7554/eLife.62576
624 Lin H-H, Chu L-A, Fu T-F, Dickson BJ, Chiang A-S. 2013. Parallel neural pathways mediate CO2 avoidance
625 responses in Drosophila. *Science* **340**:1338–1341.
626 Lin H-H, Lai JS-Y, Chin A-L, Chen Y-C, Chiang A-S. 2007. A Map of Olfactory Representation in the
627 Drosophila Mushroom Body. *Cell* **128**:1205–1217.
628 Liu C, Plaçais P-Y, Yamagata N, Pfeiffer BD, Aso Y, Friedrich AB, Siwanowicz I, Rubin GM, Preat T,
629 Tanimoto H. 2012. A subset of dopamine neurons signals reward for odour memory in Drosophila.

Nature. doi:10.1038/nature11304
Liu WW, Mazor O, Wilson RI. 2015. Thermosensory processing in the Drosophila brain. *Nature* **519**:353–357.
Luan H, Diao F, Scott RL, White BH. 2020. The Drosophila Split Gal4 System for Neural Circuit Mapping. *Frontiers in Neural Circuits*. doi:10.3389/fncir.2020.603397
Luan H, Peabody NC, Vinson CR, White BH. 2006. Refined spatial manipulation of neuronal function by combinatorial restriction of transgene expression. *Neuron* **52**:425–436.
Mao Z, Davis RL. 2009. Eight different types of dopaminergic neurons innervate the Drosophila mushroom body neuropil: anatomical and physiological heterogeneity. *Front Neural Circuits* **3**:612.
Marin EC, Büld L, Theiss M, Sarkissian T, Roberts RJV, Turnbull R, Tamimi IFM, Pleijzier MW, Laursen WJ, Drummond N, Schlegel P, Bates AS, Li F, Landgraf M, Costa M, Bock DD, Garrity PA, Jefferis GSXE. 2020. Connectomics Analysis Reveals First-, Second-, and Third-Order Thermosensory and Hygrosensory Neurons in the Adult Drosophila Brain. *Curr Biol* **30**:3167–3182.e4.
Martinez-Cervantes J, Shah P, Phan A, Cervantes-Sandoval I. 2022. Higher-order unimodal olfactory sensory preconditioning in. *Elife* **11**. doi:10.7554/eLife.79107
Masek P, Worden K, Aso Y, Rubin GM, Keene AC. 2015. A dopamine-modulated neural circuit regulating aversive taste memory in Drosophila. *Curr Biol* **25**:1535–1541.
Masse NY, Cachero S, Ostrovsky AD, Jefferis GSXE. 2012. A mutual information approach to automate identification of neuronal clusters in Drosophila brain images. *Front Neuroinform* **6**:21.
Matheson AMM, Lanz AJ, Medina AM, Licata AM, Currier TA, Syed MH, Nagel KI. 2022. A neural circuit for wind-guided olfactory navigation. *Nat Commun* **13**:1–21.
McCurdy LY, Sareen P, Davoudian PA, Nitabach MN. 2021. Dopaminergic mechanism underlying reward-encoding of punishment omission during reversal learning in Drosophila. *Nat Commun* **12**:1115.
McKellar CE, Siwanowicz I, Dickson BJ, Simpson JH. 2020. Controlling motor neurons of every muscle for fly proboscis reaching. *Elife* **9**:e54978.
Meissner GW, Nern A, Dorman Z, DePasquale GM, Forster K, Gibney T, Hausenfluck JH, He Y, Iyer NA, Jeter J, Johnson L, Johnston RM, Lee K, Melton B, Yarbrough B, Zugates CT, Clements J, Goina C, Otsuna H, Rokicki K, Svirskas RR, Aso Y, Card GM, Dickson BJ, Ehrhardt E, Goldammer J, Ito M, Kainmueller D, Korff W, Mais L, Minegishi R, Namiki S, Rubin GM, Sterne GR, Wolff T, Malkesman O. 2023. A searchable image resource of Drosophila GAL4 driver expression patterns with single neuron resolution. doi:10.7554/eLife.80660
Miyamoto T, Slone J, Song X, Amrein H. 2012. A fructose receptor functions as a nutrient sensor in the Drosophila brain. *Cell* **151**:1113–1125.
Miyazaki T, Lin T-Y, Ito K, Lee C-H, Stopfer M. 2015. A gustatory second-order neuron that connects sucrose-sensitive primary neurons and a distinct region of the gnathal ganglion in the Drosophila brain. *J Neurogenet* **29**:144–155.
Modi MN, Shuai Y, Turner GC. 2020. The Drosophila Mushroom Body: From Architecture to Algorithm in a Learning Circuit. *Annu Rev Neurosci* **43**:465–484.
Namiki S, Dickinson MH, Wong AM, Korff W, Card GM. 2018. The functional organization of descending sensory-motor pathways in Drosophila. doi:10.7554/eLife.34272
Nern A, Pfeiffer BD, Rubin GM. 2015. Optimized tools for multicolor stochastic labeling reveal diverse stereotyped cell arrangements in the fly visual system. *Proc Natl Acad Sci U S A* **112**:E2967–76.
Ohyama T, Schneider-Mizell CM, Fetter RD, Aleman JV, Franconville R, Rivera-Alba M, Mensh BD, Branson KM, Simpson JH, Truman JW, Cardona A, Zlatic M. 2015. A multilevel multimodal circuit enhances action selection in Drosophila. *Nature* **520**:633–639.
Otsuna H, Ito M, Kawase T. n.d. Color depth MIP mask search: a new tool to expedite Split-GAL4 creation. doi:10.1101/318006
Otto N, Pleijzier MW, Morgan IC, Edmondson-Stait AJ, Heinz KJ, Stark I, Dempsey G, Ito M, Kapoor I, Hsu

678 J, Schlegel PM, Bates AS, Feng L, Costa M, Ito K, Bock DD, Rubin GM, Jefferis GSXE, Waddell S. 2020.
679 Input Connectivity Reveals Additional Heterogeneity of Dopaminergic Reinforcement in Drosophila.
680 *Curr Biol* **30**:3200–3211.e8.
681 Owald D, Felsenberg J, Talbot CB, Das G, Perisse E, Huetteroth W, Waddell S. 2015. Activity of defined
682 mushroom body output neurons underlies learned olfactory behavior in Drosophila. *Neuron*
683 **86**:417–427.
684 Park J-H, Kwon JY. 2011. A systematic analysis of Drosophila gustatory receptor gene expression in
685 abdominal neurons which project to the central nervous system. *Mol Cells* **32**:375–381.
686 Pavlowsky A, Schor J, Plaçais P-Y, Preat T. 2018. A GABAergic Feedback Shapes Dopaminergic Input on
687 the Drosophila Mushroom Body to Promote Appetitive Long-Term Memory. *Curr Biol* **28**:1783–
688 1793.e4.
689 Perez-Orive J, Mazor O, Turner GC, Cassenaer S, Wilson RI, Laurent G. 2002. Oscillations and sparsening
690 of odor representations in the mushroom body. *Science* **297**:359–365.
691 Pettersson J. 1970. An Aphid Sex Attractant. *Insect Syst Evol* **1**:63–73.
692 Pfeiffer BD, Ngo T-TB, Hibbard KL, Murphy C, Jenett A, Truman JW, Rubin GM. 2010. Refinement of tools
693 for targeted gene expression in Drosophila. *Genetics* **186**:735–755.
694 Pfeiffer BD, Truman JW, Rubin GM. 2012. Using translational enhancers to increase transgene
695 expression in Drosophila. *Proc Natl Acad Sci U S A* **109**:6626–6631.
696 Plaçais P-Y, de Tredern É, Scheunemann L, Trannoy S, Goguel V, Han K-A, Isabel G, Preat T. 2017.
697 Upregulated energy metabolism in the Drosophila mushroom body is the trigger for long-term
698 memory. *Nat Commun* **8**:15510.
699 Rajagopalan AE, Darshan R, Fitzgerald JE, Turner GC. 2022. Expectation-based learning rules underlie
700 dynamic foraging in Drosophila. *bioRxiv*. doi:10.1101/2022.05.24.493252
701 Rodrigues V, Siddiqi O. 1978. Genetic analysis of chemosensory pathway. *Proceedings / Indian Academy*
702 *of Sciences* **87**:147–160.
703 Rubin GM, Aso Y. 2023. New genetic tools for mushroom body output neurons in Drosophila. *bioRxiv*.
704 doi:10.1101/2023.06.23.546330
705 Saumweber T, Rohwedder A, Schleyer M, Eichler K, Chen Y-C, Aso Y, Cardona A, Eschbach C, Kobler O,
706 Voigt A, Durairaja A, Mancini N, Zlatic M, Truman JW, Thum AS, Gerber B. 2018. Functional
707 architecture of reward learning in mushroom body extrinsic neurons of larval Drosophila. *Nat*
708 *Commun* **9**:1104.
709 Sayin S, De Backer J-F, Siju KP, Wosniack ME, Lewis LP, Frisch L-M, Gansen B, Schlegel P, Edmondson-
710 Stait A, Sharifi N, Fisher CB, Calle-Schuler SA, Lauritzen JS, Bock DD, Costa M, Jefferis GSXE,
711 Gjorgjieva J, Grunwald Kadow IC. 2019. A Neural Circuit Arbitrates between Persistence and
712 Withdrawal in Hungry Drosophila. *Neuron* **104**:544–558.e6.
713 Scheffer LK, Xu CS, Januszewski M, Lu Z, Takemura S-Y, Hayworth KJ, Huang GB, Shinomiya K, Maitlin-
714 Shepard J, Berg S, Clements J, Hubbard PM, Katz WT, Umayam L, Zhao T, Ackerman D, Blakely T,
715 Bogovic J, Dolafi T, Kainmueller D, Kawase T, Khairy KA, Leavitt L, Li PH, Lindsey L, Neubarth N,
716 Olbris DJ, Otsuna H, Trautman ET, Ito M, Bates AS, Goldammer J, Wolff T, Svirskas R, Schlegel P,
717 Neace E, Knecht CJ, Alvarado CX, Bailey DA, Ballinger S, Borycz JA, Canino BS, Cheatham N, Cook M,
718 Dreher M, Duclos O, Eubanks B, Fairbanks K, Finley S, Forknall N, Francis A, Hopkins GP, Joyce EM,
719 Kim S, Kirk NA, Kovalyak J, Lauchie SA, Lohff A, Maldonado C, Manley EA, McLin S, Mooney C,
720 Ndama M, Ogundeyi O, Okeoma N, Ordish C, Padilla N, Patrick CM, Paterson T, Phillips EE, Phillips
721 EM, Rampally N, Ribeiro C, Robertson MK, Rymer JT, Ryan SM, Sammons M, Scott AK, Scott AL,
722 Shinomiya A, Smith C, Smith K, Smith NL, Sobeski MA, Suleiman A, Swift J, Takemura S, Talebi I,
723 Tarnogorska D, Tenshaw E, Tokhi T, Walsh JJ, Yang T, Horne JA, Li F, Parekh R, Rivlin PK, Jayaraman
724 V, Costa M, Jefferis GS, Ito K, Saalfeld S, George R, Meinertzhagen IA, Rubin GM, Hess HF, Jain V,
725 Plaza SM. 2020. A connectome and analysis of the adult central brain. *Elife* **9**.

726 doi:10.7554/eLife.57443
727 Schretter CE, Aso Y, Robie AA, Dreher M, Dolan M-J, Chen N, Ito M, Yang T, Parekh R, Branson KM, Rubin
728 GM. 2020. Cell types and neuronal circuitry underlying female aggression in Drosophila. *eLife*.
729 doi:10.7554/elife.58942
730 Schroll C, Riemensperger T, Bucher D, Ehmer J, Völler T, Erbguth K, Gerber B, Hendel T, Nagel G, Buchner
731 E, Fiala A. 2006. Light-induced activation of distinct modulatory neurons triggers appetitive or
732 aversive learning in Drosophila larvae. *Curr Biol* **16**:1741–1747.
733 Schwaerzel M, Monastirioti M, Scholz H, Friggi-Grelin F, Birman S, Heisenberg M. 2003. Dopamine and
734 octopamine differentiate between aversive and appetitive olfactory memories in Drosophila. *J*
735 *Neurosci* **23**:10495–10502.
736 Shimono K, Fujimoto A, Tsuyama T, Yamamoto-Kochi M, Sato M, Hattori Y, Sugimura K, Usui T, Kimura K-
737 I, Uemura T. 2009. Multidendritic sensory neurons in the adult Drosophila abdomen: origins,
738 dendritic morphology, and segment- and age-dependent programmed cell death. *Neural Dev* **4**:37.
739 Shuai Y, Hirokawa A, Ai Y, Zhang M, Li W, Zhong Y. 2015. Dissecting neural pathways for forgetting in
740 Drosophila olfactory aversive memory. *Proc Natl Acad Sci U S A* **112**:E6663–72.
741 Shyu W-H, Chiu T-H, Chiang M-H, Cheng Y-C, Tsai Y-L, Fu T-F, Wu T, Wu C-L. 2017. Neural circuits for
742 long-term water-reward memory processing in thirsty Drosophila. *Nat Commun* **8**:15230.
743 Smith MA-Y, Honegger KS, Turner G, de Bivort B. 2022. Idiosyncratic learning performance in flies. *Biol*
744 *Lett* **18**:20210424.
745 Sterne GR, Otsuna H, Dickson BJ, Scott K. 2021. Classification and genetic targeting of cell types in the
746 primary taste and premotor center of the adult brain. *Elife* **10**. doi:10.7554/eLife.71679
747 Stocker RF, Lienhard MC, Borst A, Fischbach KF. 1990. Neuronal architecture of the antennal lobe in
748 Drosophila melanogaster. *Cell Tissue Res* **262**:9–34.
749 Strother JA, Wu S-T, Wong AM, Nern A, Rogers EM, Le JQ, Rubin GM, Reiser MB. 2017. The Emergence
750 of Directional Selectivity in the Visual Motion Pathway of Drosophila. *Neuron* **94**:168–182.e10.
751 Suh GSB, Wong AM, Hergarden AC, Wang JW, Simon AF, Benzer S, Axel R, Anderson DJ. 2004. A single
752 population of olfactory sensory neurons mediates an innate avoidance behaviour in Drosophila.
753 *Nature* **431**:854–859.
754 Takagi S, Cocanougher BT, Niki S, Miyamoto D, Kohsaka H, Kazama H, Fetter RD, Truman JW, Zlatic M,
755 Cardona A, Nose A. 2017. Divergent Connectivity of Homologous Command-like Neurons Mediates
756 Segment-Specific Touch Responses in Drosophila. *Neuron* **96**:1373–1387.e6.
757 Tanaka NK, Awasaki T, Shimada T, Ito K. 2004. Integration of chemosensory pathways in the Drosophila
758 second-order olfactory centers. *Curr Biol* **14**:449–457.
759 Tanaka NK, Endo K, Ito K. 2012. Organization of antennal lobe-associated neurons in adult Drosophila
760 melanogaster brain. *J Comp Neurol* **520**:4067–4130.
761 Tanaka NK, Tanimoto H, Ito K. 2008. Neuronal assemblies of the Drosophila mushroom body. *J Comp*
762 *Neurol* **508**:711–755.
763 Thoma V, Knapek S, Arai S, Hartl M, Kohsaka H, Sirigrivatanawong P, Abe A, Hashimoto K, Tanimoto H.
764 2016. Functional dissociation in sweet taste receptor neurons between and within taste organs of
765 Drosophila. *Nat Commun* **7**:10678.
766 Ting C-Y, Gu S, Guttikonda S, Lin T-Y, White BH, Lee C-H. 2011. Focusing transgene expression in
767 Drosophila by coupling Gal4 with a novel split-LexA expression system. *Genetics* **188**:229–233.
768 Tirian L, Dickson BJ. 2017. The VT GAL4, LexA, and split-GAL4 driver line collections for targeted
769 expression in the Drosophila nervous system. *bioRxiv*. doi:10.1101/198648
770 Truman JW, Price J, Miyares RL, Lee T. 2023. Metamorphosis of memory circuits in Drosophila reveals a
771 strategy for evolving a larval brain. doi:10.7554/eLife.80594
772 Tsao C-H, Chen C-C, Lin C-H, Yang H-Y, Lin S. 2018. mushroom bodies integrate hunger and satiety signals
773 to control innate food-seeking behavior. *Elife* **7**. doi:10.7554/eLife.35264

774 Turner GC, Bazhenov M, Laurent G. 2008. Olfactory Representations by Drosophila Mushroom Body
775 Neurons. *J Neurophysiol*. doi:10.1152/jn.01283.2007
776 Tuthill JC, Nern A, Holtz SL, Rubin GM, Reiser MB. 2013. Contributions of the 12 neuron classes in the fly
777 lamina to motion vision. *Neuron* **79**:128–140.
778 Vogt K, Aso Y, Hige T, Knapek S, Ichinose T, Friedrich AB, Turner GC, Rubin GM, Tanimoto H. 2016. Direct
779 neural pathways convey distinct visual information to Drosophila mushroom bodies. *Elife* **5**.
780 doi:10.7554/eLife.14009
781 Wang K, Wang F, Forknall N, Yang T, Patrick C, Parekh R, Dickson BJ. 2021. Neural circuit mechanisms of
782 sexual receptivity in Drosophila females. *Nature* **589**:577–581.
783 Wang Z, Singhvi A, Kong P, Scott K. 2004. Taste representations in the Drosophila brain. *Cell* **117**:981–
784 991.
785 Wan Y, Otsuna H, Chien C-B, Hansen C. 2012. FluoRender: An Application of 2D Image Space Methods
786 for 3D and 4D Confocal Microscopy Data Visualization in Neurobiology Research. *IEEE Pac Vis Symp*
787 201–208.
788 Winding M, Pedigo BD, Barnes CL, Patsolic HG, Park Y, Kazimiers T, Fushiki A, Andrade IV, Khandelwal A,
789 Valdes-Aleman J, Li F, Randel N, Barsotti E, Correia A, Fetter RD, Hartenstein V, Priebe CE,
790 Vogelstein JT, Cardona A, Zlatic M. 2023. The connectome of an insect brain. *Science*
791 **379**:eadd9330.
792 Wolff T, Rubin GM. 2018. Neuroarchitecture of the Drosophila central complex: A catalog of nodulus and
793 asymmetrical body neurons and a revision of the protocerebral bridge catalog. *J Comp Neurol*
794 **526**:2585–2611.
795 Wu J-K, Tai C-Y, Feng K-L, Chen S-L, Chen C-C, Chiang A-S. 2017. Long-term memory requires sequential
796 protein synthesis in three subsets of mushroom body output neurons in Drosophila. *Sci Rep* **7**:7112.
797 Wu M, Nern A, Williamson WR, Morimoto MM, Reiser MB, Card GM, Rubin GM. 2016. Visual projection
798 neurons in the lobula link feature detection to distinct behavioral programs. *Elife* **5**.
799 doi:10.7554/eLife.21022
800 Xie Q, Brbic M, Horns F, Kolluru SS, Jones RC, Li J, Reddy AR, Xie A, Kohani S, Li Z, McLaughlin CN, Li T, Xu
801 C, Vacek D, Luginbuhl DJ, Leskovec J, Quake SR, Luo L, Li H. 2021. Temporal evolution of single-cell
802 transcriptomes of olfactory projection neurons. *Elife* **10**. doi:10.7554/eLife.63450
803 Yamada D, Bushey D, Li F, Hibbard KL, Sammons M, Funke J, Litwin-Kumar A, Hige T, Aso Y. 2023.
804 Hierarchical architecture of dopaminergic circuits enables second-order conditioning in Drosophila.
805 *Elife* **12**. doi:10.7554/eLife.79042
806 Yamagata N, Ichinose T, Aso Y, Plaçais P-Y, Friedrich AB, Sima RJ, Preat T, Rubin GM, Tanimoto H. 2015.
807 Distinct dopamine neurons mediate reward signals for short- and long-term memories. *Proc Natl*
808 *Acad Sci U S A* **112**:578–583.
809 Yavuz A, Jagge C, Slone J, Amrein H. 2014. A genetic tool kit for cellular and behavioral analyses of insect
810 sugar receptors. *Fly* **8**:189–196.
811 Zhang X, Noyes NC, Zeng J, Li Y, Davis RL. 2019. Aversive Training Induces Both Presynaptic and
812 Postsynaptic Suppression in. *J Neurosci* **39**:9164–9172.
813 Zheng Z, Lauritzen JS, Perlman E, Robinson CG, Nichols M, Milkie D, Torrens O, Price J, Fisher CB, Sharifi
814 N, Calle-Schuler SA, Kmecova L, Ali IJ, Karsh B, Trautman ET, Bogovic JA, Hanslovsky P, Jefferis GSXE,
815 Kazhdan M, Khairy K, Saalfeld S, Fetter RD, Bock DD. 2018. A Complete Electron Microscopy Volume
816 of the Brain of Adult Drosophila melanogaster. *Cell* **174**:730–743.e22.
817 Zheng Z, Li F, Fisher C, Ali IJ, Sharifi N, Calle-Schuler S, Hsu J, Masoodpanah N, Kmecova L, Kazimiers T,
818 Perlman E, Nichols M, Li PH, Jain V, Bock DD. 2022. Structured sampling of olfactory input by the fly
819 mushroom body. *Curr Biol* **32**:3334–3349.e6.

820

821 **Figures and figure legends**
822
823 **Figure 1 Generation and annotation of split-GAL4 lines**
824 (A) In associative learning, flies adjust their behavioral responses to conditioned stimuli (CS), such as odors
825 and colors, based on the contingency with innately rewarding or punishing unconditioned stimuli (US),
826 such as sugar, bitter, shock and heat. A schematic of *Drosophila* melanogaster is from (Namiki et al., 2018).
827 (B) An image of the right half of an adult fly brain showing the mushroom bodies (MB). Projections
828 neurons (PN) convey information from the antennal lobes (AL) to the calyx of the MB and the lateral horn
829 (LH).
830 (C) A simplified diagram of the mushroom body circuit. The identity of sensory stimuli is represented by
831 sparse activity patterns of Kenyon cells (KCs). A subset of dopaminergic neurons (DANs) respond to
832 punishment/reward. Dopamine modulates weights of synapses between KCs and MB output neurons
833 (MBONs) depending on the activity status of KCs. The skewed activity patterns of MBONs across
834 compartments in response to the learned stimulus drive memory-based actions and feedback pathways
835 to DANs.
836 (D) A summary of the workflow to generate split-GAL4 lines.
837 (E) Coverage of the collection. The crepine (CRE), the superior medial protocerebrum (SMP), the superior
838 intermediate protocerebrum (SIP) and the superior lateral protocerebrum (SLP) are MB adjacent brain
839 areas where MBONs and DANs most often have arborizations. CX, central complex. LAL, lateral accessory
840 lobes.
841 (F) Examples of cell types covered by the collection. Expression patterns of CsChrimson-mVenus (green)
842 are shown with neuropil counterstaining of Bruchpilot (Brp) with nc82 antibody (magenta).
843
844 **Figure 1-figure supplement 1 Examples of cell types covered by the split-GAL4 lines in this collection**
845 Additional examples of cell types covered by the collection. Expression patterns of CsChrimson-mVenus
846 (green) are shown with neuropil counterstaining of Brp (magenta). Only one brain hemisphere is shown.
847
848 **Figure 2 LM-EM match of CRE011 driver**
849 (A) Expression pattern of SS45245-split-GAL4 in a brain.
850 (B) MCFO image of SS45245 showing individual labeled neurons.
851 (C) Frontal and ventral views of segmented light microscopy (LM) images of an exemplary split-Gal4 line
852 (SS45245) visualized with a membrane reporter (myr-smGFP-FLAG) that was aligned to the JRC2018
853 standard brain. Frontal (top) and dorsal (bottom) projections are shown with outline of relevant
854 neuropils.
855 (D) The skeleton reconstructed from electron microscopy (EM) data of the matched cell type CRE011 in
856 the hemibrain connectome. The CRE011 cell on the right hemisphere is shown.
857 (E) Synaptic connectivity of CRE011 with MBONs and DANs in the MB derived from the hemibrain
858 connectome.
859
860
861
862

Figure 2-figure supplement 1 LM-EM match of SS00460

(A) Frontal and ventral views of segmented light microscopy (LM) images of SS00460 in the JRC2018 standard brain. Projections are shown with the outline of relevant neuropils. A' (ventral) is a rotated view of A (frontal) with the reference axis indicated.

(B) The skeleton reconstructed from electron microscopy (EM) data in the hemibrain volume of the matched cell type I2LN44.

(C) EM images of neurons with the most input connections (upstream) to I2LN44 in the hemibrain connectome. The number after "#" indicates the number of connections between the matched cell type (i.e. v2LN44) and its synaptic partners. The color code and EM BodyId for each EM-reconstructed neuron are also listed.

(D) EM images of neurons with the most output connections (downstream) from I2LN44 in the hemibrain connectome. In Figure 2-figure supplement 1-20, sensory neurons and KCs are not displayed as top upstream or downstream neurons.

Figure 2-figure supplement 2 LM-EM match of SS34963

Figure 2-figure supplement 3 LM-EM match of SS33915

Figure 2-figure supplement 4 LM-EM match of SS35020

Figure 2-figure supplement 5 LM-EM match of SS34979

Figure 2-figure supplement 6 LM-EM match of SS34947

Figure 2-figure supplement 7 LM-EM match of SS00486

Figure 2-figure supplement 8 LM-EM match of SS49308

Figure 2-figure supplement 9 LM-EM match of SS49361

Figure 2-figure supplement 10 LM-EM match of SS49868

Figure 2-figure supplement 11 LM-EM match of SS49352

Figure 2-figure supplement 12 LM-EM match of SS32228

Figure 2-figure supplement 13 LM-EM match of SS32219

Figure 2-figure supplement 14 LM-EM match of SS48890

Figure 2-figure supplement 15 LM-EM match of SS48799

Figure 2-figure supplement 16 LM-EM match of SS32259

Figure 2-figure supplement 17 LM-EM match of SS48341

Figure 2-figure supplement 18 LM-EM match of SS35040

Figure 2-figure supplement 19 LM-EM match of SS33905

Figure 2-figure supplement 20 LM-EM match of SS39538

Figure 3 Drivers for MBON downstream and DAN upstream neurons.

(A) Examples of confocal microscopy images of split-GAL4 lines (bottom) and their matching cell types in the hemibrain connectome (top). CsChrimson-mVenus (green); Brp (magenta).

(B) The number of cell types that receive synaptic output from MBONs and supply synaptic input to DANs. Only cell types with connection (conn) over the indicated thresholds (i.e., more than 4 synapses for DAN upstream and more than 9 synapses for MBON downstream) were considered. The number of covered cell types are indicated in the brackets.

905 (C) A scatter plot of MB interneuron cell types connected with DANs and MBONs. Cell types covered by
906 Split-GAL4 lines are highlighted in red.
907
908 **Figure 3-figure supplement 1 New or improved drivers for MB cell types**
909 (A) Confocal images and matched EM cell types. CsChrimson-mVenus (green); Brp (magenta).
910 (B) Summary of within-MB split-GAL4 coverage. See Supplementary File 4 for details.
911
912 **Figure 4 Driver lines for uni-glomerular projection neurons**
913 (A) Examples of covered uni-glomerular PN (uPN) cell types.
914 (B) Coverage of the 51 antennal lobe glomeruli. The new collection of split-GAL4 covers uPN in the colored
915 glomeruli.
916 (C) Split-GAL4 coverage summary.
917
918 **Figure 5 Driver lines for multi-glomerular projection neurons**
919 Examples of multi-glomerular projection neurons (mPN) types. M_l2PN3t18 [VC5++ l2PN1], M_lPNm11A
920 [VP4++ lPN], and M_smPNm1 [VP3+ smPN] are predicted to receive majority non-olfactory input (Marin
921 et al., 2020).
922
923 **Figure 6 Driver lines for non-olfactory projection neurons and sensory neurons**
924 Examples of non-olfactory PN types and sensory neurons covered by this collection
925
926 **Figure 7 Drivers for gustatory sensory neurons**
927 (A) A summary of new transgenic lines generated by this study.
928 (B) Schematic of the screening strategy used here to subdivide the Gr64f-DBD pattern by intersecting it
929 with GMR and VT AD lines.
930 (C) A schematic of the sensory neuron projection types that compose the Gr64f-DBD pattern.
931 (D) A summary of expression patterns of 6 of the Gr64f split-GAL4 lines derived from the screening
932 strategy in (B), using the anatomical notation described in (C).
933 (E) Expression pattern of SS87269 in the brain and VNC.
934 (F) Expression of SS87269 in the labellum.
935 (G) Expression of SS87269 in tarsi of fore (f), middle (m) and hind (h) legs.
936 (H) Expression of SS87272 in the labral sense organ (LSO).
937 (I) Expression of SS88801 in tarsi.
938 (J) Expression of SS87278 in the abdominal body wall.
939 (K-P) Expression patterns of designated driver lines in the Gnathal Ganglia (GNG) and VNC.
940
941 **Figure 7-figure supplement 1 The original Gr64f-GAL4.**
942 (A) Expression pattern of Gr64f-GAL4 driving 20xUAS-CsChrimson-mVenus in the brain and VNC (green)
943 with neuropil counterstaining of Brp (magenta). The line used contains two copies of Gr64f-Gal4, with
944 one copy on the second and one copy on the third chromosome.
945 (B) Training protocol schematics for experiments completed in the optogenetic olfactory arena (Aso and
946 Rubin, 2016).

947 (C) Preference index (PI) memory scores 2 min after various training protocols are shown. Data are shown
948 as mean ± SEM. n = 4 for each group. Each PI was calculated from two movies of reciprocal experiments,
949 in which the CS odor paired with optogenetic reward was exchanged. Approximately twenty flies were
950 tested in each movie.
951
952
953 **Figure 8 Associative learning with Gr64f-split-GAL4 lines**
954 (A) In the optogenetic olfactory arena, odors are delivered from the periphery and sucked out from the
955 central vacuum port to deliver odors only to defined quadrants. Red LEDs (627nm peak) enable
956 programmed optogenetic activation of neurons expressing CsChrimson.
957 (B) Training and testing protocol for experiments shown in (E). The training protocol consisted of 3 x 20s
958 optogenetic activation training followed by the first preference test, 1x 1 min training followed by the
959 2nd test, and additional 2x 1 min training followed by the last test. Odors delivered to the two zones and
960 odor durations in each period are indicated. LED intensities were 4.3 µW/mm2 in early 20s training and
961 34.9 µW/mm2 in later training. Activation LED was applied with 1s ON and 1s OFF during pairing with
962 odor A. Odors were trained reciprocally. Pentyl acetate and Ethyl lactate were used as odor A and B,
963 respectively, in half of the experiments. The two odors were swapped in the other half of experiments.
964 (C) Protocol to characterize Gr64f split-GAL4 activation phenotypes in the absence of an odor. During
965 each trial, flies were illuminated with a red LED light continuously for 10 seconds.
966 (D) Summary diagram of the expression patterns of the original Gr64f-GAL4 (far left) and 6 Gr64f-split-
967 GAL4s. The expression of the original Gr64f-GAL4 in olfactory sensory neurons is not depicted here.
968 (E) Associative memory scores after the training protocol in (B). Mean, standard error of the mean (SEM),
969 and the number of groups are shown.
970 (F) The kinematic parameters of trajectories measured with Caltech FlyTracker during split-GAL4
971 activation in the absence of odor as shown in (C). Each group of flies received 6 activation trials.
972 Summarization was based on the trial average of each group. The number of groups is indicated. The thick
973 lines and shadows are mean and SEM. Gray lines are Empty-split-GAL4 control.
974 (G) Average walking speed in each of 6 trials.
975 (H) An image of a fly on a floating ball. Flies were tracked for proboscis extension (PE) activity with the
976 Animal Part Tracker. The annotated points, in the order of numbers, consisted of the tip of the abdomen
977 (1), the highest point on the thorax (2), the midpoint between the root of the antennae (3), the base of
978 the proboscis (4) and the tip of the proboscis (5). PE activity was quantified as the change of proboscis
979 length, i.e., the distance from the tip to the base of the proboscis, or the distance between points 4 and
980 5.
981 (I) SS87269 and SS88801 activation and proboscis extension. Each fly was recorded over 6 activation trials
982 in which the 624 nm LED was turned on for 1 second. LED intensity for SS87269 and SS88801, 1.1
983 mW/cm^2; for empty Gal4 (pBDPGal4), 5.0 mW/cm^2. Less saturated traces indicate behavior during LED
984 off trials, while more saturated traces indicate behavior during LED on trials.
985
986 **Figure 8-figure supplement 1 Activation phenotype of Gr64f-split-GAL4 lines**
987 The data points during the time bin shown in Figure 8F.
988 (A) Probability of return during the post-activation period.

989 (B) Change of walking speed during the onset of activation period.
990 (C) Change of curvature during the onset of activation period.
991 (D) Change of curvature during the post-activation period.
992 One-way ANOVA followed by Dunnett's multiple comparisons test. ***, P<0.001. Individual data points
993 are shown with minimum, maximum, median, and interquartile ranges.
994
995 **Figure 8-figure supplement 2 Examples of covered SEZ neurons.**
996 (Top two rows) New or improved split-GAL4 drivers for cell types already covered by the SEZ Split-GAL4
997 Collection (Sterne et al., 2021). (Bottom row) Split-GAL4 drivers for cell types not included in the SEZ Split-
998 GAL4 Collection. Cell types are from Hemibrain 1.2.1, Sterne 2021 or mn2V (McKellar et al., 2020).
999
1000 **Figure 9 Examples of covered ascending neurons**
1001 (A) Activation preference screen of 581 split-GAL4 lines (342 lines from this study). SS01159 (blue arrow)
1002 is one of the lines that flies showed strong avoidance at optogenetic activation.
1003 (B) Time course of flies' preference to quadrants with red LED light by SS01159>CsChrimson (blue) or
1004 empty-GAL4>CsChrimson (gray). A preference score to red LED quadrants was quantified from the
1005 distribution during the last 5s of two 30s activation periods. n = 8 groups for SS01159, n = 15 for empty
1006 Gal4. Mean (thick lines) and SEM (shadow) are plotted.
1007 (C) The mean normalized movement speed at the LED onset for flies in the LED quadrants. The 3-s period
1008 before LED onset was used as the baseline for normalization.
1009 (D) The mean cumulative turning angles in 5 movie frames (total elapsed time of 167 ms) when flies
1010 encountered the LED boundary. The boundary was defined as a 4-mm zone in between the LED and dark
1011 quadrants. Trajectories too close to the center (< 0.2*radius) or the wall (> 0.6*radius) of the arena were
1012 not analyzed.
1013 (E) Examples of split-GAL4 lines for ascending neurons. SS35227 and SS35256 shared a split half (R41C05-
1014 AD) with SS01159. SS32217 matched with TPN1 (Kim et al., 2017). No cell types were assigned to the
1015 other lines shown due to missing information in the hemibrain volume.
1016
1017 **Figure 10 Stereotypy and erroneous projections**
1018 (A) V_l2PN from both hemispheres send axonal projections to the right hemisphere in an atypical case
1019 (arrowhead).
1020 (B) In this atypical case, there are two MB-DPM neurons in one hemisphere (arrowhead) and the
1021 arborizations extend beyond the pedunculus into the calyx.
1022 (C) MBON-α1 occasionally has additional arborizations in the ellipsoid body (arrowhead)
1023 (D) The localization of MBON-α3 soma widely varied along the dorso-ventral axis. It occasionally had an
1024 additional axonal branch (arrowhead).
1025 (E) A table to summarize erroneous projections of MBONs and MB-DPM. In all the cases except for the
1026 DPM, "different number of cells" was likely due to stochastic expression of the drivers (i.e., lack of
1027 labeling) rather than biological difference. In some MB310C samples, we observed third soma attached
1028 to MBON-α3 but they lacked any neurites. See Figure 11 for variability of MBON08/09 in MB083C.
1029

1030 **Figure 11 Individuality and asymmetry of MBON08 and MBON09**
1031 (A) A typical image of two MBONs in MB083C-split-GAL4 driver.
1032 (B) Abnormal axonal projection of MBON08/09 observed in one of 169 samples.
1033 (C-D) MCFO images of MB083C driver from different flies show that the two cells can either be both
1034 MBON09-γ3β'1 (C) or one MBON09-γ3β'1 and one MBON08-γ3 (D).
1035 (E-G) An example of MCFO image of MB083C, which visualized one MBON08 and two MBON09 in the
1036 same brain. The projection (E) and image sections at the γ3 (F) or β'1 (G) are shown.
1037 (H) Diagrams of the three MBONs shown in E-G.
1038 (I) A summary table for observation of MBON08 and MBON09 in male and female brains.
1039 (J) All possible variations of 4 MBONs in MB083C driver, and estimated probability for each case.
1040
1041 **Figure 11-figure supplement 1 MB083C invariantly label two MBONs**
1042 Maximum intensity projection images of individual samples are shown. Note that two somas in each
1043 hemisphere are labeled in all samples. Reporters used are indicated in each panel.
1044
1045 **Figure 11-figure supplement 2 Subdivisions of medial and lateral γ3 compartments**
1046 (A) Overlay between the dendrites of MBON08/09 and axons of PAM-γ4 DANs.
1047 (B) Overlay between the dendrites of MBON08/09 and axons of PAM-γ3 DANs.
1048 (C) A subset of PAM-γ3 arborizes in the medial part of the γ3 compartment. Asterisk indicates the position
1049 of the lateral γ3 that is not labeled in this line.
1050
1051 **Figure 12 Examples of split-LexA conversion**
1052 Split-LexA shares the same enhancers with split-GAL4 but with the Gal4DBD replaced by LexADBD. Among
1053 34 conversions tested, 22 were successful, with the split-LexA showing identical or similar expression
1054 patterns as the split-GAL4. The remaining 12 had weak/no expression or showed unintended
1055 intersectional patterns. See Supplementary File 2 for the hemidriver lines with p10 translational
1056 enhancers to enhance expression level.

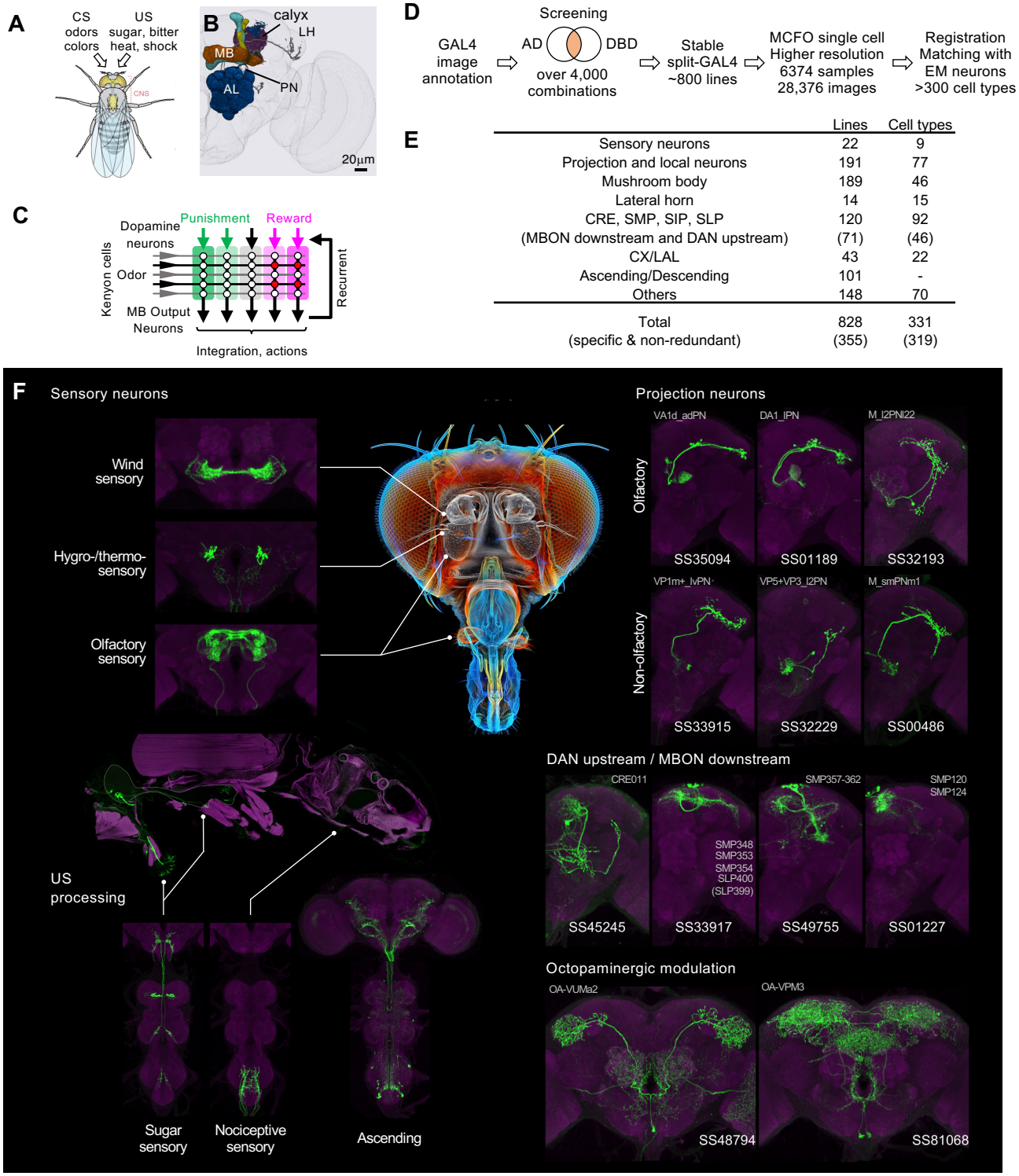

	Lines	Cell types
Sensory neurons	22	9
Projection and local neurons	191	77
Mushroom body	189	46
Lateral horn	14	15
CRE, SMP, SIP, SLP	120	92
(MBON downstream and DAN upstream)	(71)	(46)
CX/LAL	43	22
Ascending/Descending	101	-
Others	148	70
Total	828	331
(specific & non-redundant)	(355)	(319)

Figure 1 Generation and annotation of split-GAL4 lines

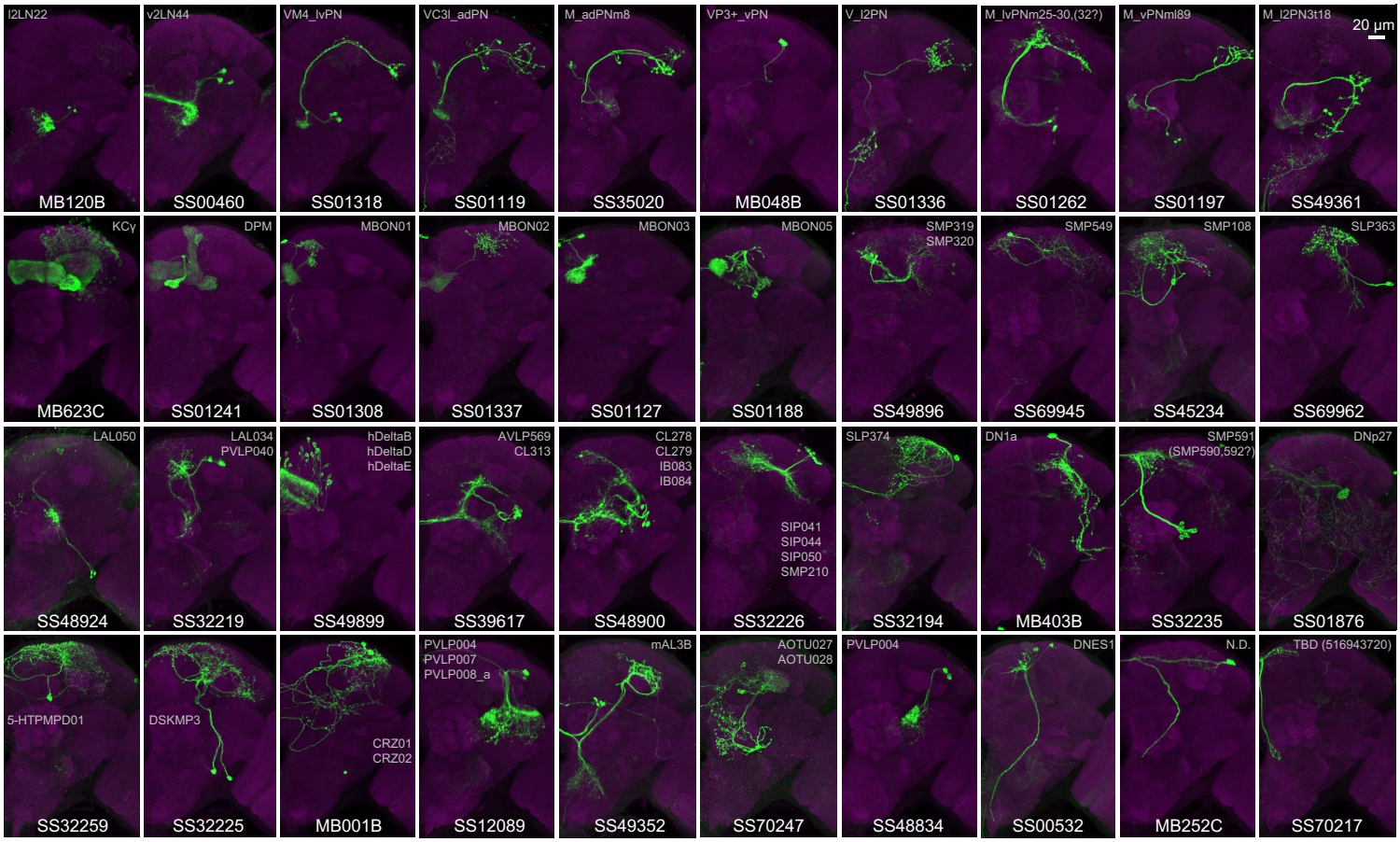

Figure 1-figure supplement 1 Examples of cell types covered by the split-GAL4 lines in this collection

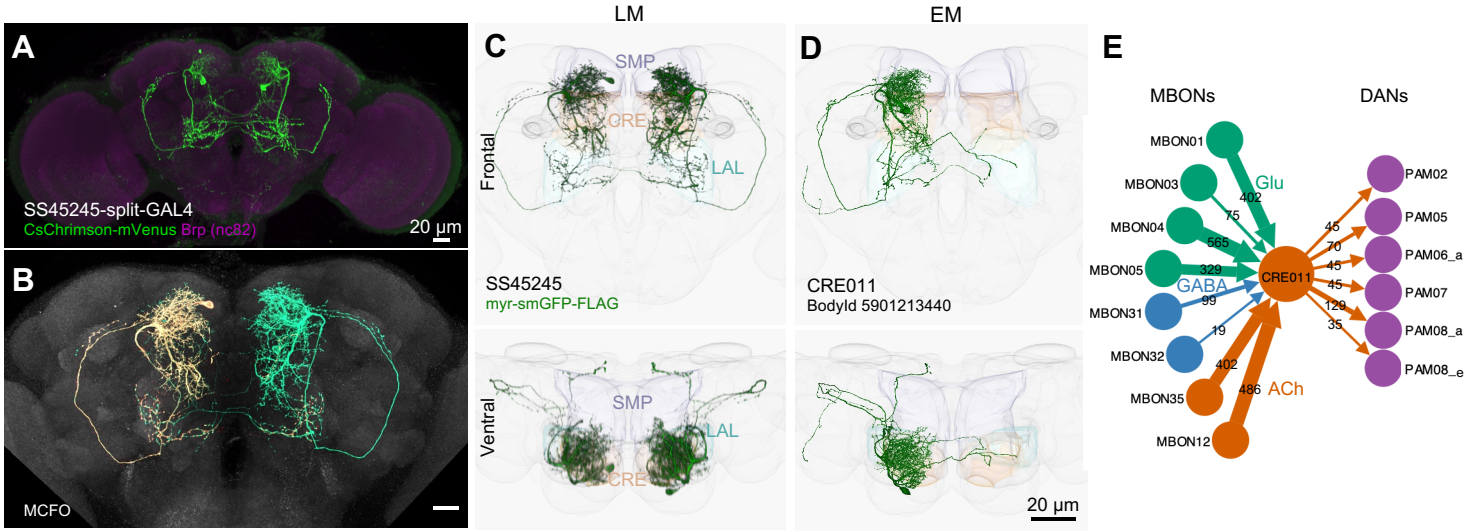

Figure 2 LM-EM match of CRE011 driver

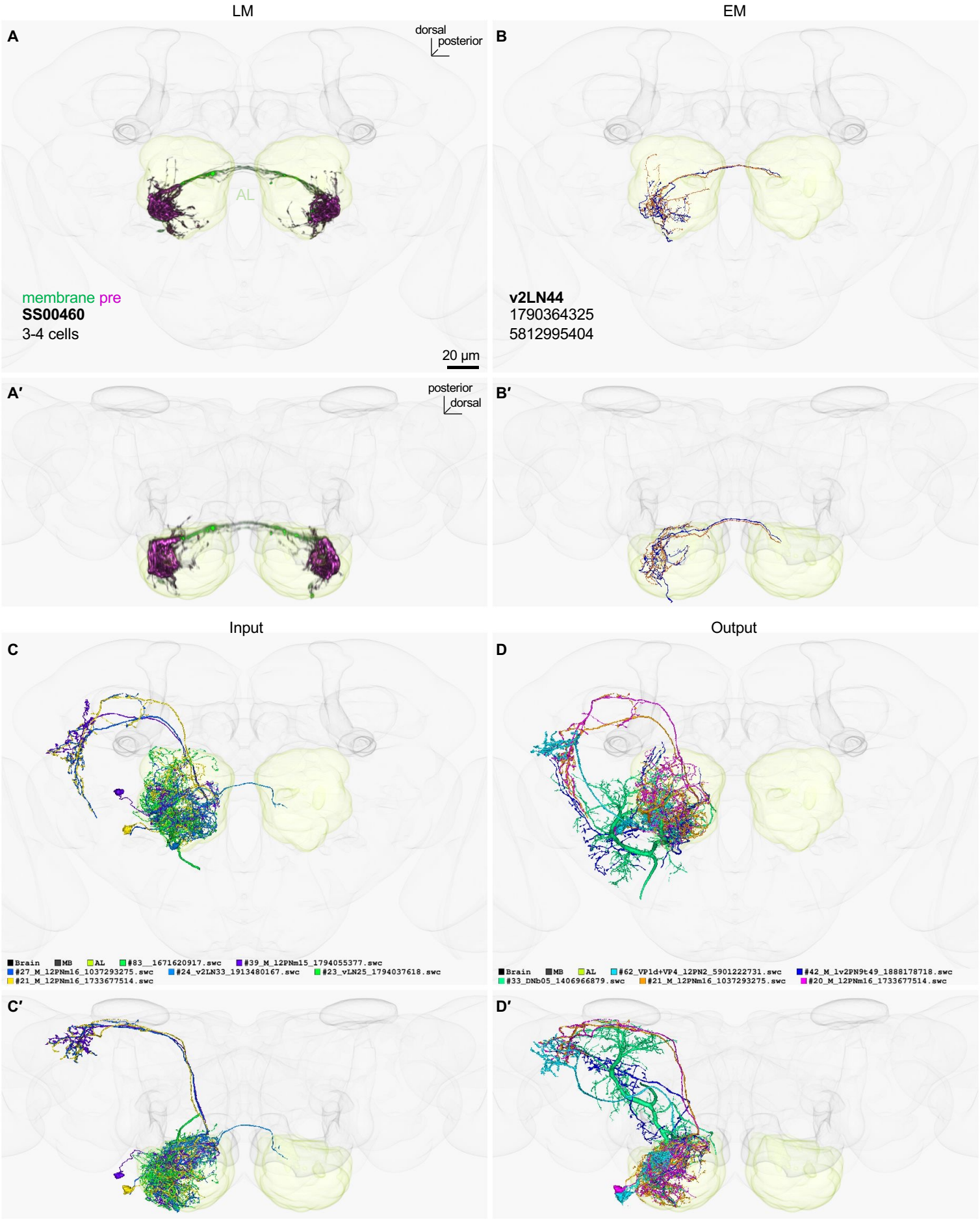

Figure 2 – figure supplement 1

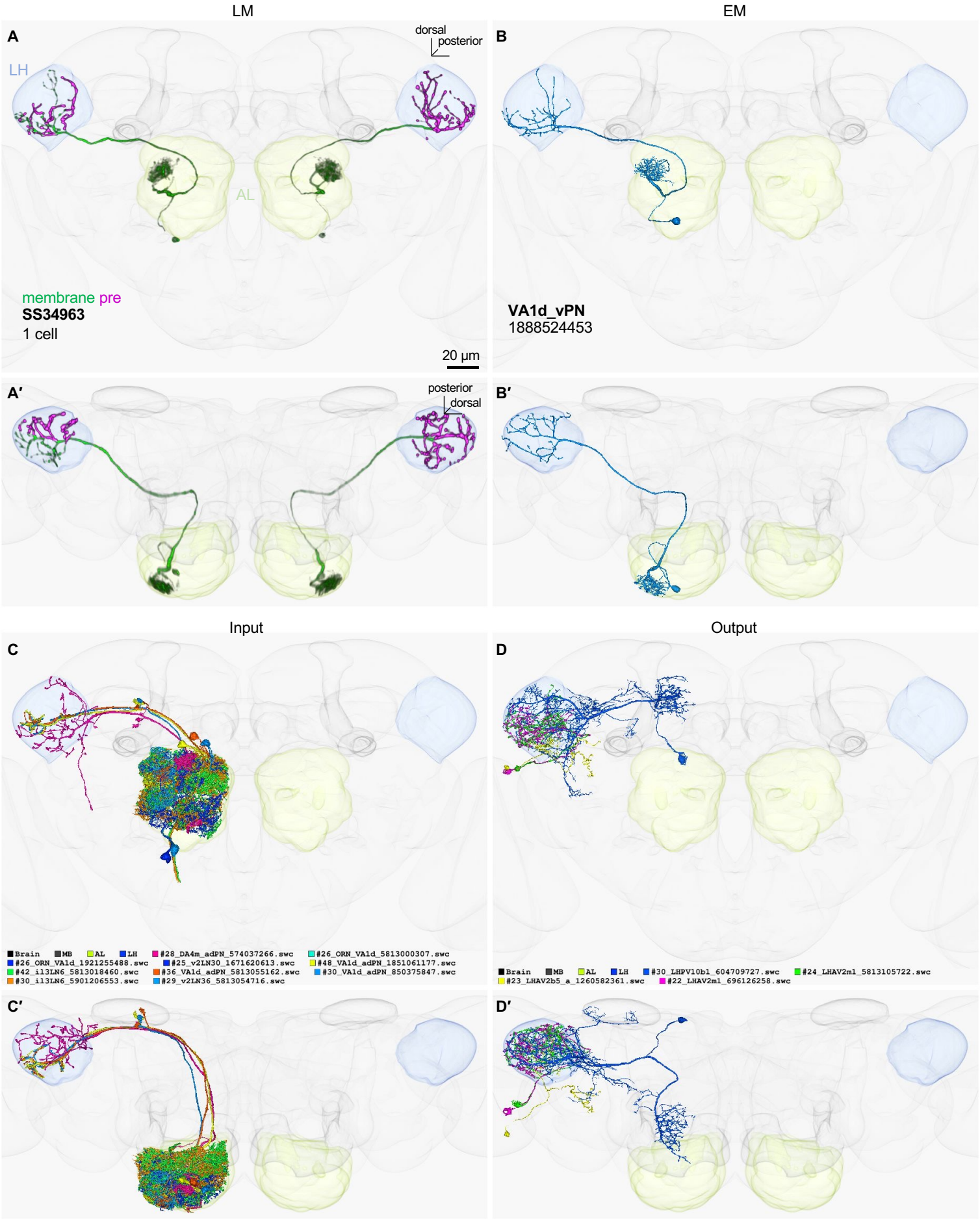

Figure 2 – figure supplement 2

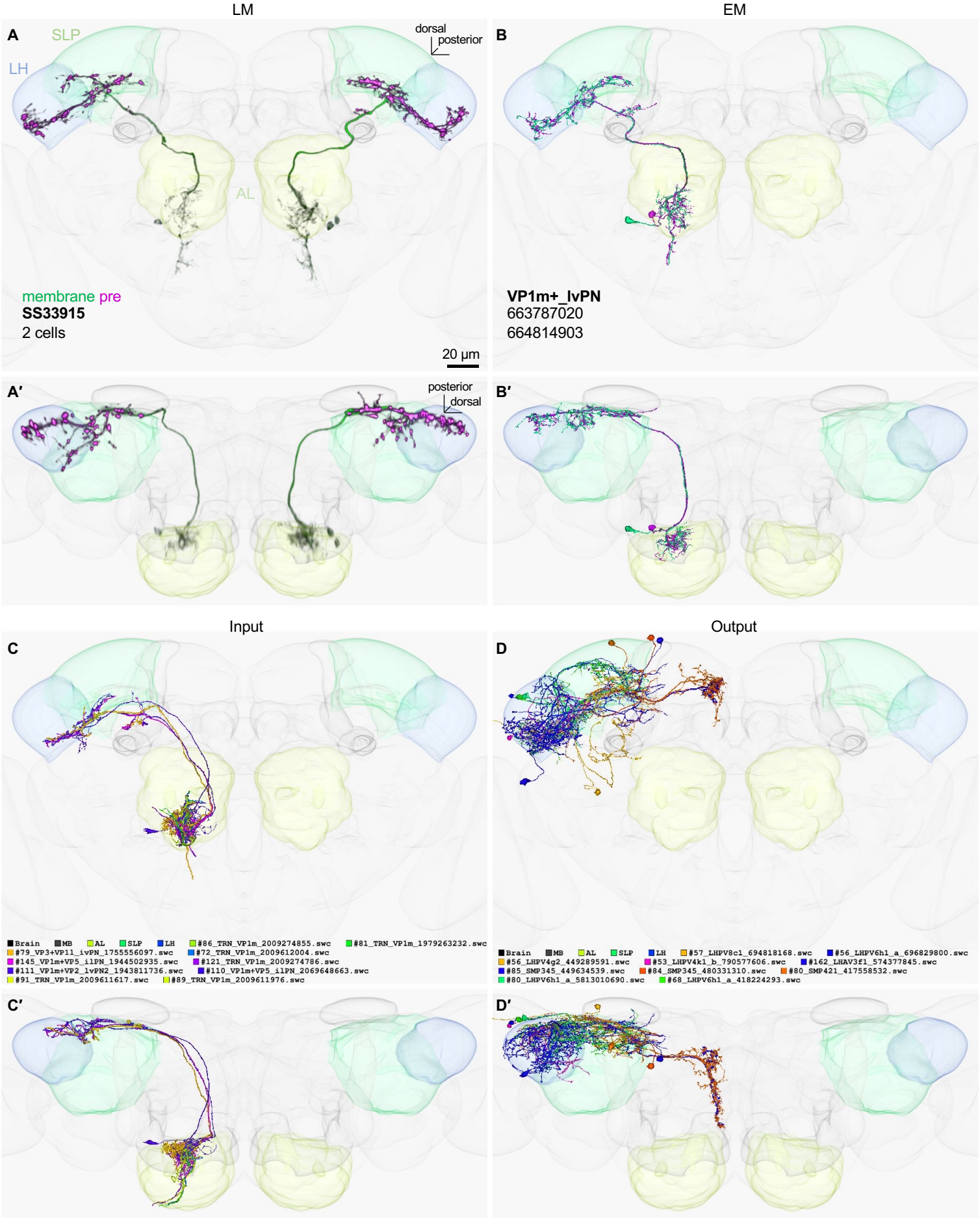

Figure 2 – figure supplement 3

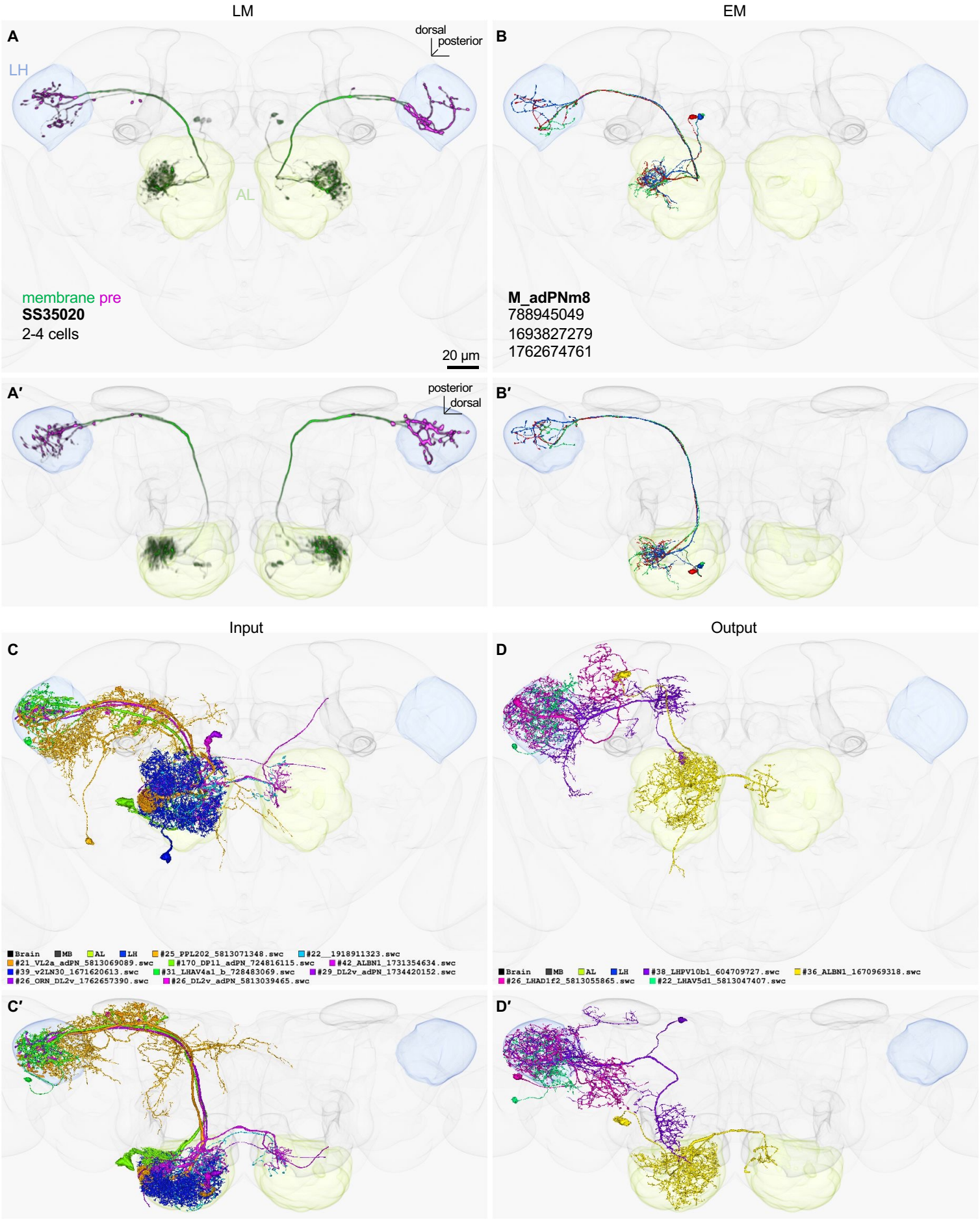

Figure 2 – figure supplement 4

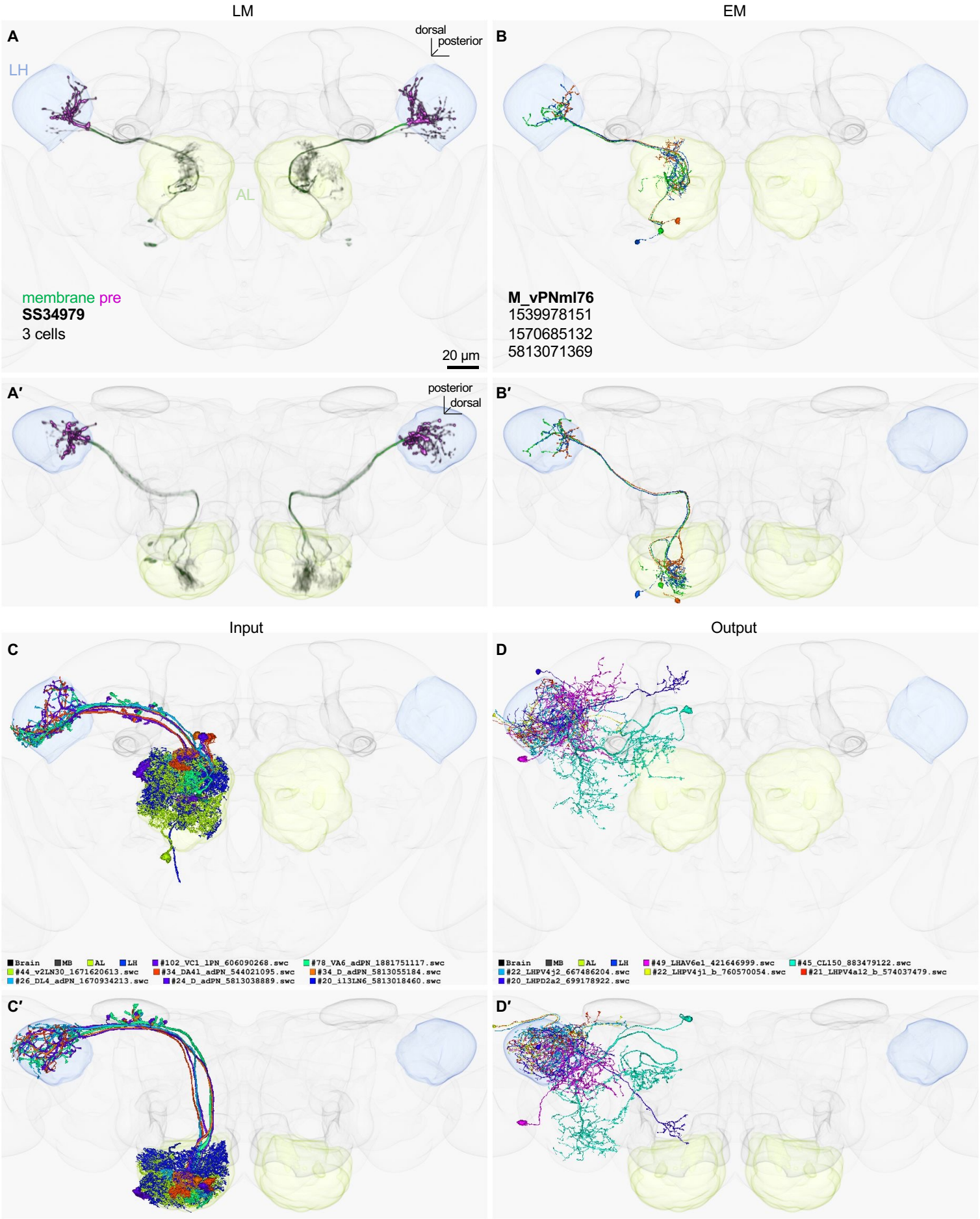

Figure 2 – figure supplement 5

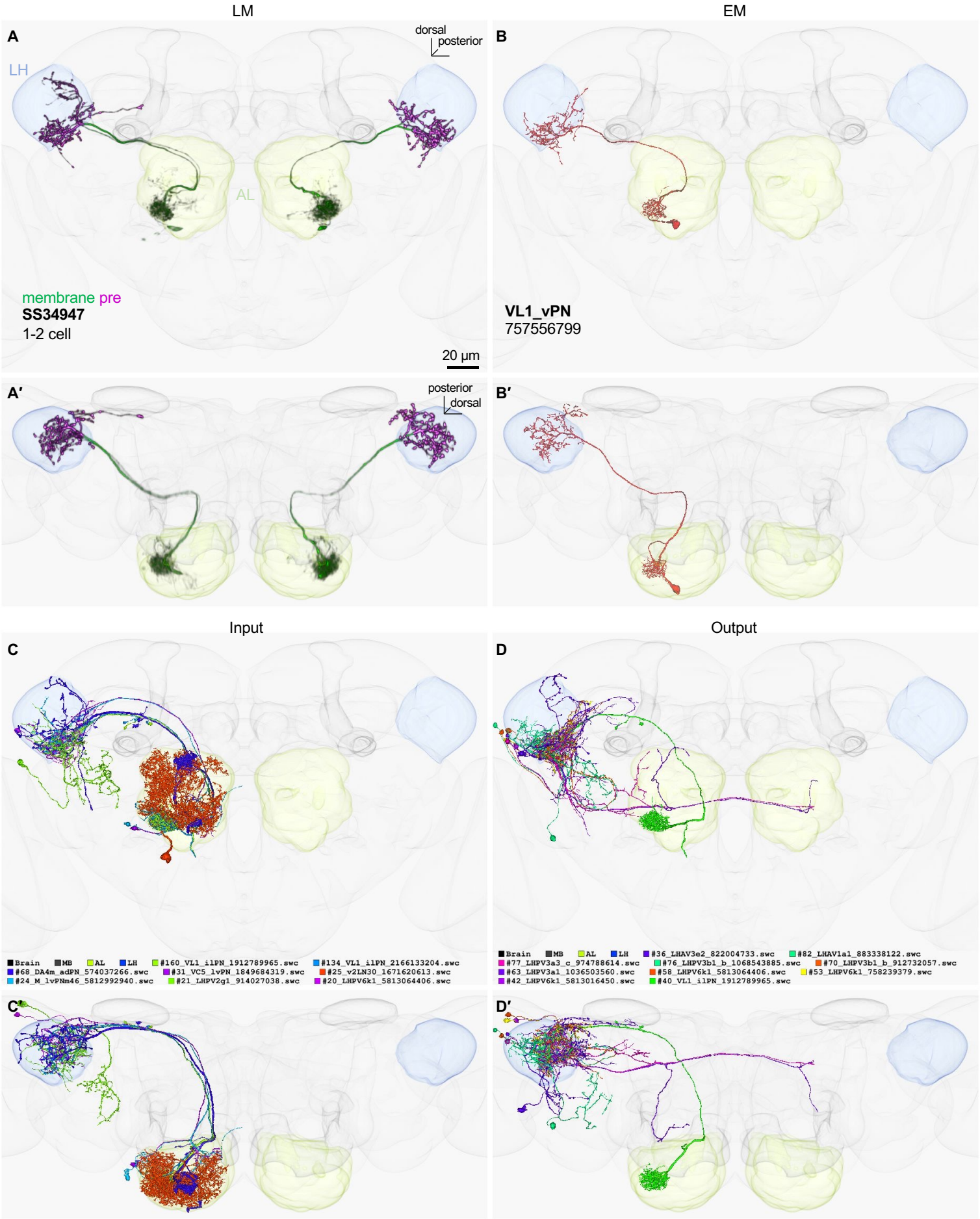

Figure 2 – figure supplement 6

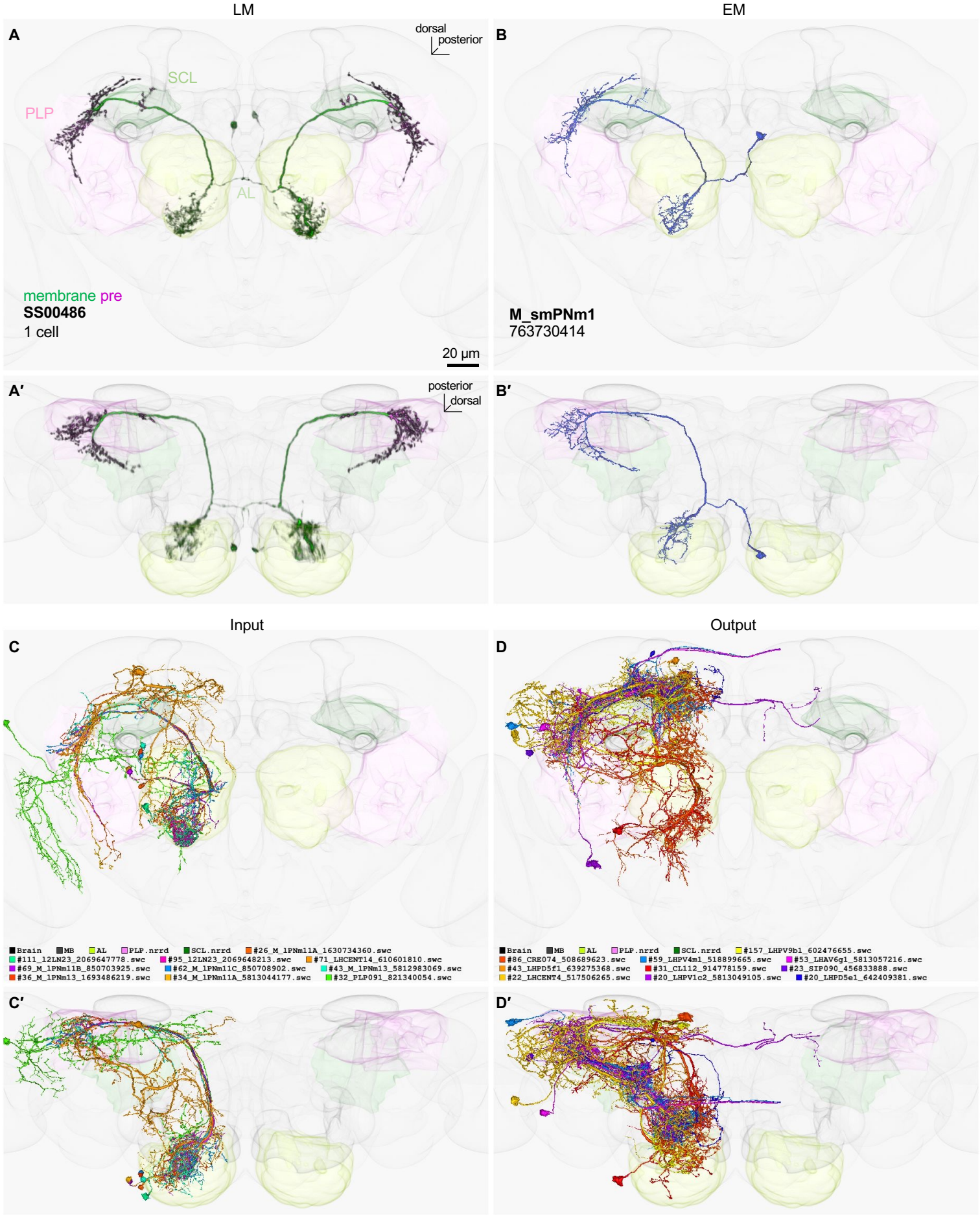

Figure 2 – figure supplement 7

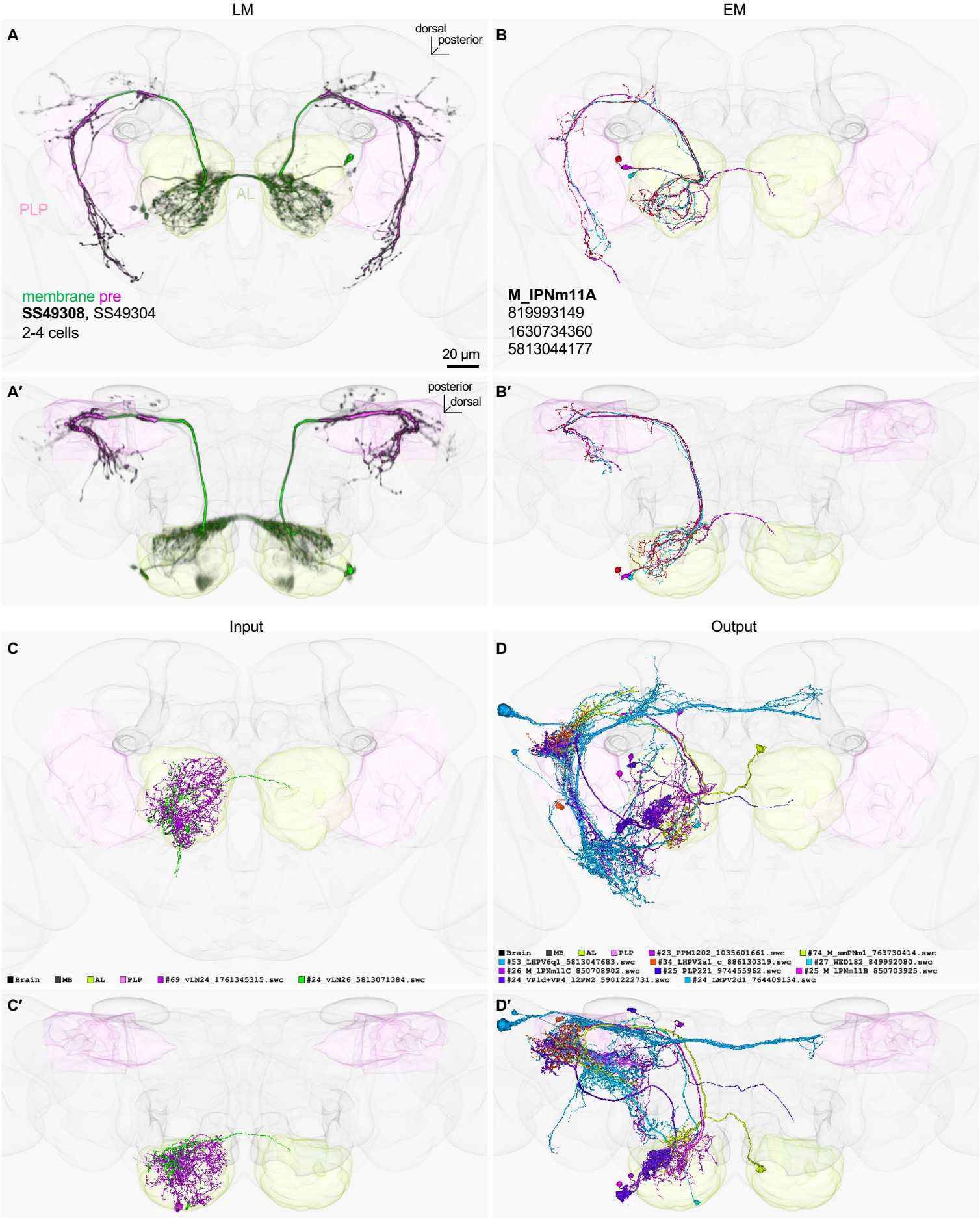

Figure 2 – figure supplement 8

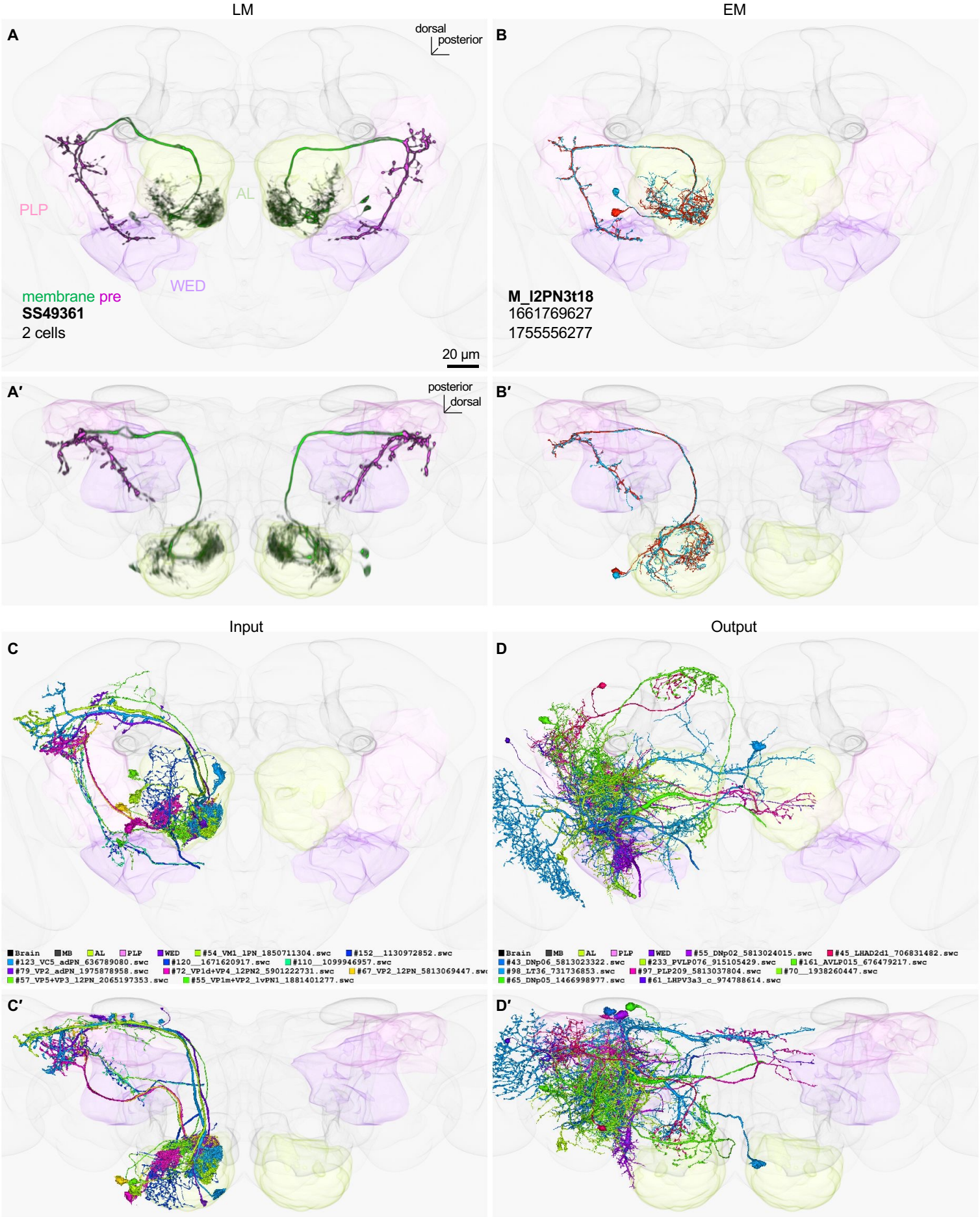

Figure 2 – figure supplement 9

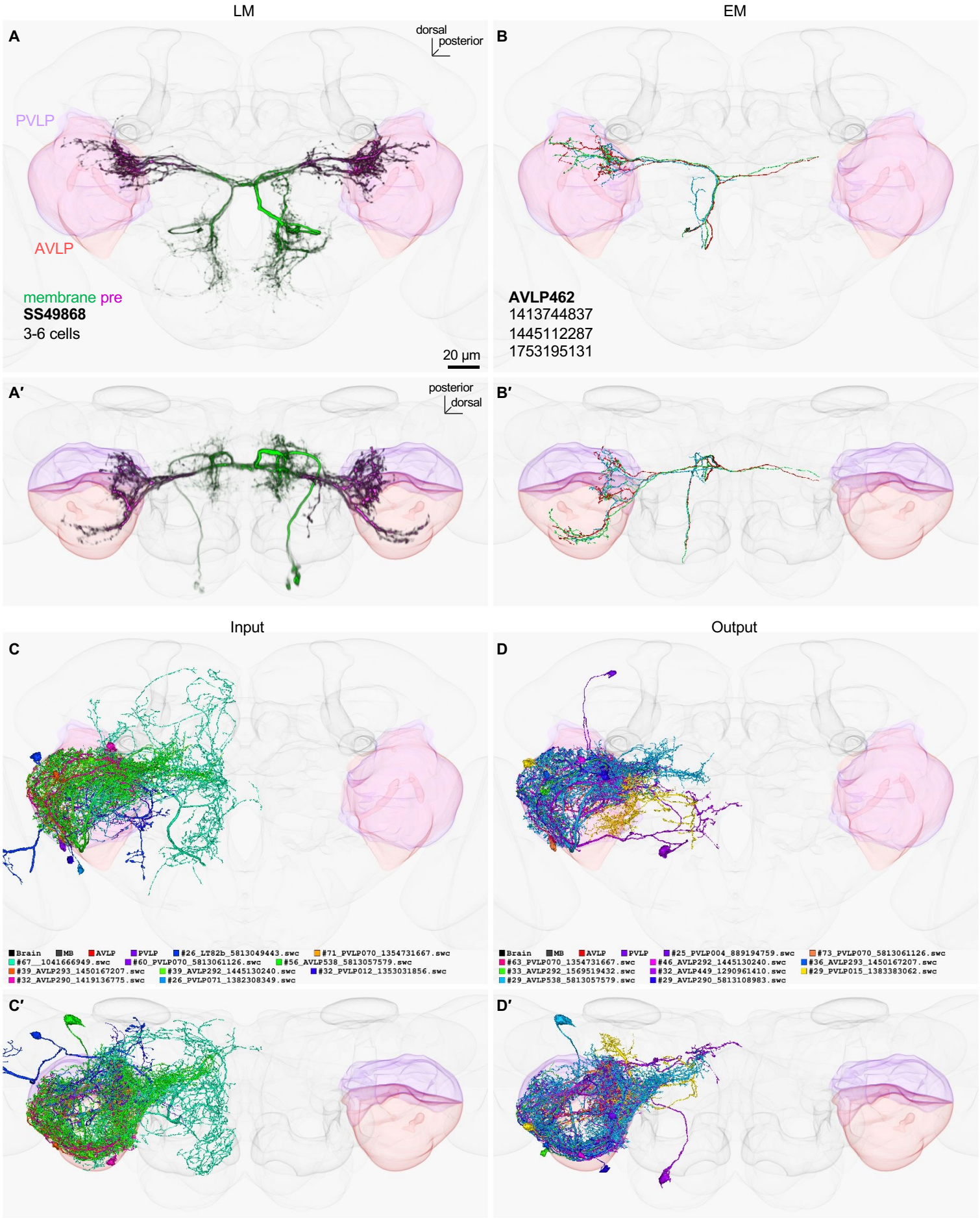

Figure 2 – figure supplement 10

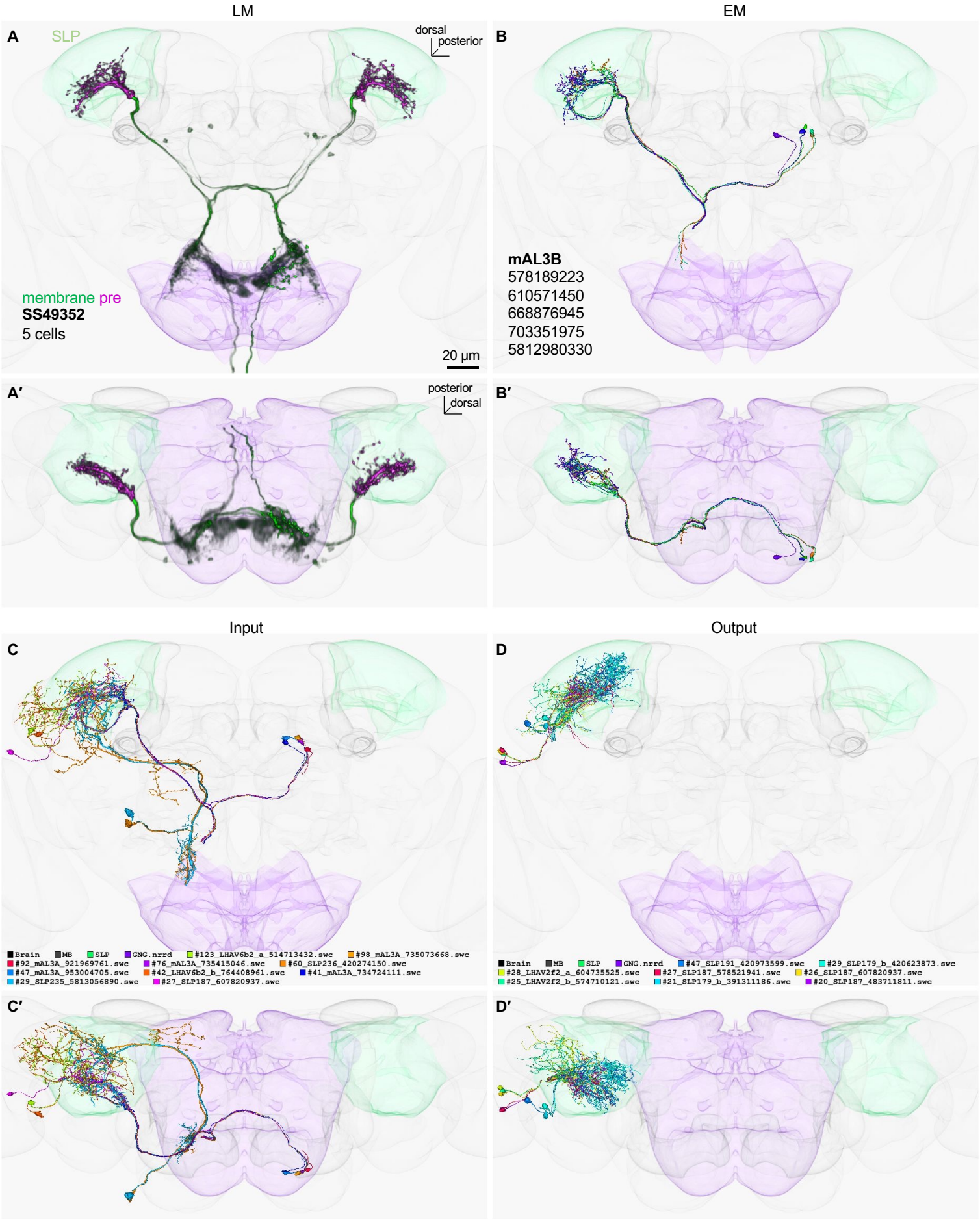

Figure 2 – figure supplement 11

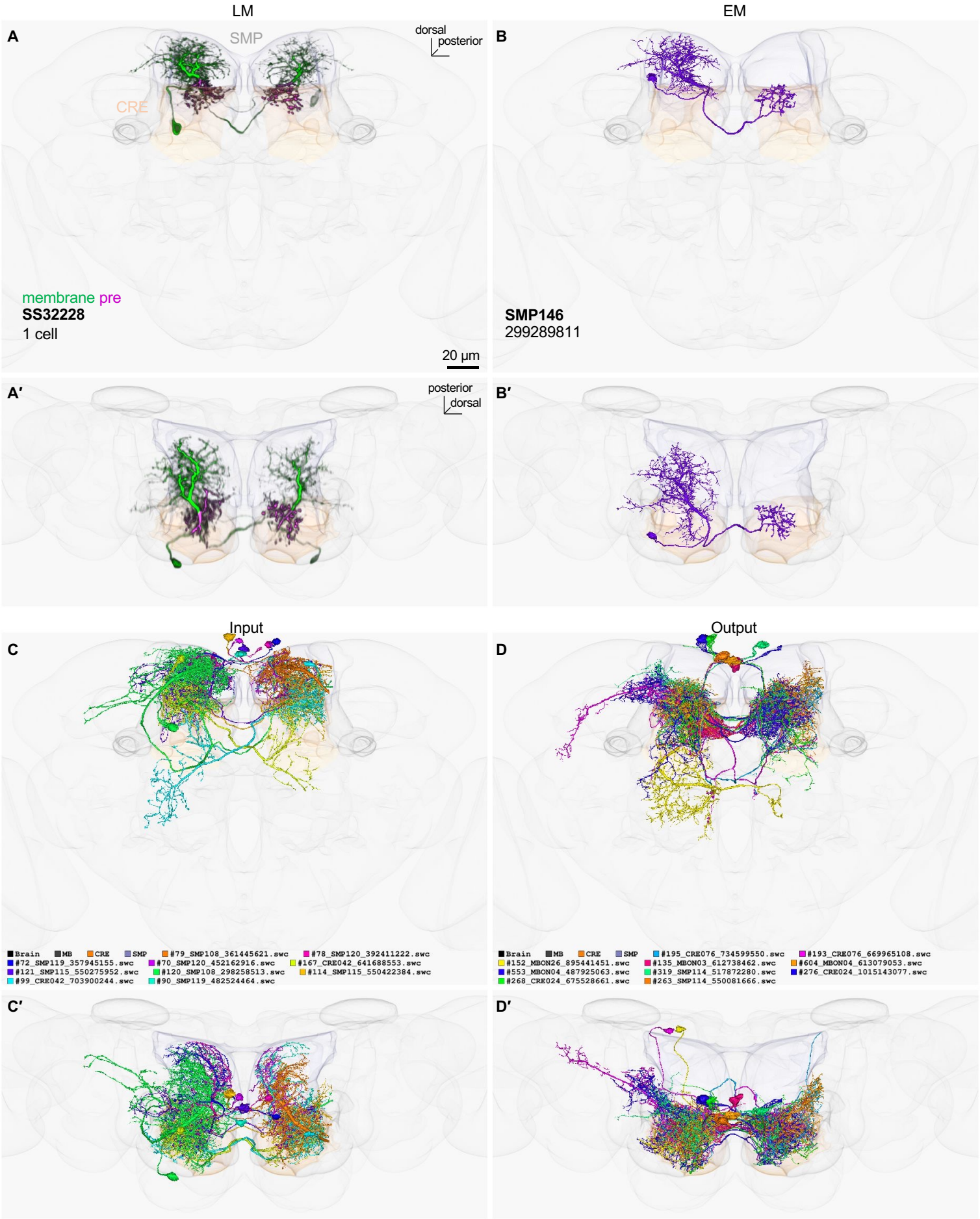

Figure 2 – figure supplement 12

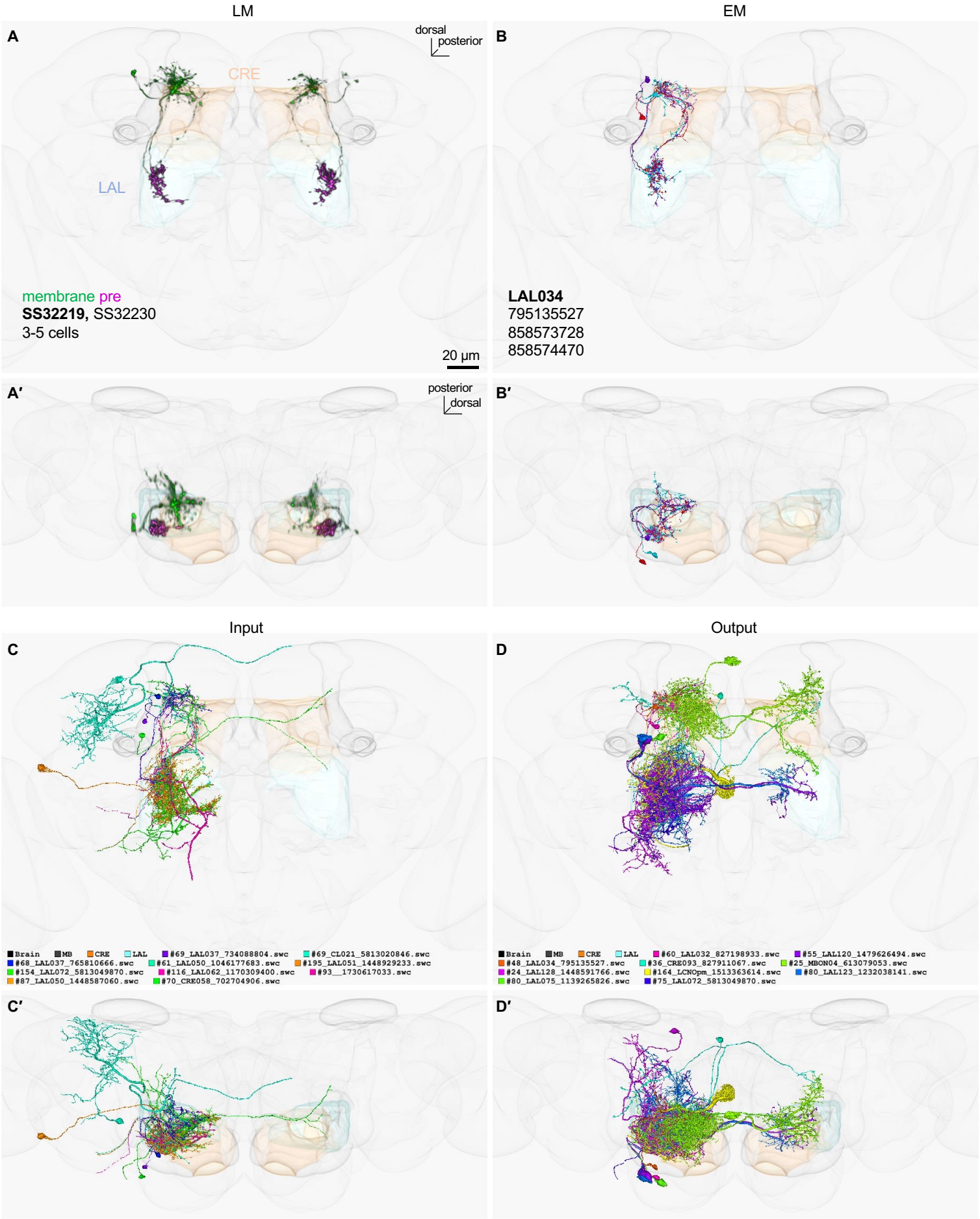

Figure 2 – figure supplement 13

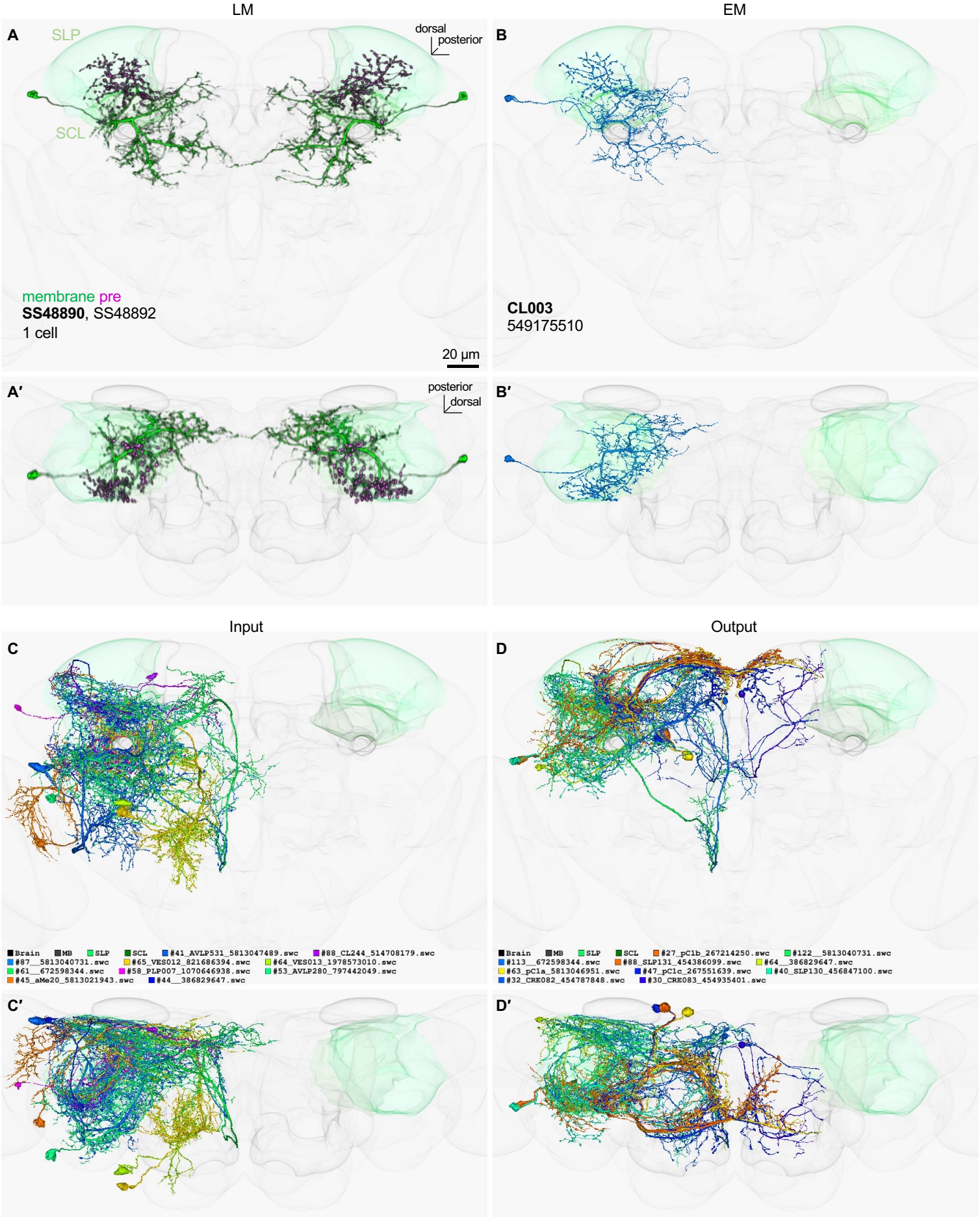

Figure 2 – figure supplement 14

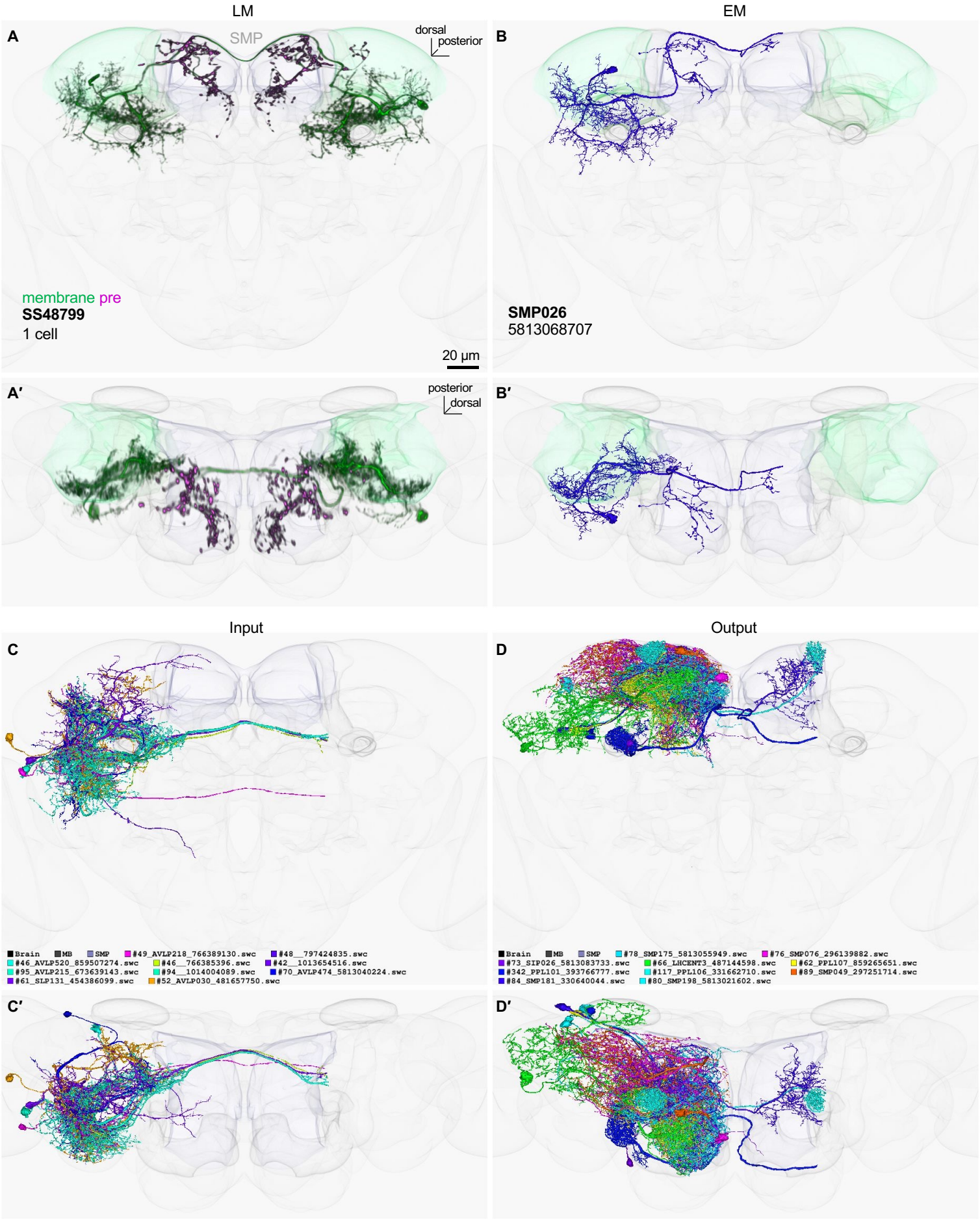

Figure 2 – figure supplement 15

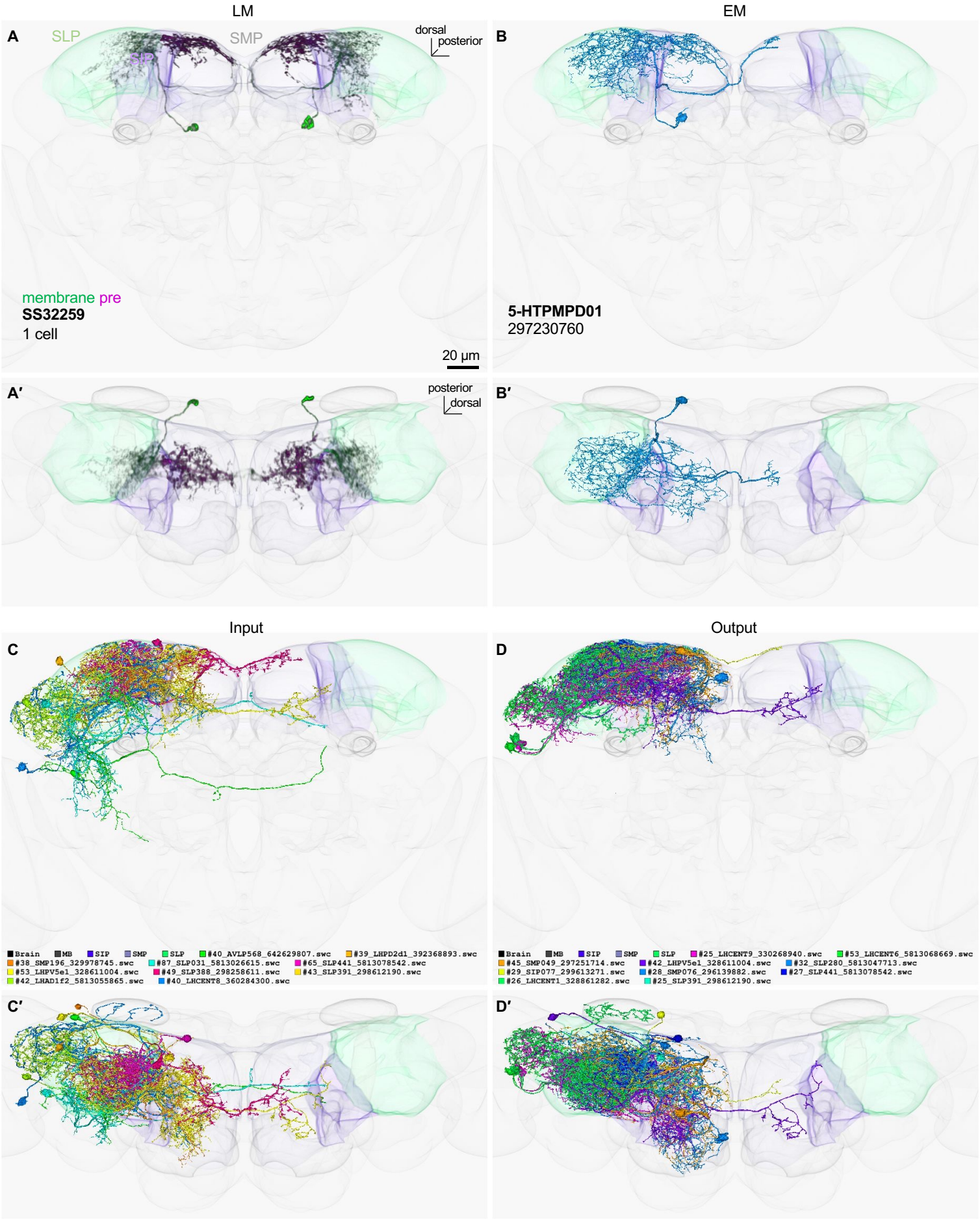

Figure 2 – figure supplement 16

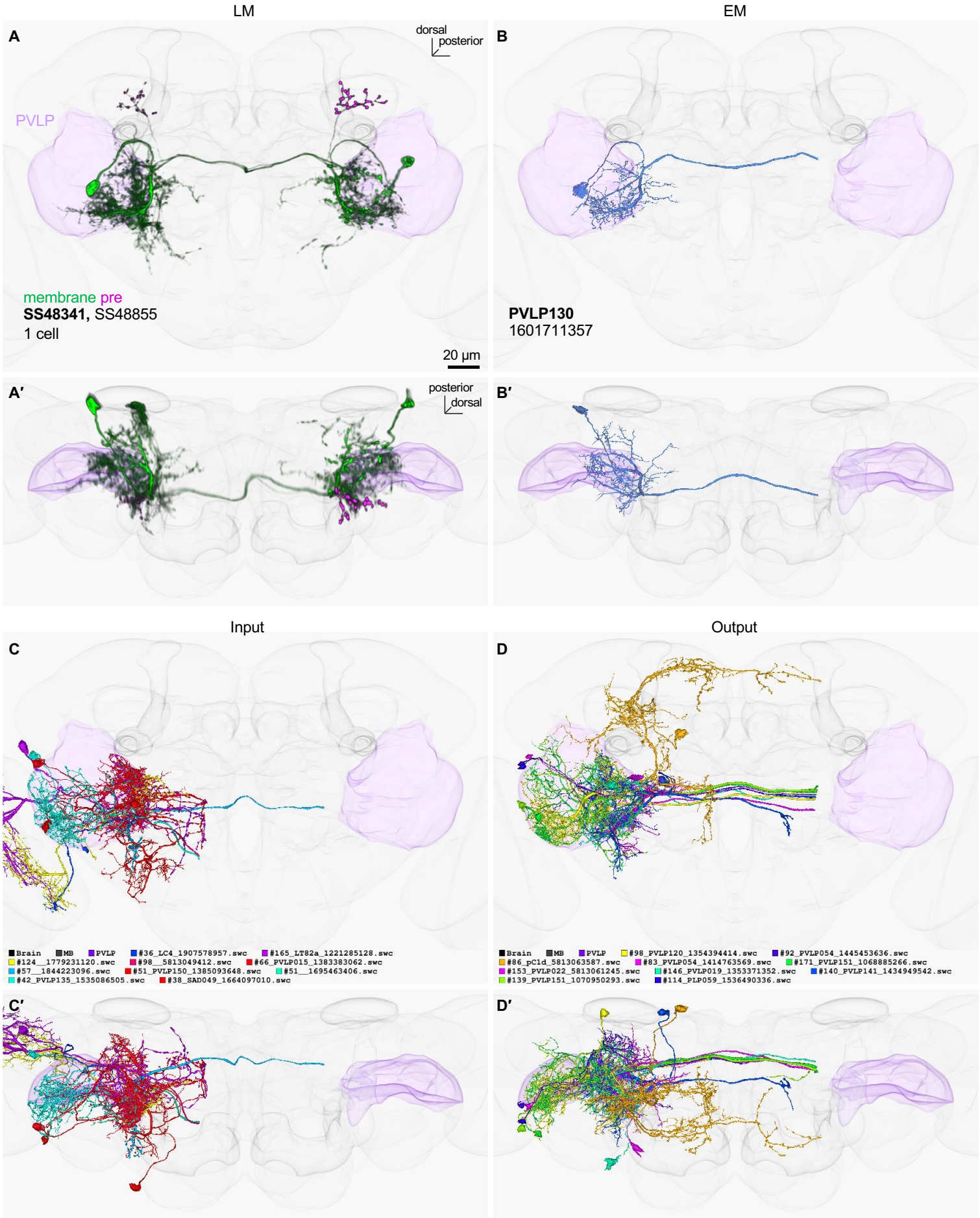

Figure 2 – figure supplement 17

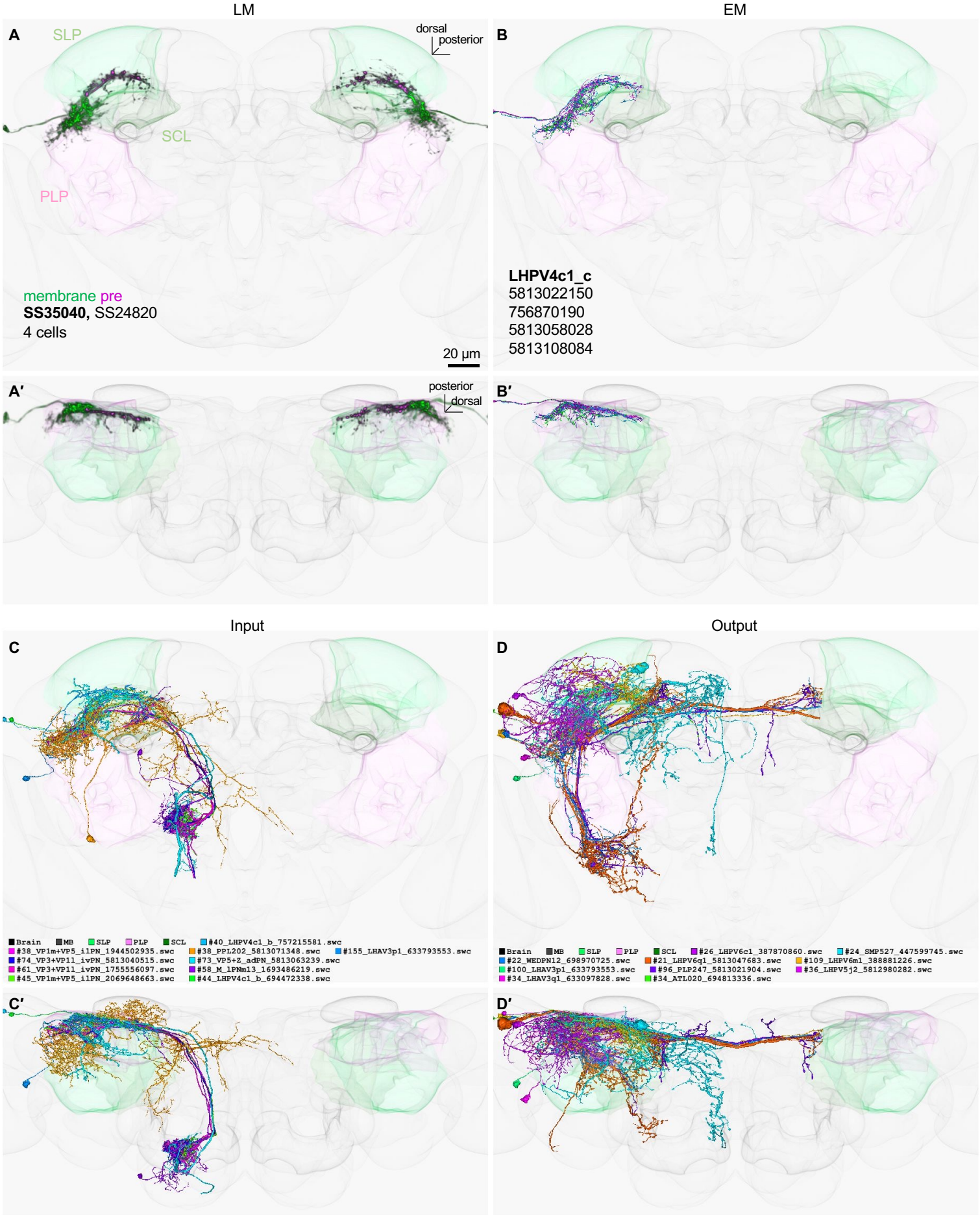

Figure 2 – figure supplement 18

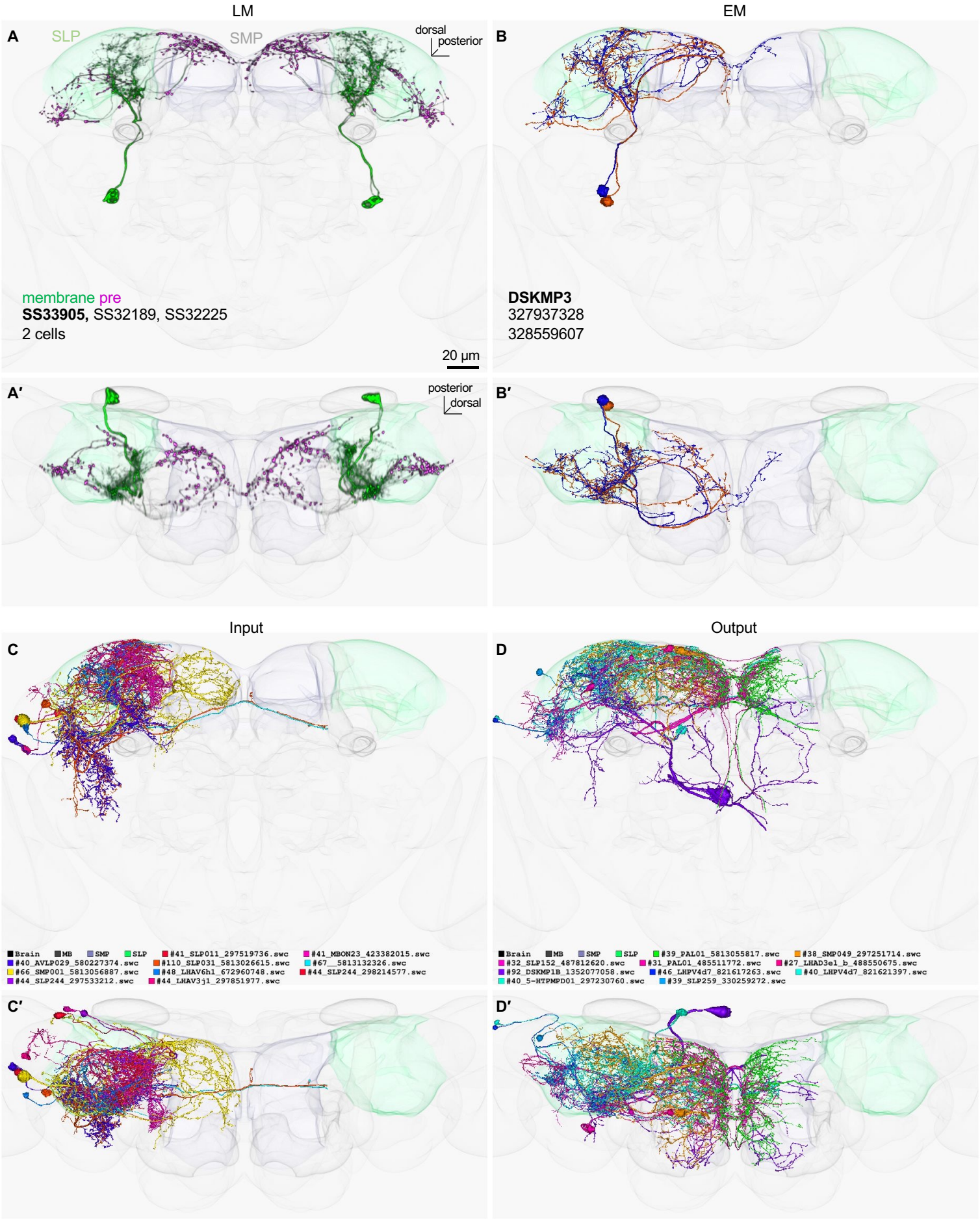

Figure 2 – figure supplement 19

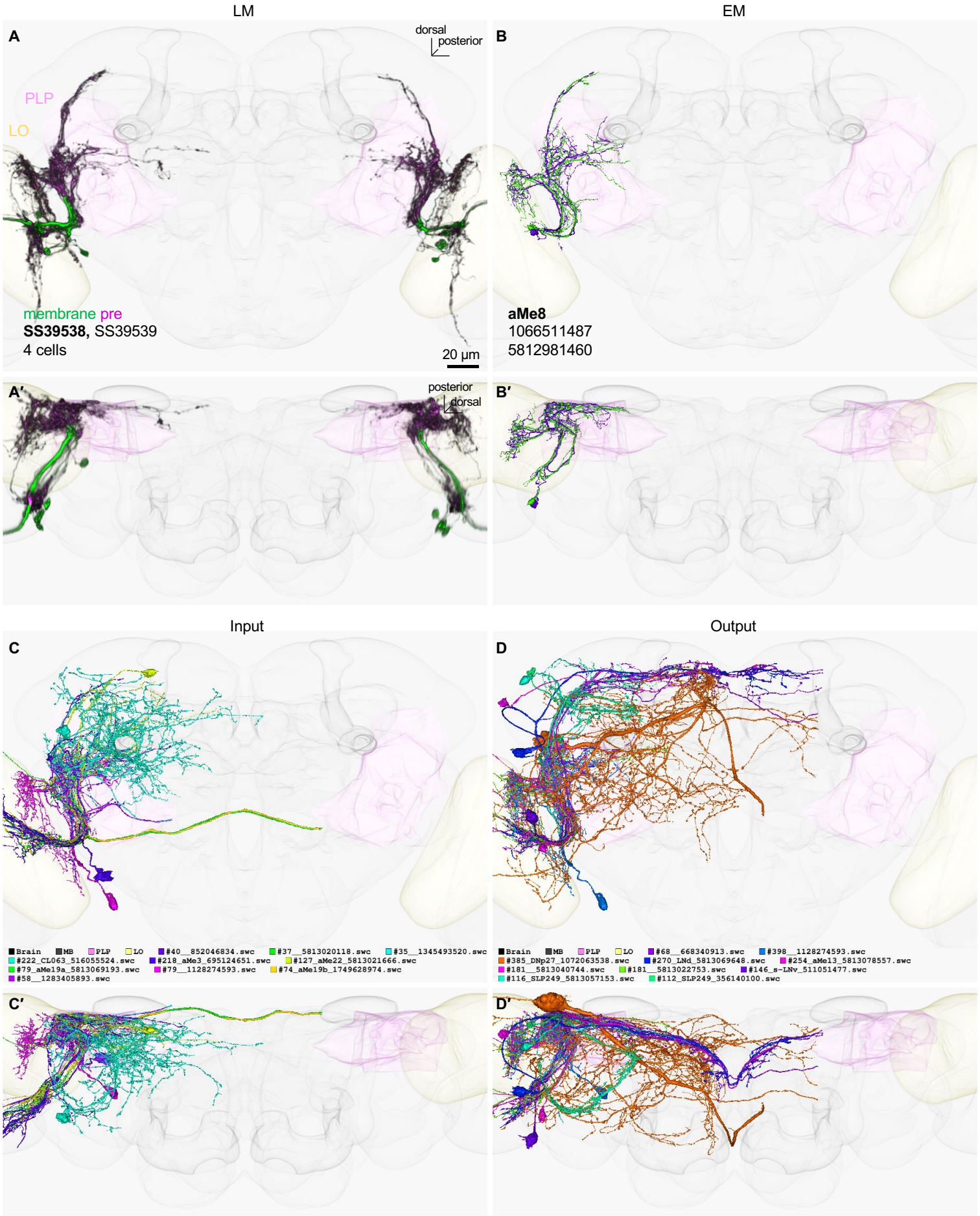

Figure 2 – figure supplement 20

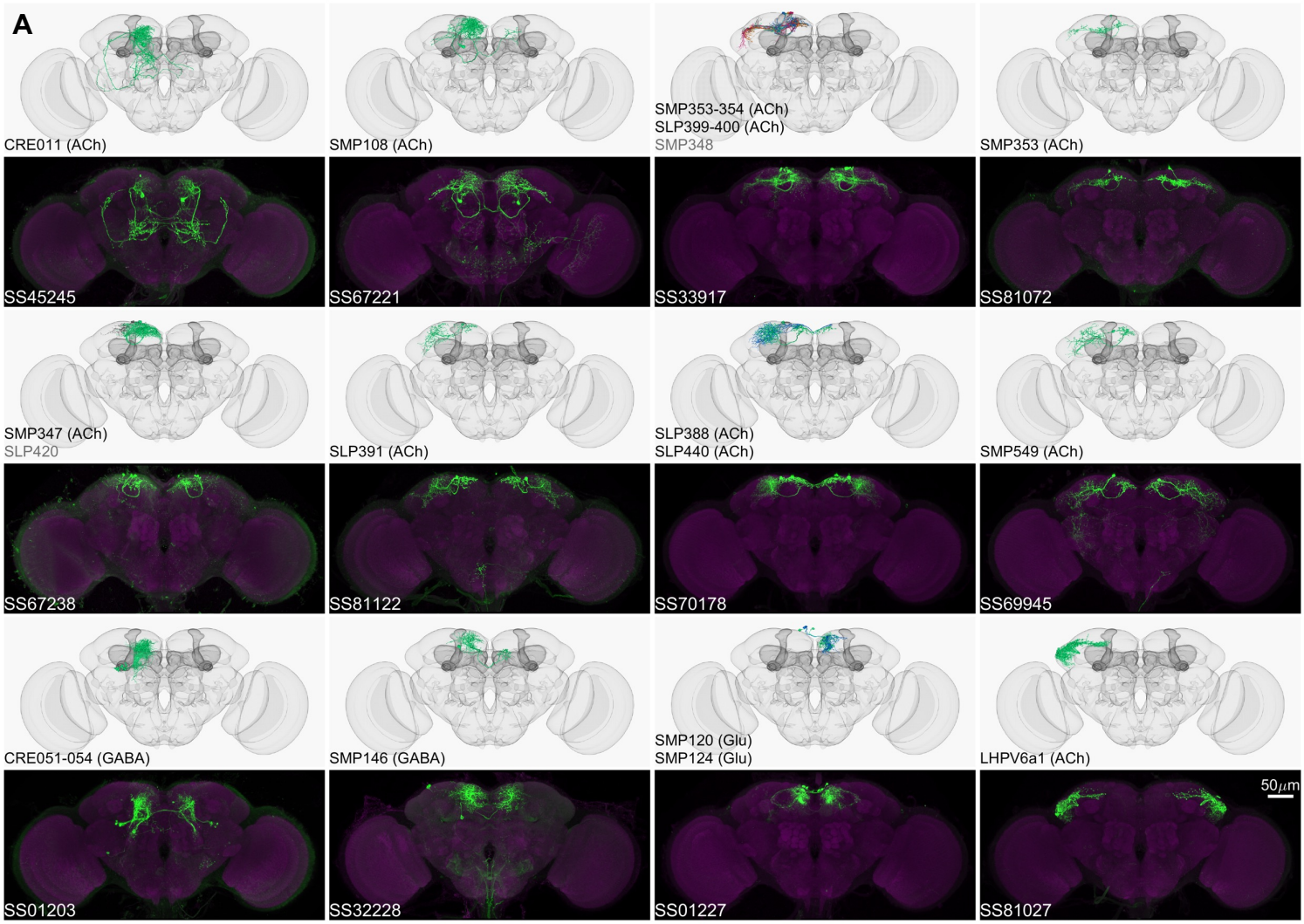

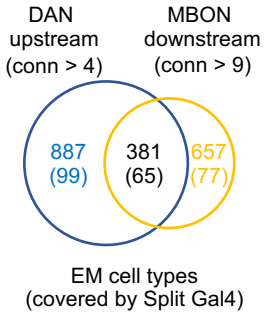

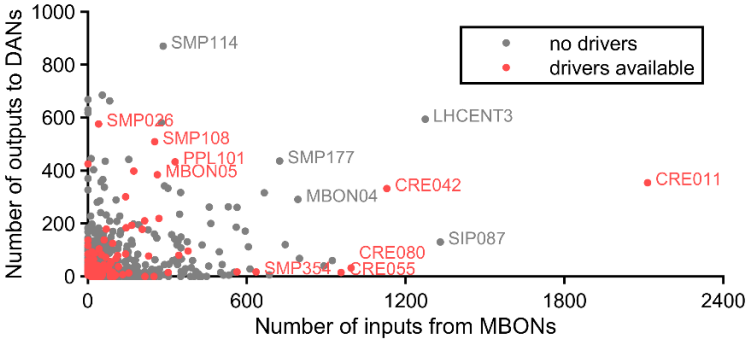

Figure 3 Coverage of MBON downstream and DAN upstream neurons

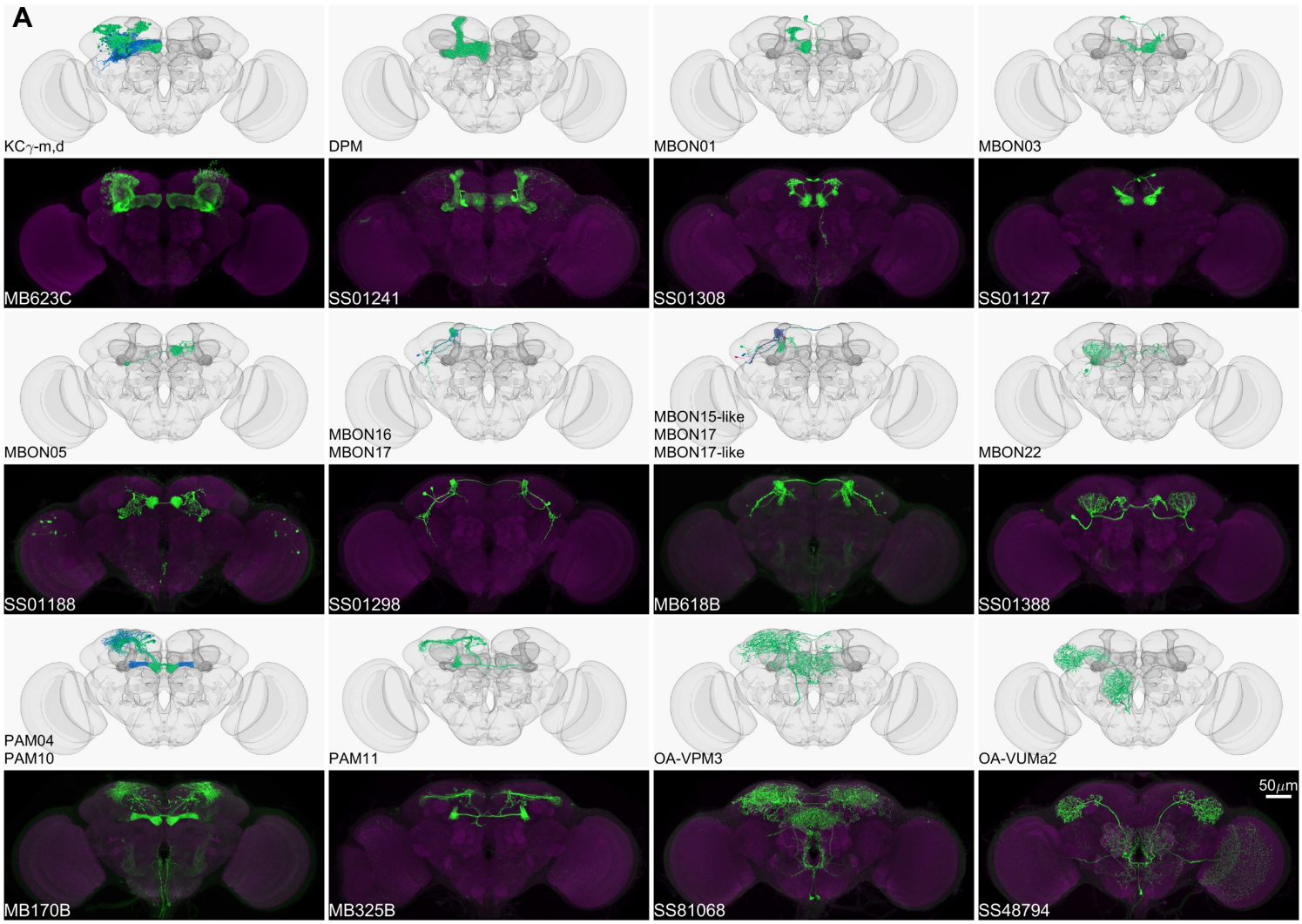

B

MB cell types	Covered cell types	Total cell types	Missed cell types
Intrinsic neurons (excluding KCs)	1	2	APL
MBONs	33	37	MBON24-25, 27, 34
DANs	18	23	PPL102, 201-202, PAM09,15
Other modulatory	6	6	
Total	58	68	

Figure 3-supplemental figure 1 New or improved drivers for MB cell types

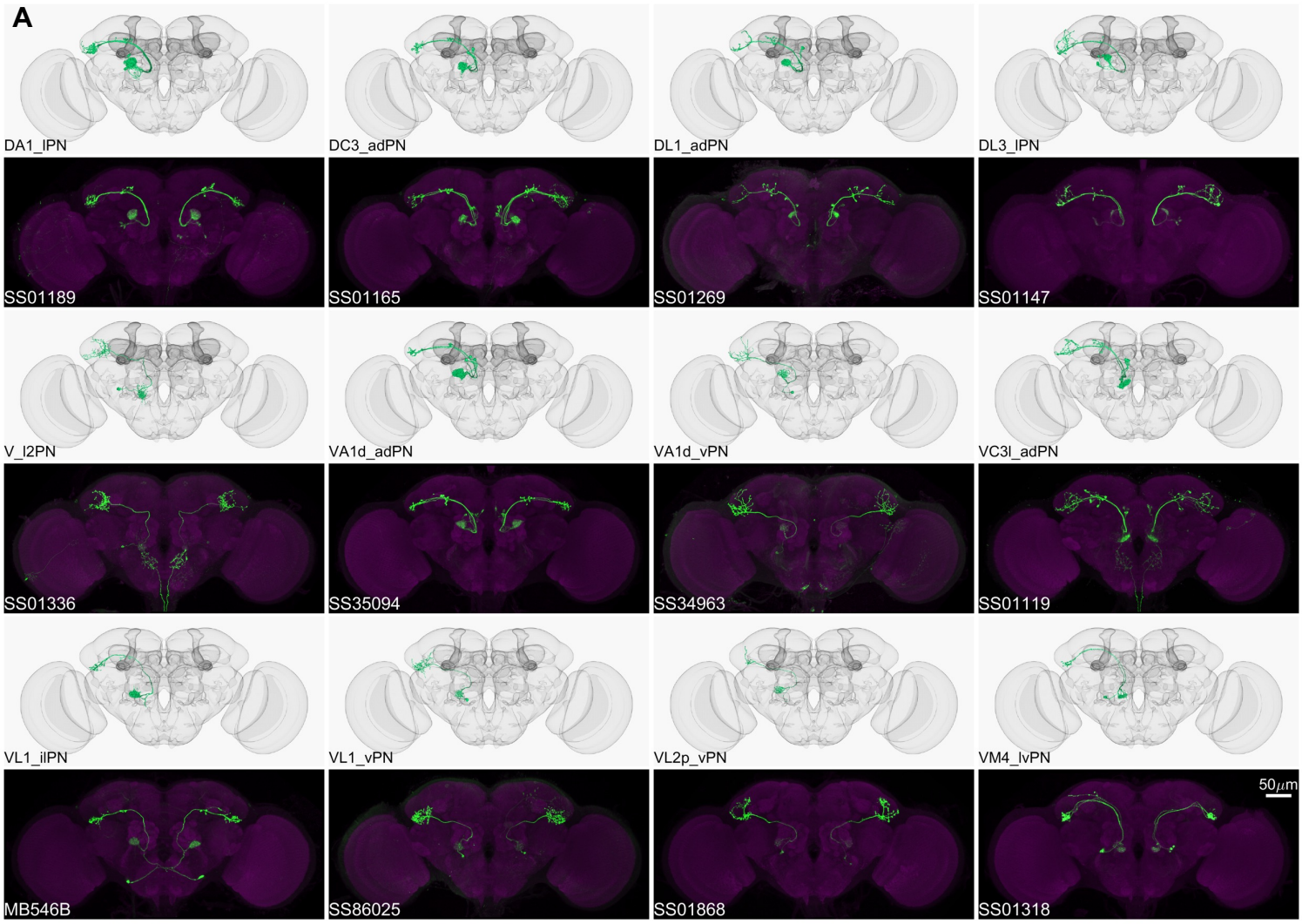

B

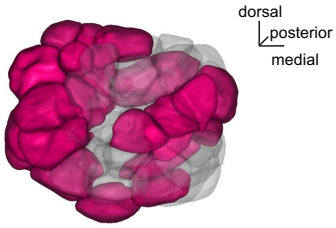

C

PN types	Covered cell types	Total cell types
Olfactory uni-glomerular PNs	26	~80
Multi-glomerular PNs and non-olfactory PNs	> 22	~120
Total	> 48	~200

Figure 4 Examples of covered PN cell types (uni-glomerular)

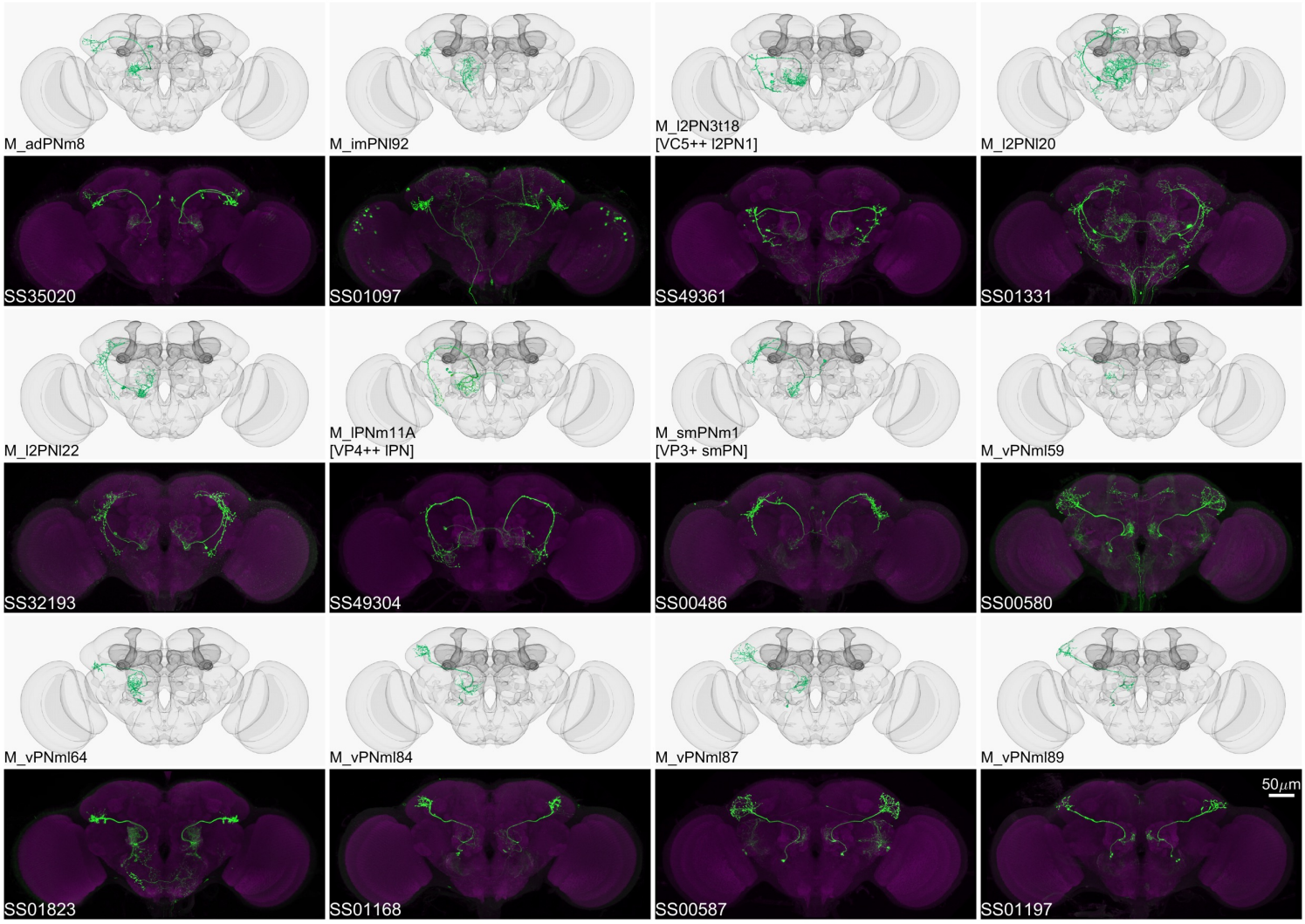

Figure 5 Examples of covered PN cell types (multi-glomerular)

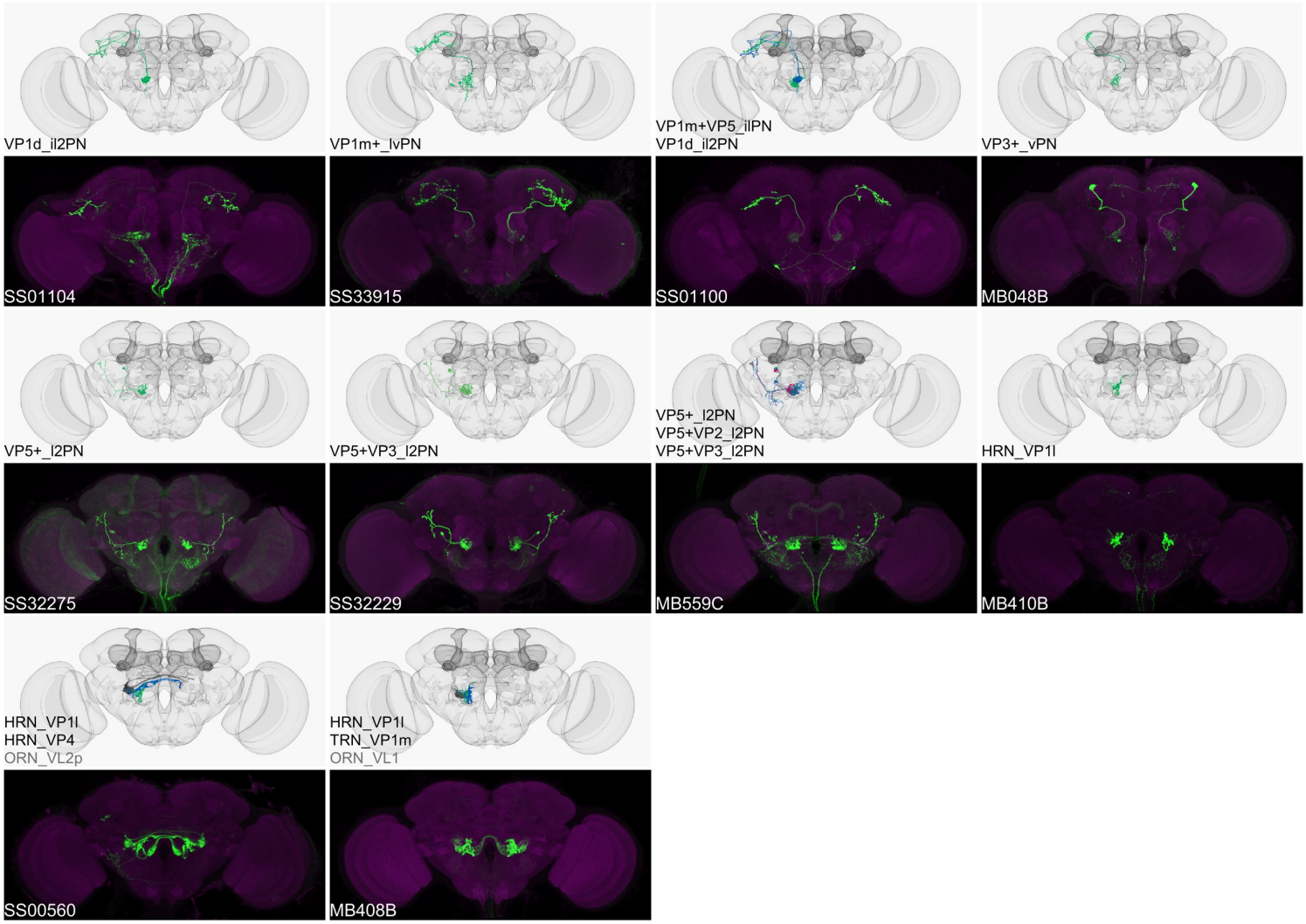

Figure 6 Examples of covered non-olfactory PNs cell types and sensory neurons

A

promoter	Gal4 DBD	LexA DBD	LexA
Gr64f	1	6	1
Gr43a	-	1	-
Gr66a	-	1	-
Gr28b	-	1	-
dTrpA	-	-	1
GMR/VT	-	24	-

B

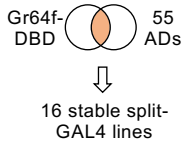

C

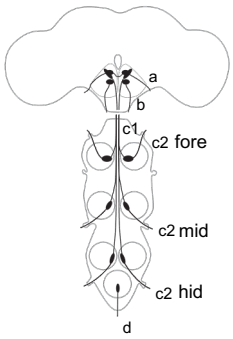

D

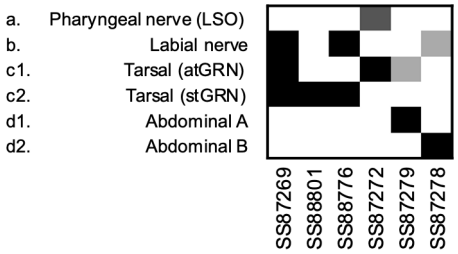

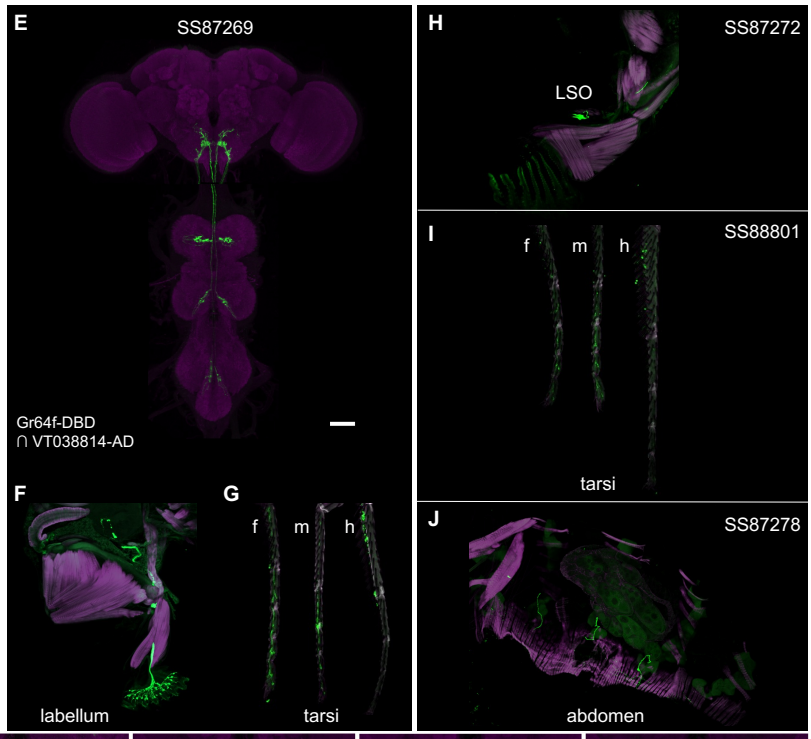

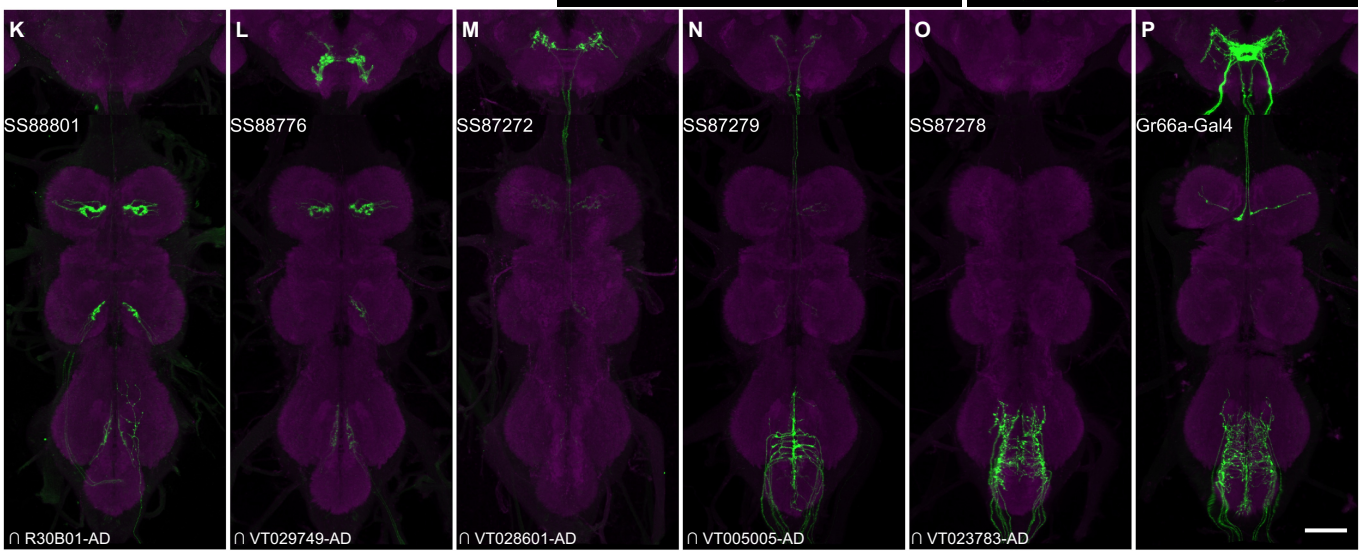

Figure 7 Gr64f split-Gal4

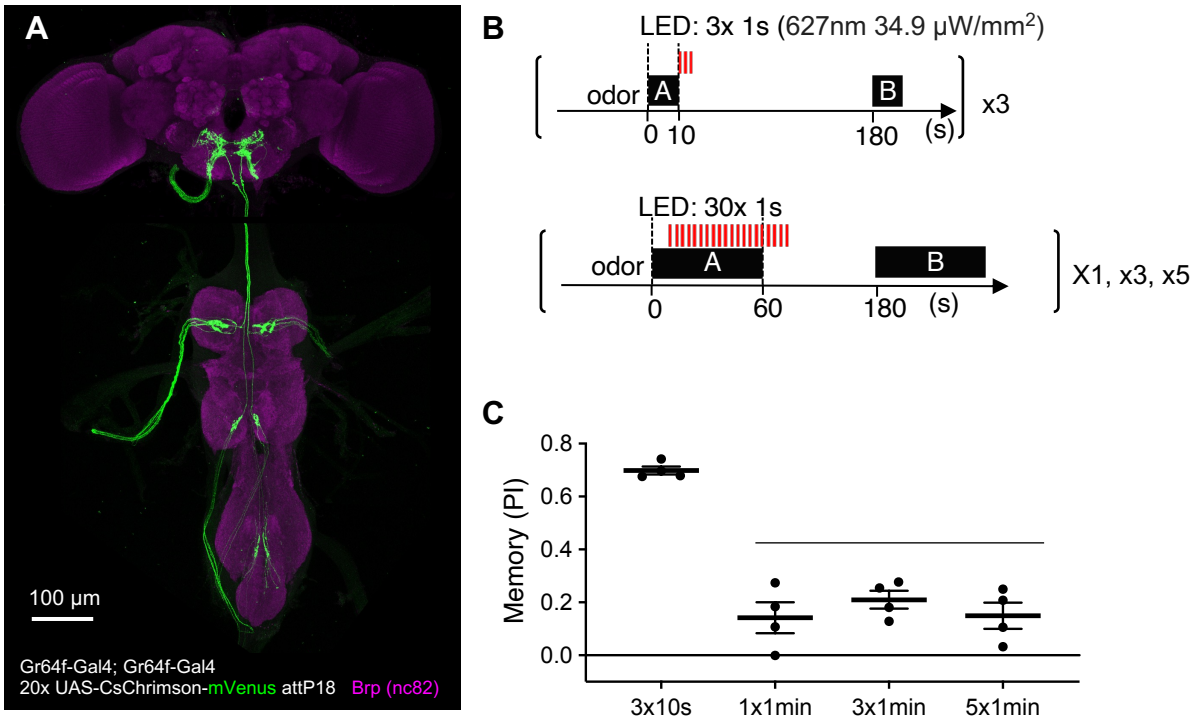

Figure 7-figure supplement 1 US substitution experiment with Gr64f-Gal4

Missing statistics

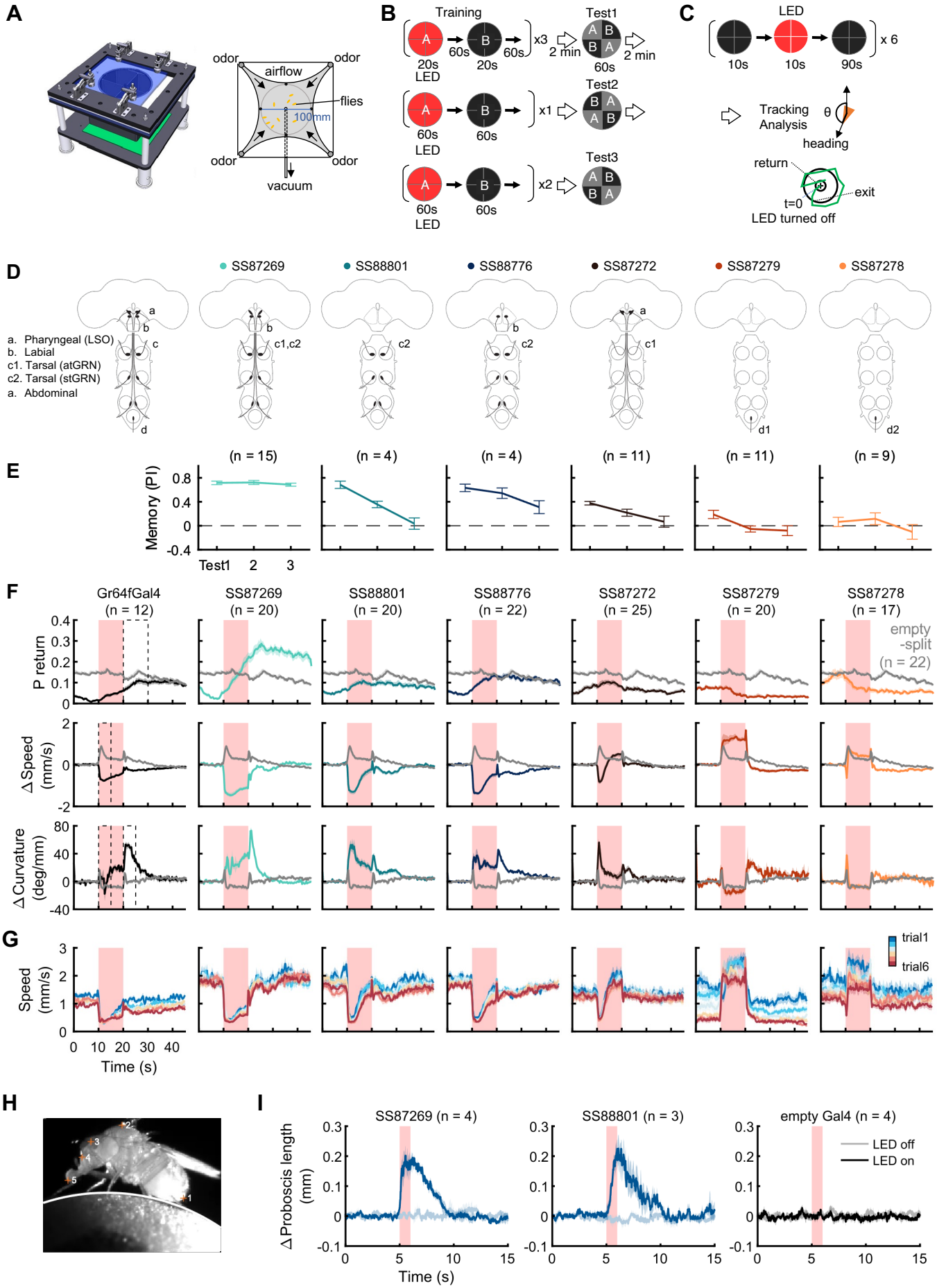

Figure 8 Gr64f-split behavior

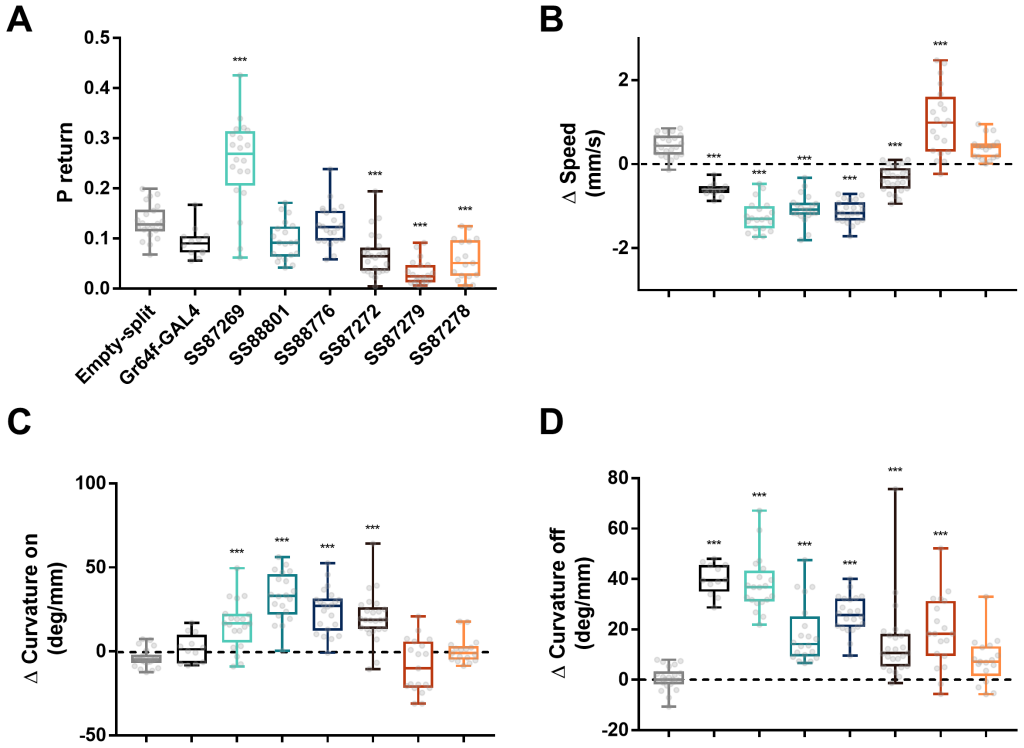

Figure 8-figure supplement 1 Summary data of Gr64f activation phenotypes

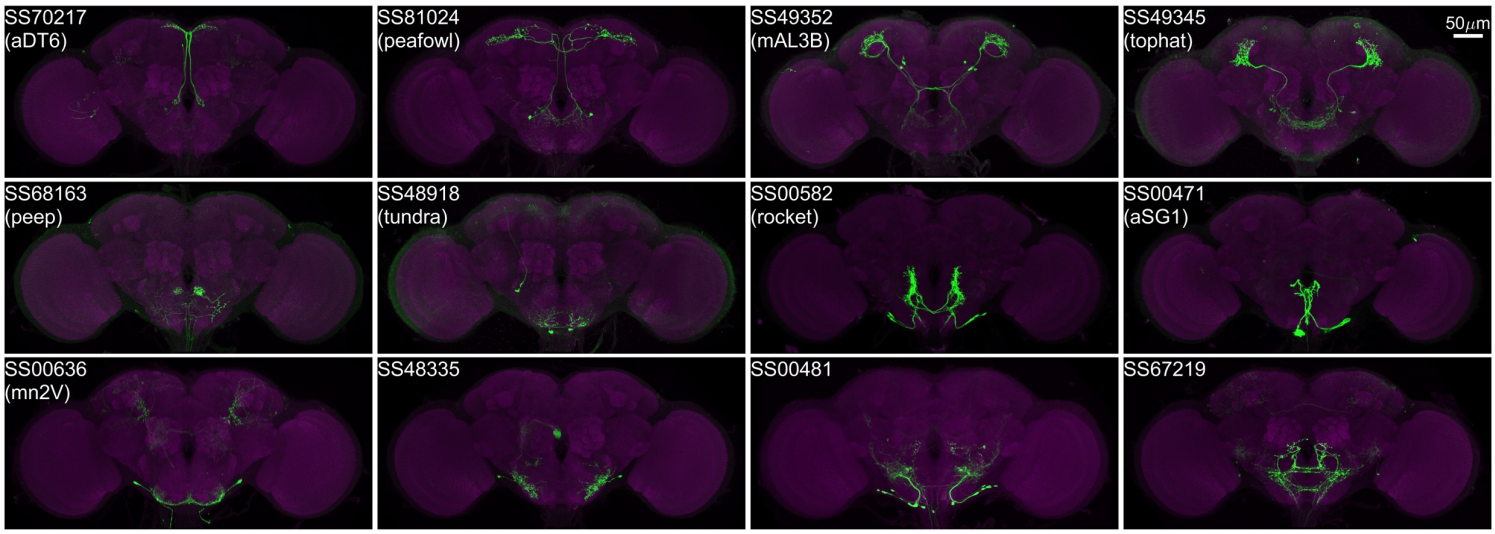

Figure 8-figure supplement 2 Examples of covered SEZ neurons

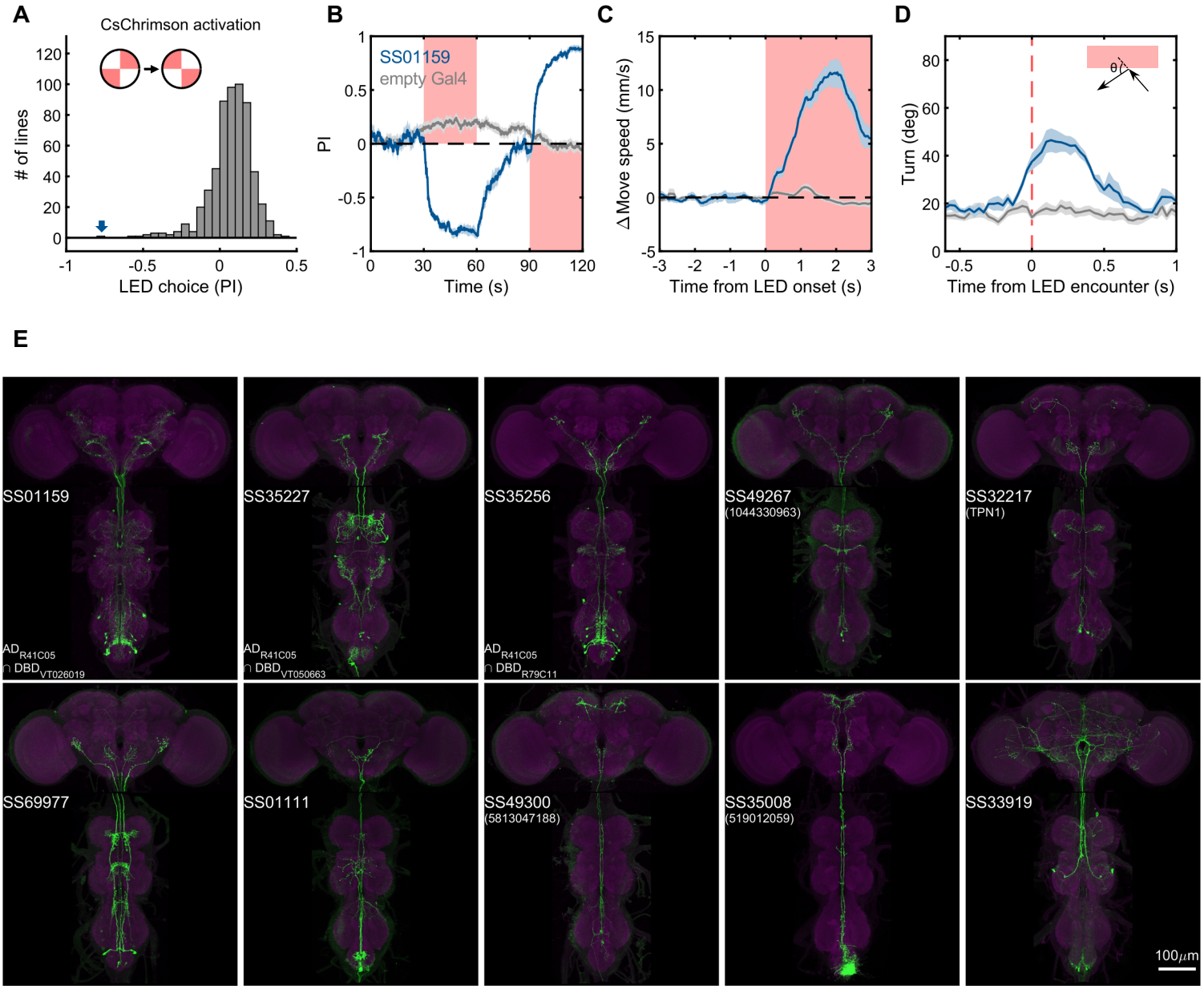

Figure 9 Examples of covered ascending neurons

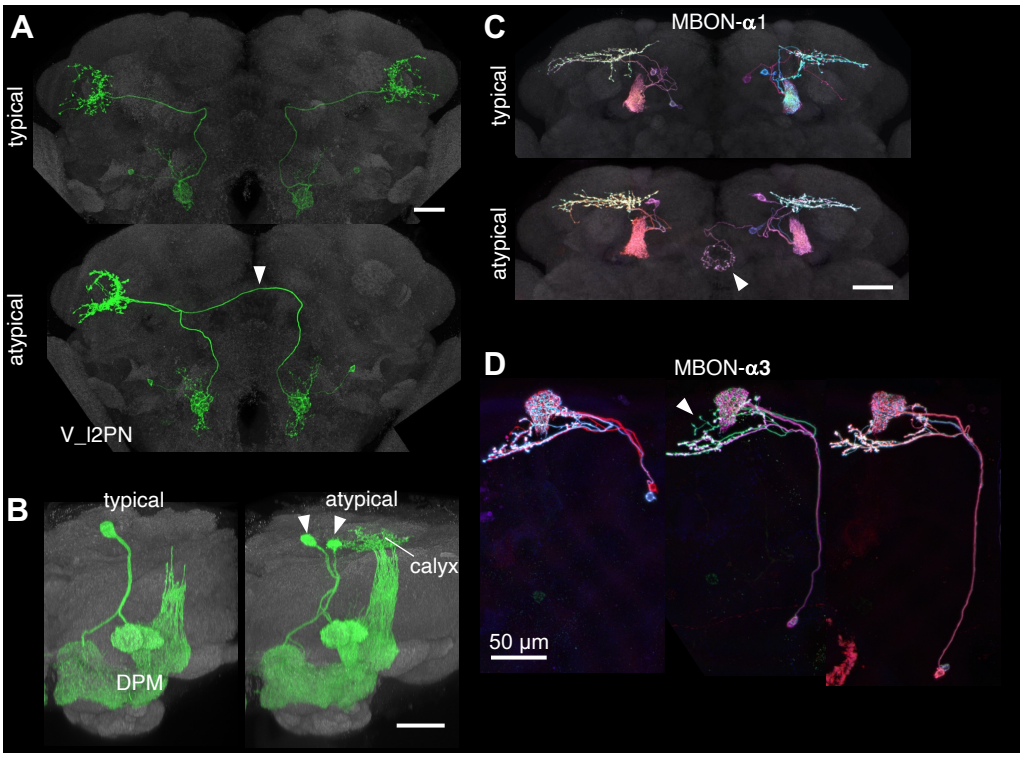

E

Cell Type	MB compartments	N hemisphere examined	Typical number of cells	Different number of cells (%)	Mislocalization (%) Dendrite	Mislocalization (%) Axon	mode of errors
MBON01	Y5, β'2a	16	1	0.0	0.0	12.5	mislocalization of axons
MBON02	β2, β'2a	96	1	1.0	1.0	1.0	mislocalization of axons
MBON03	β'2mp	56	1	0.0	0.0	0.0	
MBON05	Y4	50	1	0.0	0.0	0.0	
MBON06	β1	38	1	0.0	0.0	0.0	
MBON07	α1	105	2	0.0	22.9	1.9	dendrites outside the MB axon in the ellipsoid body third soma without neurites
MBON08/09	Y3, β'1	338	2	0*	*	0.6	see Figure 11
MBON11	Y1, pedc	136	1	0.7	0.7	1.5	dendrites in Y2 axon in the calyx lack of axon in α3
MBON12	Y2, α'1	106	2	0.0	0.0	0.0	
MBON13	α'2	82	1	0.0	1.2	0.0	dendrites outside the MB
MBON14	α3	44	1	0.0	0.0	2.3	additional axon branch
MBON18	α2sc	36	1	0.0	0.0	0.0	
MBON19	α2p3p	34	2	0.0	0.0	0.0	
MBON22	calyx	56	1	1.8	17.9	0.0	dendriets outside the calyx
MB-DPM	all	48	1	8.3	4.2	4.2	Second DPM axons/dendrites in the calyx

Figure 10 Atypical morphology of neurons

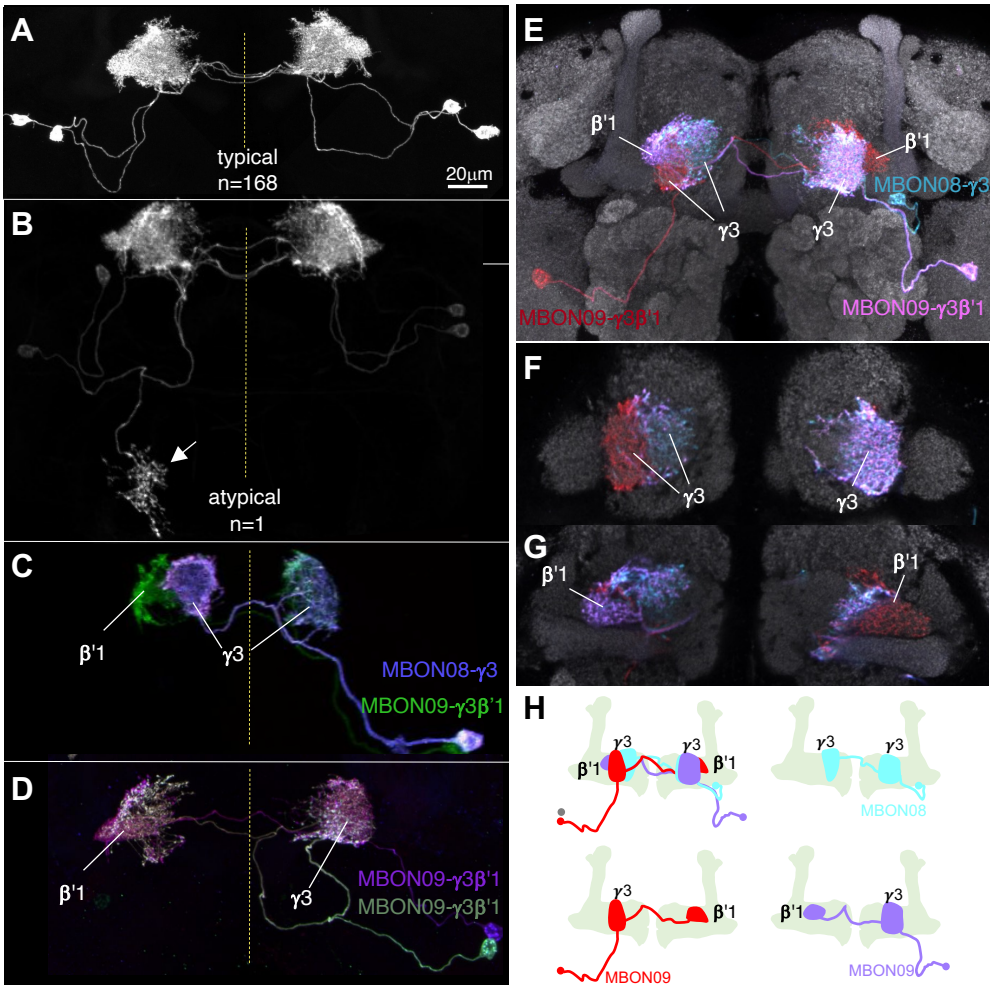

I

	Female	Male	Total
MBON08	7	14	21
MBON09	102	86	188
% MBON08	6.4	14.0	10.0
P only MBON09	0.77	0.55	0.65
P at least One MBON08	0.23	0.45	0.35

J

Left #1	Left #2	Right #1	Right #2	Left γ3	Left β'1	Right γ3	Right β'1	
8	8	8	8	+		+		P = 2% (No occurrence in 169 flies)
8	8	8	9	+	+	+		
8	8	9	8	+	+	+		
8	8	9	9	+	+	+		
8	9	8	8	+		+	+	
9	8	8	8	+		+	+	
9	9	8	8	+		+	+	
8	9	8	9	+	+	+	+	P = 3% (No occurrence In MCFO)
8	9	9	8	+	+	+	+	
9	8	8	9	+	+	+	+	
9	8	9	8	+	+	+	+	
8	9	9	9	+	+	+	+	P = 29%
9	8	9	9	+	+	+	+	
9	9	8	9	+	+	+	+	
9	9	9	8	+	+	+	+	
9	9	9	9	+	+	+	+	P = ~65% of flies
MBON type				MB compartments				

Figure 11 Morphological individuality

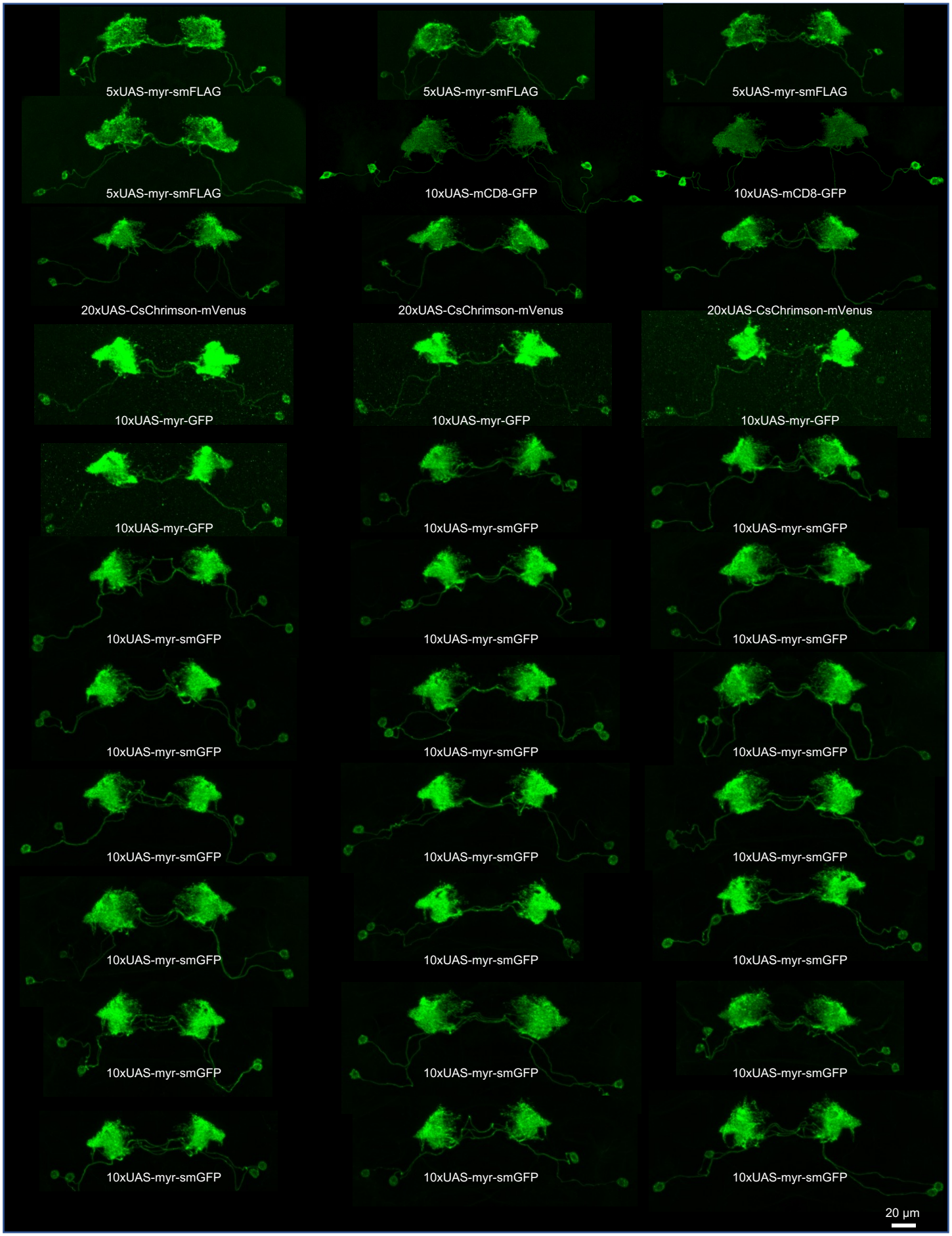

Figure 11 – figure supplement 1

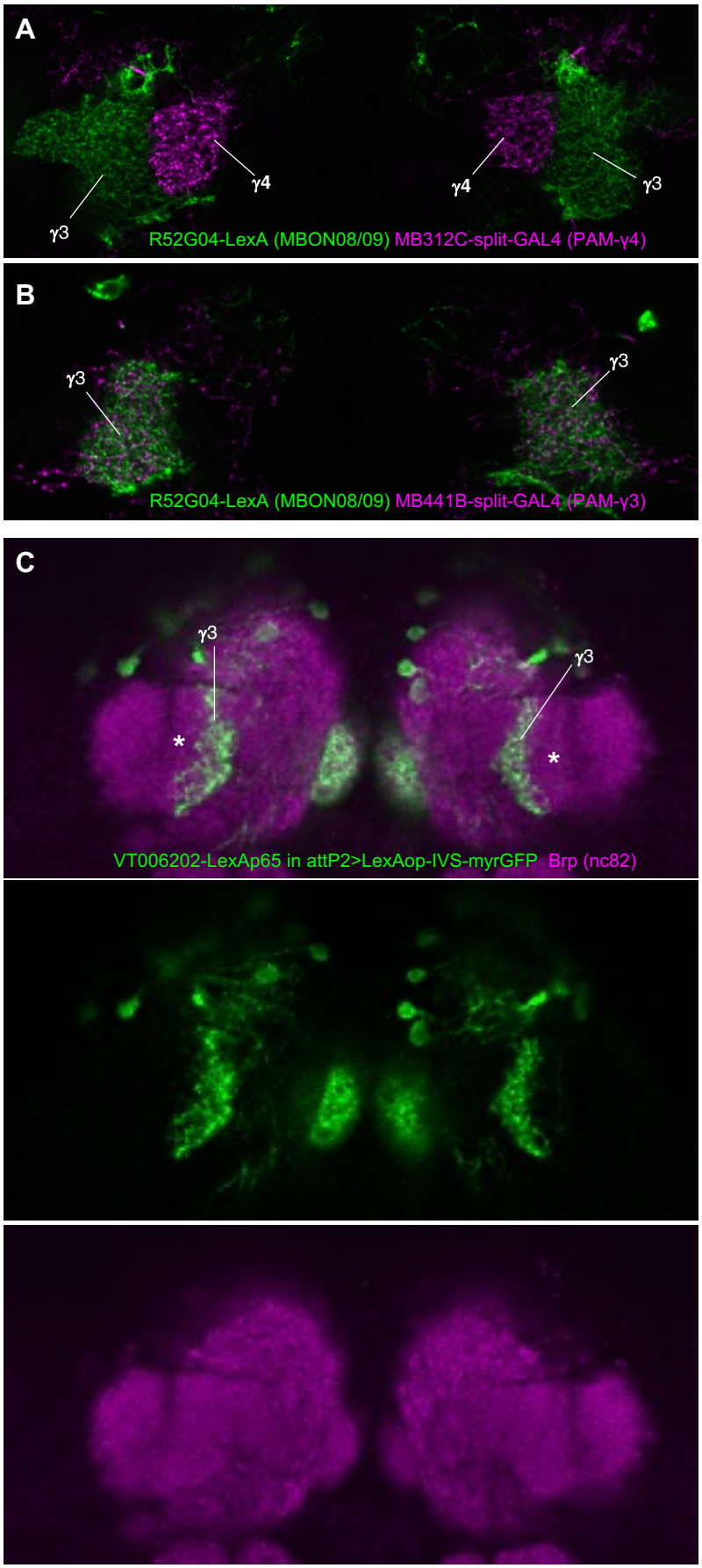

Figure 11 – figure supplement 2

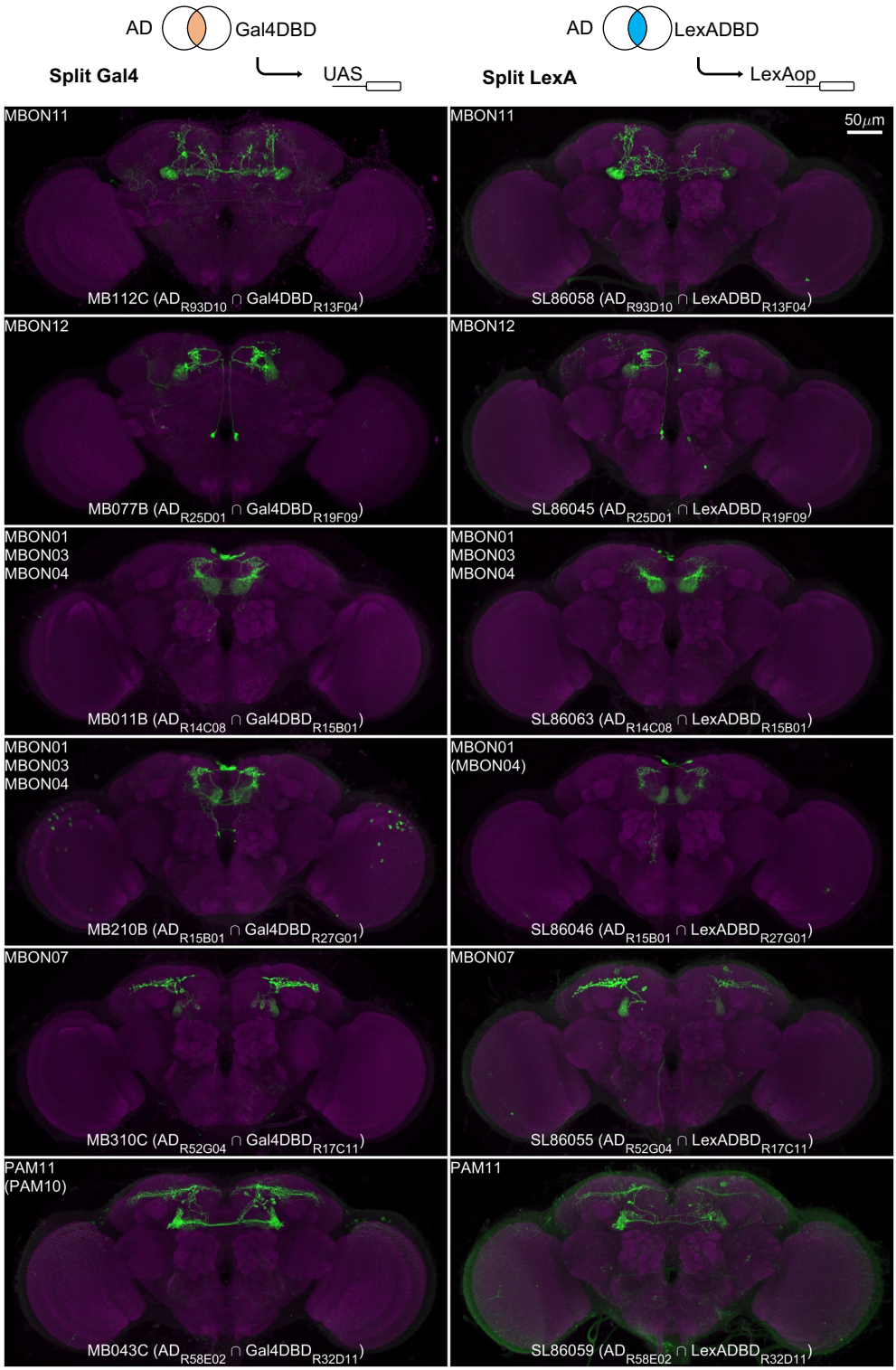

Figure 12 Examples of split-LexA conversion